DESIGN CONSIDERATIONS FOR DC-DC CONVERTERS IN FUEL CELL SYSTEMS

A Dissertation

by

LEONARDO MANUEL PALMA FANJUL

Submitted to the Office of Graduate Studies of
Texas A&M University
in partial fulfillment of the requirements for the degree of

DOCTOR OF PHILOSOPHY

December 2006

Major Subject: Electrical Engineering

DESIGN CONSIDERATIONS FOR DC-DC CONVERTERS IN FUEL CELL SYSTEMS

A Dissertation

by

LEONARDO MANUEL PALMA FANJUL

Submitted to the Office of Graduate Studies of
Texas A&M University
in partial fulfillment of the requirements for the degree of

DOCTOR OF PHILOSOPHY

Approved by:

Chair of Committee,	Prasad Enjeti
Committee Members,	Shankar Bhattacharyya
	Hamid Toliyat
	Emil Straube
Head of Department,	Costas Georghiades

December 2006

Major Subject: Electrical Engineering

ABSTRACT

Design Considerations for DC-DC Converters in Fuel Cell Systems.

(December 2006)

Leonardo Manuel Palma Fanjul, B.S., Universidad de Concepción;

M.S., Texas A&M University

Chair of Advisory Committee: Dr. Prasad Enjeti

Rapidly rising fossil fuel costs along with increased environmental awareness has encouraged the development of alternative energy sources. Such sources include fuel cells, wind, solar and ocean tide power. Among them, fuel cells have received increased interest in the recent years. This is mainly due to their high efficiency, modularity, and simple construction. However, due to their low output voltage and wide variation from no load to full load, a power electronics converter is required to interface the fuel cell with its loads.

This dissertation focuses on developing a set of considerations that will assist designers of the power electronics converter in the design and optimization of the system. These design considerations are obtained analytically and verified experimentally and allow obtaining an efficient and stable fuel cell – power converter system.

In addition to the design guidelines this dissertation presents new power converter topologies that do not require the use of transformers to achieve a large voltage gain.

Further a new modular fuel cell power converter system that divides the fuel cell stack to optimize power generation is proposed. It is shown by means of mathematical analysis and experimental prototypes that the proposed solutions contribute to the reduction of size and cost of the power converter as well to increase the efficiency of the system.

TABLE OF CONTENTS

TABLE OF CONTENTS CONTINUED

TABLE OF CONTENTS CONTINUED

LIST OF FIGURES

LIST OF FIGURES CONTINUED

LIST OF FIGURES CONTINUED

LIST OF FIGURES CONTINUED

LIST OF FIGURES CONTINUED

LIST OF TABLES

TABLE Page

CHAPTER I

INTRODUCTION

1.1 Introduction

Rapidly rising costs of fossil fuels along with the fear of short term depletion of oil reserves and increased environmental awareness are moving the world in the direction of renewable and clean energy generation. Oil prices have recently reached historical heights and are expected to keep increasing as world reserves start declining. And as any other non-renewable resource oil reserves will eventually be extinguished. Although the exact date when oil will be exhausted is unknown, most projections coincide in that this will occur some time around the middle of the current century [1-3]. On the other hand environmental concerns have been raised regarding the ever increasing use of fossil fuels. Burning fossil fuels such as oil and coal produce greenhouse gasses such as CO_2. The world temperature has been increasing steadily over the past century due to the release of such gases, and if this trend continues it is expected to produce an accelerated melting of the polar caps and unpredictable changes in the world weather. This in turn will raise the sea levels worldwide with the consequent damage for costal cities.

For these reasons the development of alternative energy sources has gained acceptance in the last two decades.

The citations on this dissertation follow the style of *IEEE Transactions on Industry Applications*.

Environmentally friendly energy sources such as fuel cells, solar panels, wind mills and micro hydroelectric plants appear as good alternatives to produce electric power. Among these, fuel cells have been considered as the primary energy source for next generation power for residential, transportation and portable applications.

Fuel cells use chemical reactions to generate electricity, rather than storing it, as is typically done with conventional batteries. Fuel cells generate electrical energy by combining oxygen with a hydrogen-based fuel, such as methanol. Power is continuous while fuel and oxygen are supplied, similar to the gasoline/engine system which is used to power a car. The engine is purchased once (with the car) and gasoline is replenished as needed for continuous operation. The same is true fuel cell systems, which are expected to someday help power portable electronic products, such as notebook computers. Fuel capsules can be swapped out quickly no need to wait for recharging. In the case of portable applications users would carry spare fuel cartridges, not extra batteries to extend operation and enhance convenience. Fuel cells also find their place in residential power systems where they can be used along with solar panels to reduce the power consumed during peak hours and helping to reduce the energy bill. Another application where fuel cells appear as a good alternative is in the transportation market, where they can be used to replace internal combustion engines. In these applications the main advantage they pose in contrast with the alternative, which are batteries, is quick refueling. The hydrogen tank can be refilled in mater of seconds in comparison to hours in the case of batteries. Also there is the advantage disposal; unlike batteries fuel cells do

not contain any hazardous materials once their operational life is over they can be discarded easily.

Fuel cells can be considered as a soft voltage source, this due to the load dependent nature of its output voltage. A typical fuel cell stack output voltage experiences a 2 to 1 variation from no load to full load. Also, since each cell in a fuel cell stack has a low output voltage (0.6V to 0.7V at full load), it is necessary to stack many cells in series to obtain a reasonable output voltage.

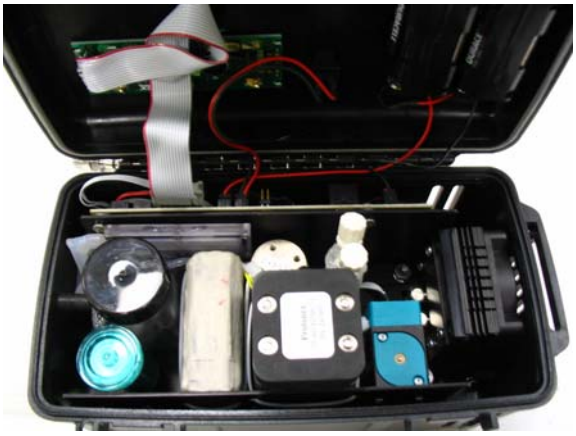

Figure 1. An example 30W portable fuel cell system

Stacking many cells in series adds to the complexity of the system, in terms of:

a) Complicated plumbing to properly distribute the fuel

b) Water/thermal management.

Due to these limitations, a lower output voltage (3V to 12V) fuel cell (with fewer cells stacked in series) becomes the optimum configuration for fuel cells under 20W (figure 1). Due to the available lower output voltage, coupled with no-load to full-load

variation of the fuel cell terminal voltage, a step-up type DC-DC converter becomes necessary (figure 2).

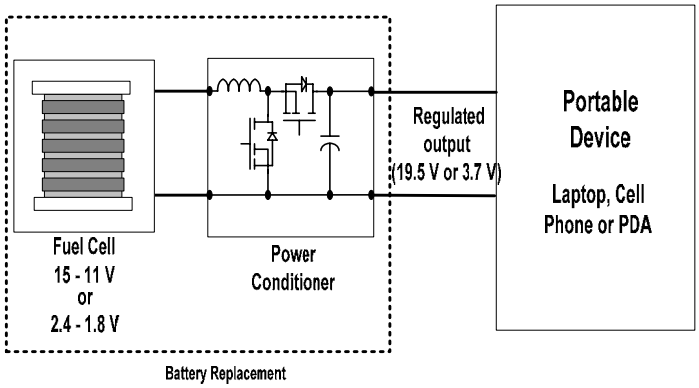

Figure 2 Fuel cell powered portable electronic system

In order to properly design and control this DC-DC converter a good understanding of the behavior of the fuel cell is needed. For this, both dynamic and steady state performance of the fuel cell needs to be studied and analyzed. Analogously the interaction of fuel cell and DC-DC converter has to be understood in order to optimize the performance of the overall system.

1.2. Fuel cell technology

Fuel Cells are electrochemical devices that convert hydrogen rich fuels into electric energy directly with a high overall efficiency. Since the process of producing electric energy avoids the intermediate steps of producing heat and mechanical work, common in most conventional methods, fuel cells are not limited by the thermal limitations such as

the Carnot efficiency. Moreover since the process does not involve any kind of combustion fuel cells produce power with a minimal amount of pollutant gases. On the other hand, unlike batteries, fuel cells produce power as long as reductant and oxidant are supplied. Although, in theory, fuel cells can use a wide range of fuels most modern systems use hydrogen rich reductants such as common fuels (methanol, natural gas, gasoline, etc) or pure hydrogen. Air is mostly used as oxidant. The basic structure of a fuel cell is shown in figure 3, and consists of an electrolyte layer in contact with an anode and a cathode on either side. The reductant or fuel is fed continuously to the anode and the oxidant is fed to the cathode.

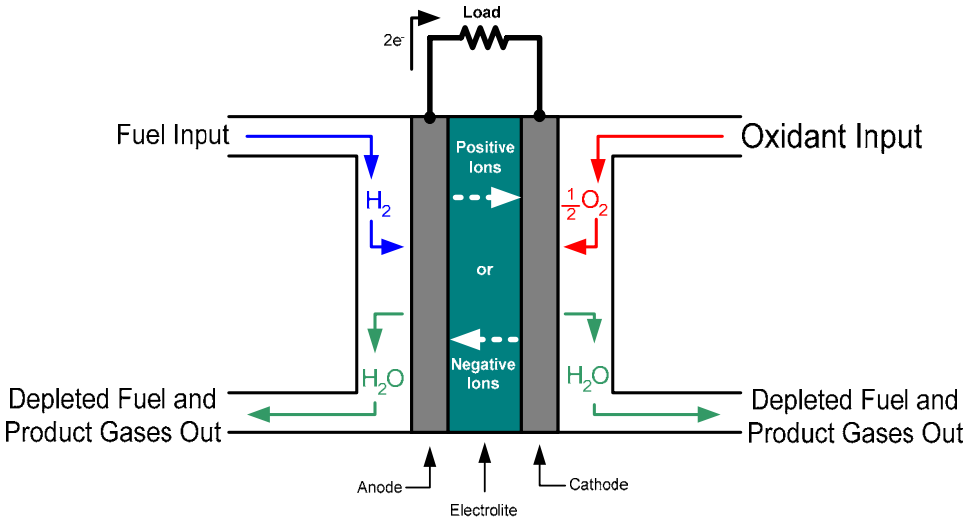

Figure 3 Fuel cell basic structure

The electrochemical reactions take place at the electrodes and to produce a current trough the electrolyte, while driving a complementary electric current that performs

work on the load. Fuel cells can be classified according to the type of electrolyte and fuel used:

a) Polymer electrolyte fuel cell (PEFC)

b) Alkaline fuel cell (AFC)

c) Phosphoric fuel cell (PAFC)

d) Molten carbonate fuel cell (MCFC)

e) Solid oxide fuel cell (SOFC)

The choice of electrolyte also dictates the operation temperature of the system. High temperature fuel cells such as solid oxide fuel cells (SOFC) are mostly suitable for large scale power generation. On the other hand low temperature fuel cells such as the polymer electrolyte fuel cell are preferred for portable power and small scale generation. Among them the proton exchange membrane fuel cell (PEMFC) has gained a wide acceptance due to several advantages such as compact design, long operating life, quick start-up times, and high efficiency. A PEMFC generates electricity directly from hydrogen fuel by means of two electrochemical reactions which take place at the proton exchange membrane/catalyst interface at low temperatures (<80° C). The electrochemical reactions are given by:

$$H_2 \rightarrow 2H^+ + 2e^- \quad (1)$$

$$O_2 + 4H^+ + 4e^- \rightarrow 2H_2O \quad (2)$$

The voltage produced by a single PEMFC varies from 1.4V at no load to 0.7V at nominal load current. Thus, in order to obtain a reasonable voltage a number of

individual cells need to be stacked in series. However stacking multiple cells in series has the disadvantage of increasing the complexity of the system.

1.3. The fuel cell promise

Some of the main advantages of PEM fuel cells are their high efficiency, simple operation and high energy density. These are the reasons, especially the later, why fuel cells appear as a direct competition for traditional power sources for portable electronics. Since the introduction of portable electronics in the mid 1950's batteries have been their de facto source of energy. However the amount of energy that can be stored in batteries is limited and their development does not keep up with the energy requirements of modern devices. In contrast the energy density of fuel cells is up to 4 times higher than that of batteries currently available as can be observed from figure 4. Moreover fuel cells offer an energy density even higher that the theoretical limit of their closes competitor (Li-ion).

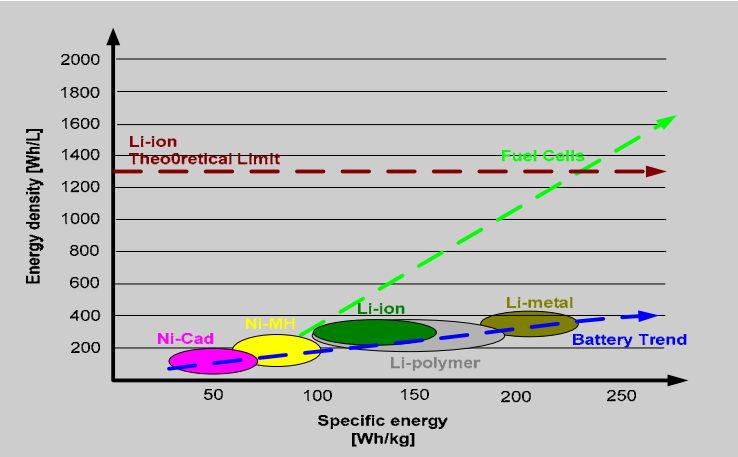

Figure 4 Fuel cell and battery energy density vs. specific energy

Another strong point of fuel cells appears when the cost of producing 1kW of energy is compared against batteries. As can be observed from Table I the total cost of generating 1kW of energy using a fuel cell is up to 5.8 times lower than using existing reusable battery technologies. Also the life span of fuel cells is up to four times longer than popular battery technologies such as Li-ion and Ni-MH. For these reasons fuel cells appear as a very promising candidate for replacing batteries in portable devices in the upcoming years. However there still are issues that have to be resolved in order to make fuel cells popular in the market place.

Table I

Cost of generating 1kW of energy

Power source	Investment of equipment to generate 1kW	Lifespan of equipment before major overhaul or replacement	Cost of fuel per kWh	Total cost per kWh, including maintenance and equipment replacement
Ni-MH	**$9400** Based on 7.5V, 1000mAh at $70/pack	**500h** based on 1C discharge	**$0.15** for electricity	**$18.50**
Li-ion	**$12000** Based on 7.2V, 1200mAh at $100/pack	**500h** , based on 1C discharge	**$0.15** for electricity	**$24.00**
Rechargeable Alkaline	**$1000** Based on 7.2V, 1400mAh at $6/pack	**10h** , based on 1C discharge	**$0.15** for electricity	**$95.00**
Ni-Cd	**$7000** Based on 7.2V, 1000mAh at $50/pack	**1500h** , based on 1C discharge	**$0.15** for electricity	**$7.50**
Fuel Cell	**$3000-7500**	**2000h**	**$0.35**	**$1.85-4.10**

1.4. Interfacing fuel cells and loads

Due to the low voltage that a fuel cell produces (0.7V at nominal current) it becomes necessary to stack a number of them in series in order to obtain a reasonable output voltage value. However by doing so the system becomes more complicated due to the fuel and oxygen distribution to each of the cells in the stack. Also by stacking many cells in series some thermal and water management issues arise. For this reason the number of cells connected in series in a fuel cell stack should be maintained at a minimal. For low power applications a stack containing between 10-20 cells appears as a good solution. Such an arrangement provides an output voltage between 6 and 12V at full load.

Also the voltage produced by the fuel cell is a function of its load current exhibiting a 2 to 1 variation from no load to full load (figure 5). Therefore a step-up type DC-DC converter is required in order to interface the fuel cell with most electronic loads which require a stable input voltage. DC-DC converters can be operated either in continuous conduction mode (CCM) or in discontinuous conduction mode (DCM).

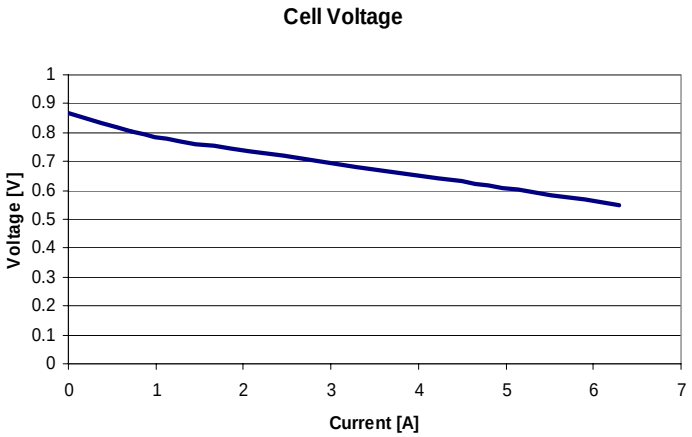

Figure 5 V-I characteristic for a single cell

When the converter is operated in continuous conduction mode the current being drawn from the fuel cell has a small high frequency ripple as seen in figure 6.

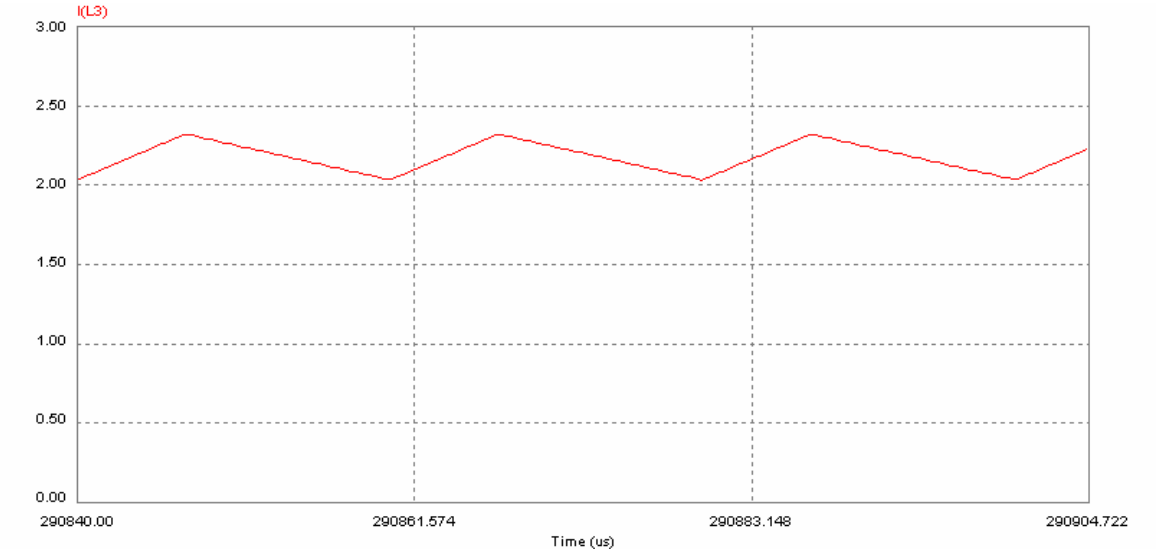

Figure 6 Inductor current for boost converter in CCM

On the other hand if the DC-DC converter is operated in discontinuous conduction mode the current drawn from the fuel cell has a large high frequency ripple (figure 7).

Since fuel cells are mainly DC power sources they are intended to supply loads that draw a DC current, and as can be seen from figures. 6 and 7 this is not the case when a DC-DC converter is used. Therefore it is needed to analyze if the presence of high frequency ripple currents degrades the performance of the fuel cell stack. Specifically this analysis should include:

- Methods to determine an electrical equivalent circuit for a commercially available 20W portable fuel cell.

- Experimentally evaluate the effects of continuous and discontinuous conduction operation of the dc-dc converter on the fuel cell performance. Note discontinuous conduction operation results in smaller inductor size, zero current switching during turn-on due to the absence of diode reverse recovery losses.

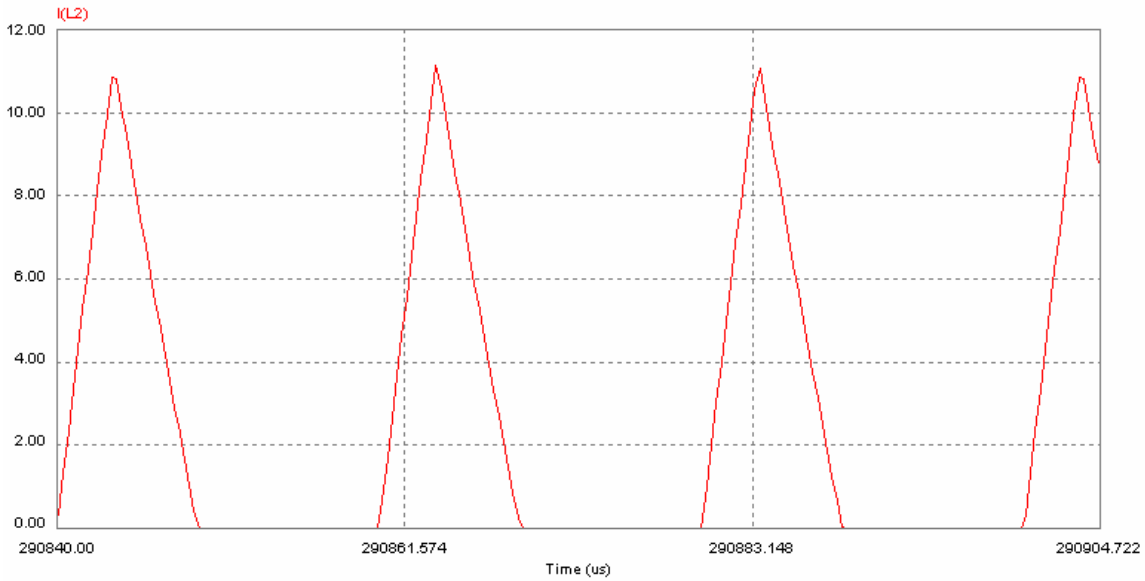

Figure 7 Inductor current for boost converter in DCM

As mentioned before DC-DC converters can be operated either in continuous conduction mode (CCM) and discontinuous conduction modes (CCM). In the continuous conduction mode, the peak currents are lower, however, the inductor size is larger and the effect of diode reverse recovery contributes to additional switching losses. On the other hand the discontinuous conduction operation results in large peak currents, lower inductor size, zero current turn-on and the absence of reverse recovery phenomenon. Therefore operating the DC-DC converter in DCM may be more attractive in portable

applications where size and efficiency are at a premium. However in both cases the current supplied by the fuel cell contains a large high frequency ripple current. The presence of these currents has an effect on the performance of the fuel cell. The performance of the fuel cell can be measured in terms of the temperature rise and hydrogen fuel consumption. The result of this type of analysis facilitates the design of DC-DC converter by giving design and optimization guidelines.

1.5. System interactions between fuel cell and power converter

In most practical applications, due to the low voltage of the fuel cell, the use of a boost type DC-DC converter is required. The interaction of the two systems has to be analyzed in order to ensure proper dynamic response as well as stability of the overall system. Normally the design of DC-DC power supplies is carried out assuming that the impedance of the source is small enough to not interfere with the operation and dynamic performance of the converter. But the use of a fuel cell as the power source, which has complex internal impedance, will alter the control characteristics of the DC-DC converter (figure 8).

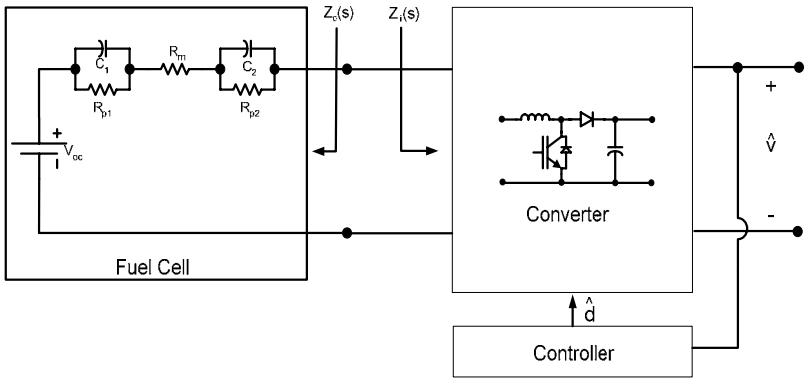

Figure 8 Fuel cell DC-DC converter system

Thus it is needed to analyze the magnitude of the impact on the control characteristics of the system to assure that the system stability and dynamics are not degraded. Another point to be analyzed is the behavior of the system during the purging of the fuel cell. For low power applications, 150W and below, dead ended PEM fuel cells are normally used. In this particular kind of fuel cell hydrogen enters the stack at the anode, and there is a solenoid valve located at the cathode which opens at regular intervals to release the by-products of the chemical reaction. The opening of the valve is referred to as purging. During the purging interval the voltage produced by the fuel cell drops due to the reduction in internal pressure (figure 9).

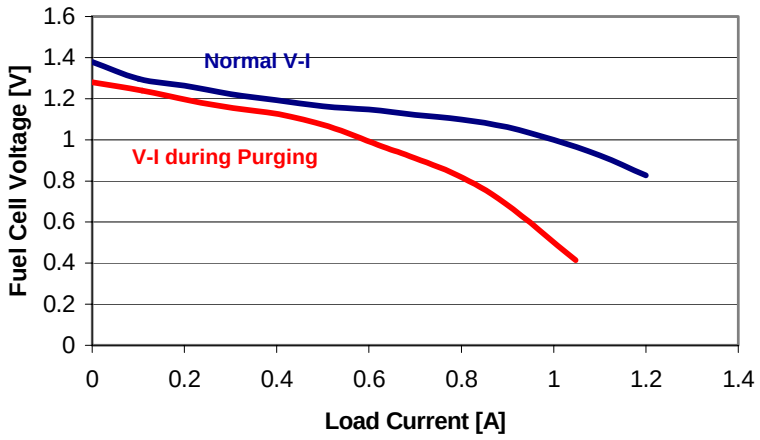

Figure 9 Fuel cell V-I characteristic

The magnitude of this voltage drop is a characteristic of the fuel cell, and it is a function of the load current, fuel cell parameters, and the duration of the purging period. During the purge interval the voltage produced by the stack is reduced, which in turn reduces the power that the fuel cell can deliver. This in turn may affect the stability of the fuel cell DC-DC converter system thus it needs to be analyzed in detail.

1.6. High gain DC-DC converters

As mentioned above a draw back of fuel cells is that the DC voltage generated by the stack varies widely, normally from 2 in per unit to 1 in per unit. Further the voltage produced by fuel cells is low in magnitude and therefore for applications where the output power is in the kilowatt range input voltages and currents can easily have the same order of magnitude. Thus they present quite challenging characteristics for the design of the power conditioning system required to interface the fuel cell to the utility

grid or ac loads common in residential applications. By the fore mentioned reason a step-up DC-DC conversion stage is essential to generate an adequate input voltage for the DC-AC inverter stage (200V typically for a 120 V AC output). A typical power conversion unit for this type of applications is shown in figure 10. Where the power conversion system is composed by two stages a DC-DC converter and a DC-AC inverter.

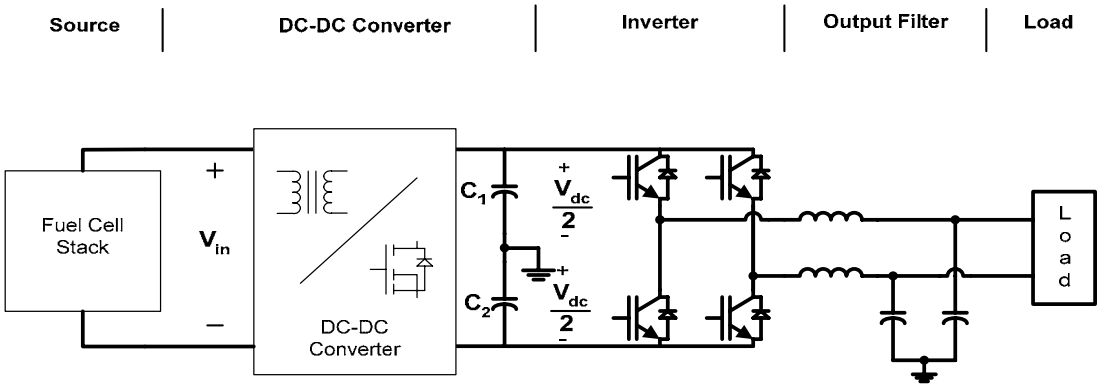

Figure 10 Typical fuel cell power conversion system for residential applications

Normally the DC-DC converters used to accomplish this task take advantage of a high frequency transformer to provide the voltage gain required. But the use of transformer based DC-DC converter has some disadvantages such as increased size and cost.

Recently transformer-less converters have been proposed to reduce the size and cost of the power conversion units in applications where no electrical isolation is required [4-5]. But they lack of an adequate voltage gain, and in some cases they require a dual input

voltage supply. For this reason is of interest to design a transformer less step-up DC-DC converter topology that can provide a large voltage gain while maintaining a stable dc-link for the operation of DC-AC inverter.

Such a converter should have the following advantages:

- Operation from a single input voltage
- No transformer required to achieve a voltage gain of 5 in per unit
- If a single phase is connected at its output the system can generate $120V_{AC}$ output from a $40V_{DC}$ input source without the use of a transformer.

1.7. Modular DC-DC converters for fuel cell systems

As previously stated due to the low voltage produced by fuel cells it becomes necessary to stack a number of them in series in order to obtain a higher voltage. However this comes at a cost of increased system complexity and additional thermal and waste water management issues. This is especially true for applications that require the fuel cell to provide a high voltage such as residential and transportation applications. An additional problem that arises when connecting many cells in series is that the voltage produced by each individual cell in the stack may not be equal. The voltage produced by each cell in the stack is affected by parameters such as fuel pressure, air pressure, and membrane humidity. In addition the presence of mal functioning cells in the stack further contributes to an un-even distribution of the voltage. All this has the end effect of reducing the maximum power that the fuel cell stack can produce. To avoid these problems the use of a modular fuel cell stack as shown in figure 11 is proposed.

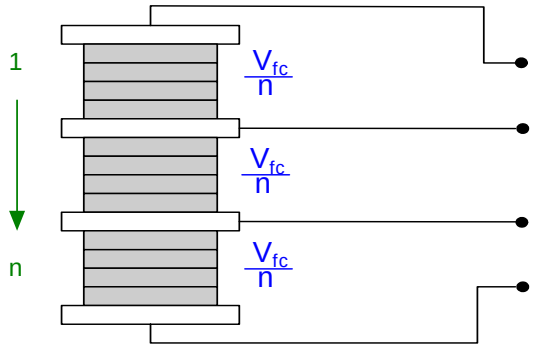

Figure 11 Sectioned fuel cell stack

To take advantage of such as fuel cell stack an appropriate DC-DC converter has to be designed and its control strategy needs to be devised.

1.8. Common mode voltage and circulating currents

Because of rapid changes in voltages and currents within a switching converter, power electronic equipment is a source of electromagnetic interference (EMI). This interference can affect the operation of other equipment as well as the one producing the interference. The EMI can be transmitted in two forms: radiated and conducted. Switching converters supplying power to the utility generate conducted noise that is normally several orders of magnitude higher than the radiated nose, this due to the fact that power converters are normally encased in metal cabinets that serve as shield that blocks the radiated component of the EMI.

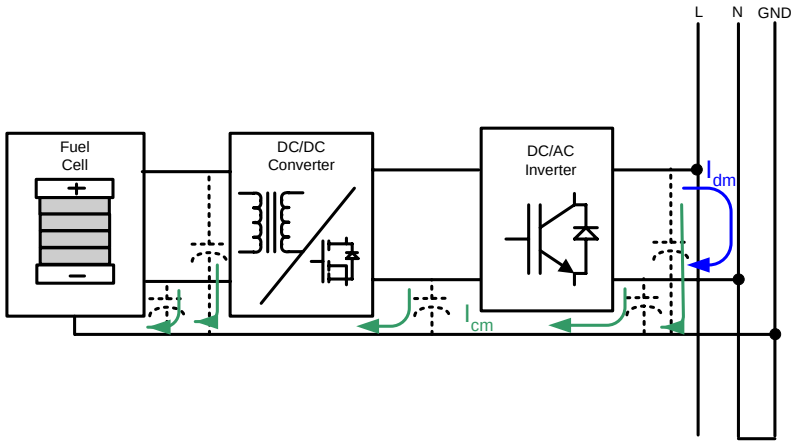

Figure 12 Conducted interference

In a utility connected fuel cell system as shown in figure 12 one can identify two different types of conducted noise, common mode and differential mode. The differential-mode noise is a current or voltage measured between the output lines of the converter, which is the actual output of the system. On the other hand common-mode noise is a voltage or current measured between the output lines of the converter and ground, such as I_{cm} in figure 12. The transmission of the common-mode noise is entirely trough "parasitic" or stray capacitors and stray electric and magnetic fields. These stray capacitances exist between various system components and between components to ground. Analysis of common mode voltage and current in fuel cell systems is required in order to minimize its effects on the system components.

1.9. Previous work

Over the years many equivalent circuit models have been proposed [6-8], which vary on complexity and accuracy. Using one of these equivalent circuit models the effect of the load current in the performance of the fuel cell has been studied by Choi and Enjeti, but their work focused only on the effect of low frequency ripple. Specifically on the effect of drawing 120 Hz ripple current from the fuel cell stack. This ripple current is typical in fuel cell systems used to supply AC loads through a DC-AC inverter. However if the fuel cell supplies a portable device the current drawn by the DC-DC converter only contains high frequency ripple currents. The frequency of the ripple current in this type of application is given by the switching frequency of the DC-DC converter, which normally ranges from 20 kHz to 200 kHz. The effect of such high frequency currents on the performance of the stack needs to be analyzed.

The effect in the dynamics of the DC-DC converter due to the internal impedance of the fuel cell has not been studied so far. However analytical tools exist that can facilitate this analysis. The use of a fuel cell as a power source for DC-DC converters can be treated in a similar fashion as when a filter is connected between the power source and a DC-DC converter. An approach to analyze this problem is presented by Erickson and Maksimović in [9] and it is shown that for the case of using a filter the stability and dynamics of the system may be compromised.

A number of transformer less step-up DC-DC converters have been presented. But most of them do not provide the voltage gain required for fuel cell applications (normally up to 10x). Moreover those that do provide a high voltage gain are only rated

for low power applications (less than 2W). A DC-DC converter that overcomes some of these problems was proposed by Luo [4]. This converter offers a high voltage gain but is intended for low power applications such as computer peripherals. Whether this converter is applicable for applications in the kW range remains to be seen. An alternative DC-DC converter to provide a high voltage gain is the flying capacitor converter. This converter is derived from inverters for medium voltage. The main problem in this type of converter is controlling the voltage on each of the flying capacitors. An approach to use this converter was presented by Bayer [5].

Modular power converters are normally used in medium voltage motor drive applications. Modular medium voltage converters such as the one presented by Cengelci, Enjeti, Singh, Blaabjerg and Pederson [10] are constructed several low voltage modules whose outputs are connected in series. The applicability of such a concept has not been used for DC-DC converters. In addition the concept of utilizing sectioned fuel cell stacks has not been presented so far.

The presence of common-mode noise in adjustable speed drives has been carried out in the past. These systems are normally composed by a three phase rectifier cascaded with a three phase inverter. The inverter may be constructed either using a two level topology for low voltage or multilevel topology for medium voltage. Most of the previous work focuses on reducing the common-mode noise by placing passive filters at the output of the inverter [11-13]. Or by modifying the switching patterns in order to cancel out most of the common-mode voltage [14-16]. However little attention has been given to the common-mode problem in systems used for co-generation, such as utility

connected fuel cell systems. These systems are normally composed by a DC-DC converter cascaded with a DC-AC inverter, thus there are two potential common-mode sources in such systems. Therefore analysis of the common-mode issue is required.

1.10. Research objective

The objective of this dissertation is to analyze and design DC-DC converters for fuel cell applications. The starting point of the analysis is by obtaining an adequate equivalent circuit for the fuel cell. For this the frequency spectroscopy method is used to obtain and systemize the element values in the equivalent circuit. This equivalent circuit is then be used to analyze the effects of high frequency ripple currents, typical of DC-DC converter operation, in the fuel cell. This is done both analytically and experimentally and the main focus is on determining whether or not the presence of high frequency currents has a negative effect on the amount of fuel that the fuel cell consumes. In addition the efficiency of the stack is studied in order to determine if the fuel cell can produce the same amount of power when supplying a load current with a high frequency ripple component. Design guidelines for the DC-DC converter are derived from this analysis.

The interaction between the DC-DC converter and the fuel cell stack is studied. The effects of the fuel cell internal impedance on the stability and dynamics of the DC-DC converter are analyzed. Also the effect on the operation of the DC-DC converter produced by the periodical release of by-products by the fuel cell will be studied. From

the results obtained design criteria optimizing the operation of the power converter is proposed and their effectiveness is shown by means of experimental results.

High gain transformer less DC-DC converter for fuel cell applications is proposed. The use of a hybrid connection of DC-DC converters to realize the high gain power converter are analyzed and designed. Analytical equations for the voltage gain and efficiency of the proposed approach are derived to show the operation of the system. The effectiveness of the proposed solution is shown by means of experimental results on laboratory prototypes.

Typically many cells are stacked in series to attain a higher output voltage. This fuel cell configuration results in un-even cell voltages, and contributes to reduced output power, and reduced reliability. To address these problems, an approach to use a modular fuel cell is investigated. To take advantage of this fuel cell arrangement a modular DC-DC converter is introduced. The proposed converter is capable of maximizing the power extracted from the fuel cell by equalizing the power extracted from each section. In addition faulty sections in the fuel cell can be bypassed without having to decommission the entire stack. The operation of the said converter is analyzed and a control strategy for the system is proposed.

Due to the high frequency switching in power electronics systems common mode noise is generated. In particular common-mode noise is of interest due to its ease of propagation trough stray capacitances. Analysis of common mode voltage and currents on fuel cell systems connected to the utility needs to be done. For this different fuel cell grounding approaches have to be studied to verify the presence of common-mode

voltages and currents in the system. An approach to reduce the conduction of common-mode currents is analyzed.

1.11. Dissertation outline

Chapter I of this dissertation presents the reasons behind the increased interest on fuel cells as an alternative power source for residential, transportation and portable applications. The basic operation principle of the fuel cell is described as well as its most relevant terminal characteristics. Also this chapter compares fuel cells with batteries in terms of energy densities and cost. It is shown that in both aspects the fuel cell appears as a good alternative for powering portable devices. The characteristics of the fuel cell as a power source are discussed and the need of DC-DC converters as an interface for electronic loads is presented. In addition some issues regarding the interaction of the fuel cell and the DC-DC converter are discussed. Finally the research objective of this work is presented.

Chapter II focuses on the modeling of the fuel cell in order to obtain an electrical equivalent circuit, and a method to extract the parameters of the equivalent circuit is presented. In addition, the effect of the load current on the performance of the fuel cell stack is studied. Since a DC-DC converter is needed to interface the fuel cell with the loads the current drawn from the fuel cell will contain a high frequency ripple. The effect of this high frequency component on the fuel consumption and power available at the fuel cell terminals is discussed. Design guidelines to optimize the fuel cell DC-DC converter system will be derived in this chapter.

Chapter III deals with the effect of the internal impedance of the fuel cell in the dynamic characteristics of the DC-DC converter. For this the output impedance and input impedance of the fuel cell and DC-DC converter along with the transfer function of the converter are derived and analyzed. In addition this chapter discusses the effect the purge of the by products of the fuel cell in the stability of the system.

Chapter IV covers the use of transformer less DC-DC converters in fuel cell systems. A hybrid connection of modules to obtain a high voltage gain is presented. The main terminal characteristics of the proposed solution are analyzed and the operation of the system is verified by means of laboratory prototypes.

Chapter V presents the use of a modular fuel cell to avoid the problems that arise from long fuel cell stacks. Also the use of modular DC-DC converters for this type of fuel cell is discussed. A modular approach fuel cell – DC-DC system is presented and its control strategy discussed.

Chapter VI deals with the problem of common-mode noise in fuel cell systems connected to the utility. The presence of common-mode voltages and currents produces conducted electromagnetic interference that may result harmful to the operation of neighboring equipment as well as to the converter itself and the fuel cell. Analysis of the problem for different system configurations is done and possible solutions are presented.

Finally Chapter VII presents the general conclusions and remarks obtained from this work.

CHAPTER II

FUEL CELL EQUIVALENT CIRCUIT

2.1. Introduction

Fuel cells use a chemical reaction to generate electricity, rather than storing it, as is typically done with conventional batteries. Fuel cells generate electrical energy by combining oxygen with a hydrogen-based fuel, such as methanol. Power is continuous while fuel and oxygen are supplied. Fuel capsules can be swapped out quickly no need to wait for recharging. Users would carry spare fuel cartridges, not extra batteries to extend operation and enhance convenience.

Fuel cells can be considered as a soft voltage source, this due to the load dependent nature of its output voltage. A typical fuel cell stack output voltage experiences a 2 to 1 variation from no load to full load.

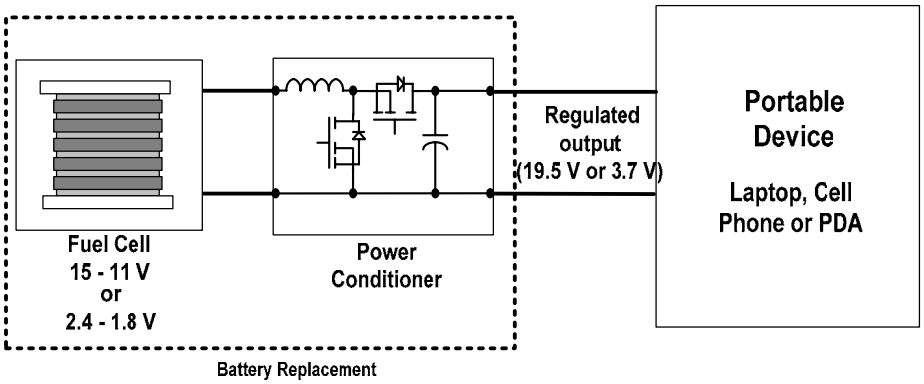

Figure 13 Fuel cell powered portable system

Also, since each cell in a fuel cell stack has a low output voltage (0.6V at full load), it is necessary to stack many in series to obtain a reasonable output voltage. Stacking many cells in series adds to the complexity of the systems, in terms of:

a) Complicated plumbing to uniformly distribute the fuel

b) Water/thermal management complexities arise when many cells are connected in series.

Due to these limitations, a lower output voltage (3V to 12V) fuel cell (with fewer cells stacked in series) becomes the optimum configuration for fuel cells under 20W. Due to the available lower output voltage, coupled with no-load to full-load variation of the fuel cell terminal voltage a dc-dc boost converter is therefore an ideal choice for such systems (figure 13). The purpose of this chapter is to explore in depth the design considerations for the fuel cell powered DC-DC converter. In particular this paper focuses on:

- Methods to determine an electrical equivalent circuit for a commercially available 20W portable fuel cell.
- Experimentally evaluate the effects of continuous and discontinuous conduction operation of the dc-dc converter on the fuel cell performance. Note discontinuous conduction operation results in smaller inductor size, zero current switching during turn-on due to the absence of diode reverse recovery losses.

DC-DC converters can be operated either in continuous conduction mode (CCM) and discontinuous conduction modes (CCM). In the continuous conduction mode, the peak currents are lower, however, the inductor size is larger and the effect of diode reverse recovery contributes to additional switching losses. On the other hand the discontinuous conduction operation results in large peak currents, lower inductor size, zero current turn-on and the absence of reverse recovery phenomenon. In both cases the current supplied by the fuel cell contains high frequency ripple. The presence of these currents has an effect on the performance of the fuel cell. The performance of the fuel cell can be measured in terms of the temperature rise and hydrogen fuel consumption. The result of this type of analysis facilitates the design of dc-dc converter by giving design and optimization guidelines. For example it is shown that the hydrogen flow rate is less than 5% higher under discontinuous conduction with a duty cycle of in the range from 40 to 100%.

2.2. Fuel cell equivalent circuit

The starting point to analyze the behavior of the fuel cell stack is to obtain an electrical equivalent circuit model. This model has to provide an accurate response for steady state as well as dynamically. Over the years many equivalent circuit models have been proposed [6-8, 17, 18], which vary on complexity and accuracy. Among them the equivalent circuit model proposed in [8] is one of the few that link the chemical reactions and measurable electric parameters.

The chemical reactions taking place in the anode and cathode of the fuel cell are given by:

$$H_2 \rightarrow 2H^+ + 2e^- \quad (3)$$

$$O_2 + 4H^+ + 4e^- \rightarrow 2H_2O \quad (4)$$

From these equations the equivalent circuit shown in figure 14 can be derived and the parameters can be obtained from the redox reactions that occur in both electrodes.

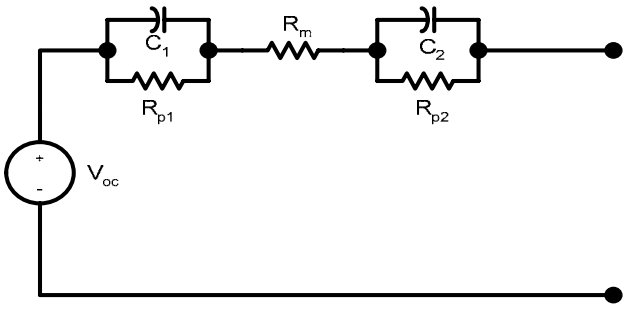

Figure 14 Equivalent circuit for a PEM fuel cell

This equivalent circuit consists of the resistance of the membrane R_m, which is related to the electrolyte resistance. Also the model contains two parallel resistor and capacitors R_{p1}-C_1 and R_{p2}-C_2 are the time constants of each electrode and are related to the electron transport phenomena in the anode and cathode. Specifically resistances R_{p1} and R_{p2} model the charge transfer at the anode and cathode of the fuel cell, on the other hand capacitances C_1 and C_2 model the capacitive effect that arises due the electrode/ electrolyte interface at the anode and cathode respectively. These parameters can be

calculated in terms of the fuel cell chemical parameters, but this information is rarely available for the power electronics designer.

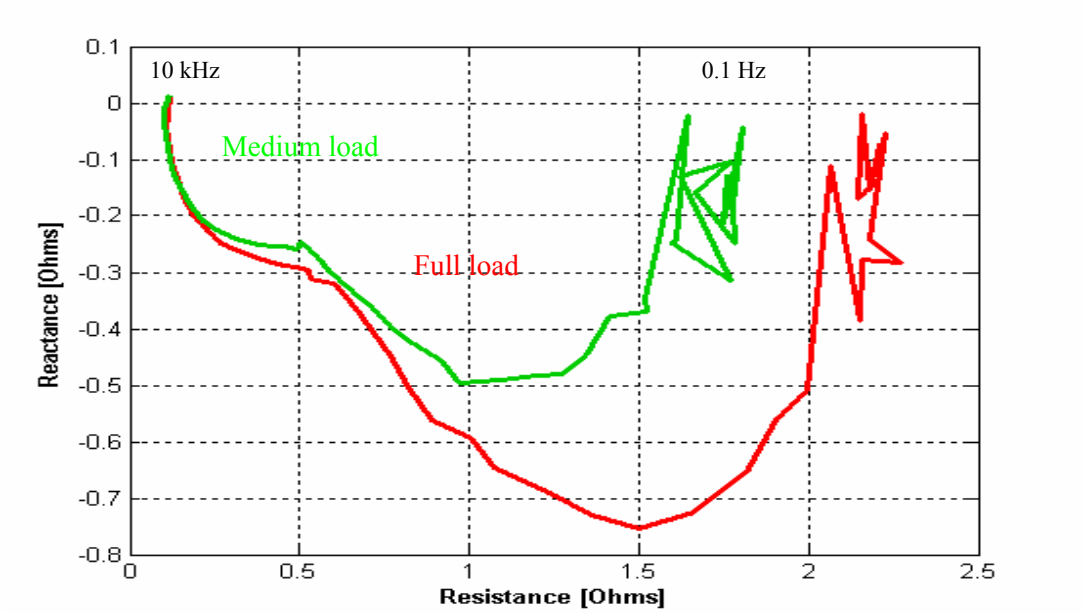

Figure 15 Nyquist plot for a 30W fuel cell stack

A straightforward method of obtaining these parameters is by means of frequency spectroscopy, i.e. using a frequency response analyzer. Figure 15 shows a Nyquist plot obtained from a 20W proton exchange membrane fuel cell for different load conditions obtained experimentally by using this method. This figure shows the resistance and reactance of the fuel cell stack for two different load conditions and for frequencies ranging from 0.1 Hz to 10 kHz. From this plot it is simple to identify the main elements of the equivalent circuit model. Also from this result it is possible to synthesize the parameters of the circuit model if the chemical data is not known. Each semi circle in the

graph corresponds to one R-C time constant, where the diameter of each semi-circle corresponds to its resistive value and the vertex corresponds to its characteristic frequency. The value of the membrane resistance can be obtained from the graph at the point were the reactance becomes zero. The equivalent circuit parameters of the fuel cell whose response is shown in figure 15 are listed in Table II.

Table II
Equivalent circuit parameters

Load Condition	R_m [mΩ]	R_{p1} [mΩ]	C_1 [mF]	R_{p2} [mΩ]	C_2 [mF]
Medium Load	80.74	440	1.70	1042	18.81
Full Load	80.74	496	1.55	1508	18.12

2.3. Effect of continuous and discontinuous conduction of the DC-DC converter on fuel cell performance

An important point when designing the DC-DC converter is to know how much current ripple can be injected into the fuel cell without degrading its performance. From the converter point of view at light loads it may be more efficient to operate in discontinuous conduction mode. Also designing a converter with higher input current ripple may lead to smaller inductor sizes and reduced converter size. To obtain an answer to this question two approaches are possible to evaluate the performance, the use of the equivalent circuit model and experimental measurements. Although the analysis of the equivalent circuit is simple it only gives information on the additional losses

produced by the switching current, which can be related indirectly to temperature rise and hydrogen consumption. However if more detailed information on these performance indexes is required, direct measurements are needed. The parameters that need to be measured include: hydrogen flow rate which is proportional to the average power being produced by the fuel cell and the temperature rise. Both these parameters have to be measured for various discontinues conduction modes of the dc-dc converter keeping the average output current of the stack constant.

2.3.1. Equivalent circuit analysis

From the equivalent circuit shown in figure 14 it is possible to derive an expression for the impedance of the fuel cell in terms of the load current frequency.

$$Z_{fc} = \left[\frac{R_1}{w^2 C_1^2 \left(R_1^2 + \frac{1}{w^2 C_1^2} \right)} + R_m + \frac{R_2}{w^2 C_2^2 \left(R_2^2 + \frac{1}{w^2 C_2^2} \right)} \right] - I \left[\frac{R_1^2}{wC_1 \left(R_1^2 + \frac{1}{w^2 C_1^2} \right)} + \frac{R_2^2}{wC_2 \left(R_2^2 + \frac{1}{w^2 C_2^2} \right)} \right] \quad (5)$$

The additional internal losses in the fuel cell produced by the switching frequency current can then be calculated using (6)

$$P_{loss,hf} = \Re(Z_{fc}(w_{sw}))I_{sw,rms}^2 \quad (6)$$

where w_{sw} is the angular frequency of the ripple current and $I_{sx,rms}$ is the rms value of the switching current.

It can be seen that from (5) that as the switching frequency increases the real part of the fuel cell impedance is reduced to the membrane resistance R_m. Thus the additional internal losses produced by the switching frequency also decrease as the switching frequency increases.

Equation (6) can be expressed in per unit form by:

$$P_{loss,hf} = \frac{R_m}{R_1 + R_m + R_2}\left(\frac{I_{sw,rms}}{I_{DC}}\right)^2 \qquad (7)$$

Figure 16 shows a typical current wave form from a pulsating current source at a switching frequency of 50 kHz. The average value of the current is 1.6A which is the nominal load current of the 20 W PEM fuel cell stack from Table II.

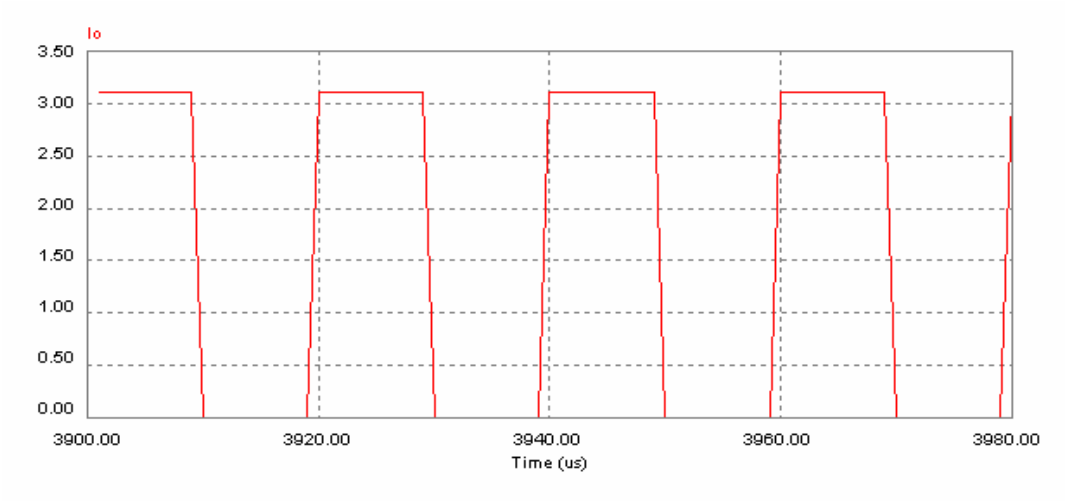

Figure 16 Input current for boost converter operating in critical conduction

Evaluating (7) for this fuel cell the plot shown in figure 17 is obtained. It can be seen from figure 17 that for ripple currents of low frequency, i.e. less than 1 kHz the power available at the terminals of the fuel cell is reduced by more than 10%. Also for frequencies above 10 kHz the reduction in the available output power is in the range of 4%.

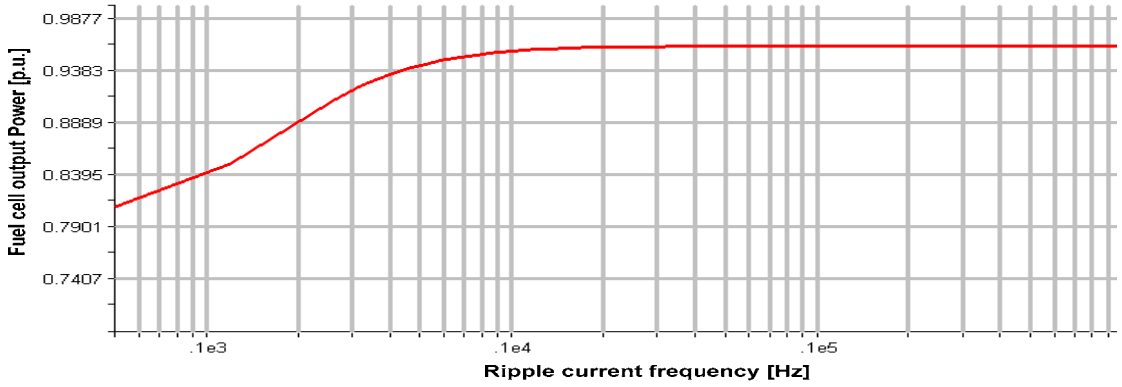

Figure 17 Fuel cell output power calculate from the equivalent circuit

2.3.2. Experimental measurements for 20W FC

To further evaluate the effects of high frequency ripple currents in the performance of the fuel cell experimental measurements on a 20W stack were made. The measurements consisted on loading the fuel cell stack with a square wave load current with a 50% duty cycle, as shown in figure 18. The peak value of the load current was set to two times the nominal current of the fuel cell stack so that its mean value coincided with its nominal current. Then the frequency of the load current was varied from 10 Hz to 200 kHz, and the hydrogen consumption and output power of the stack were recorded. This test was performed for two different fuel cells in order to contrast the results.

Figure 19, shows the hydrogen consumption and output power as function of the load current frequency as measured from a 20W PEM fuel cell. It can be observed from figure 19a that the hydrogen being consumed in the fuel cell increases due to the presence of the ripple current. The magnitude of the increase in the hydrogen consumption is a function of the frequency of the ripple current.

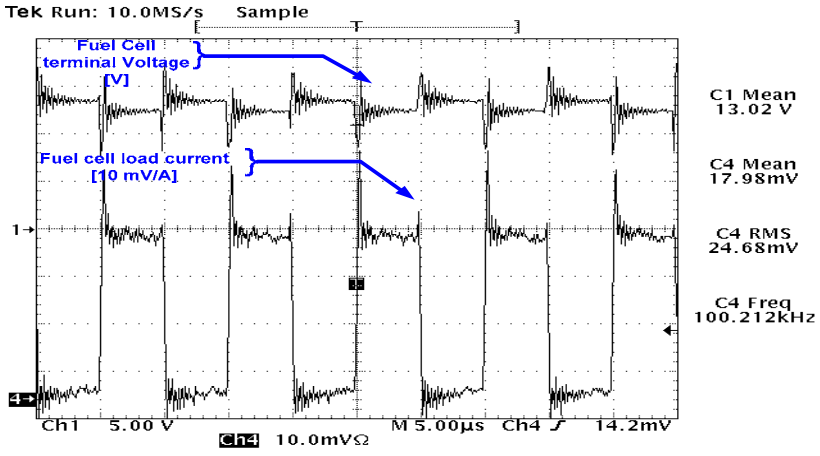

Figure 18 Test current waveform

Also from figure 19a it can be seen that for frequencies below 1 kHz the fuel cell consumes more than 4% extra hydrogen. In the same manner for frequencies between 10 kHz and 100 kHz the fuel cell consumes about 3% additional hydrogen. Figure 19b shows the output power of the fuel cell for the tested frequency range. It can be observed that the fuel cell delivers up to 20% less power for low frequency ripple currents, and as frequency increases it approaches its nominal. For load currents in the range of 10 kHz to 100 kHz the output power of the fuel cell decreases by 5%. Comparing the result obtained from the experimental measurements (figure 19b) with the analytical expression obtained from the equivalent circuit (figure 17) one can see that there are some minor differences due to the non linear behavior of the fuel cell. However if the non-linearities are discarded there is close agreement between the analytical and experimental results.

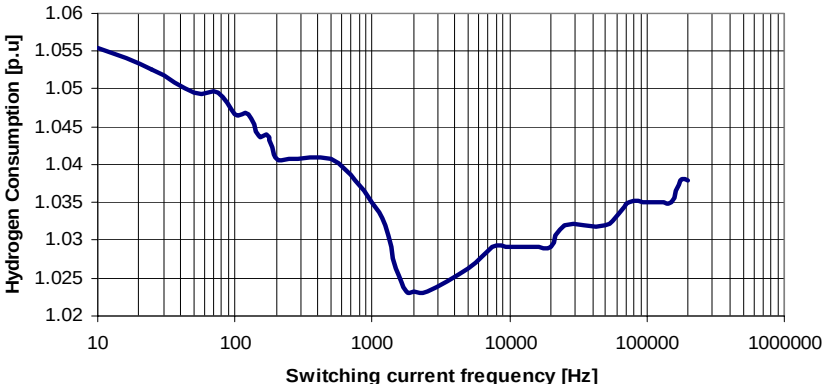

a)

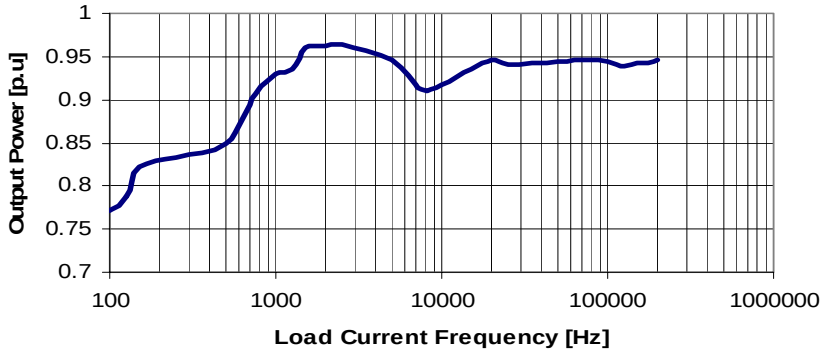

b)

Figure 19 Hydrogen and output power for the 20W fuel cell as function of load current ripple frequency

Figure 20 shows the result of the thermal analysis for the 20W fuel cell stack working with dc (figure 20a) and load current wit a 20kHz switching component (figure 20b). As can be observed from the figure in this case there is a temperature rise of 0.5 deg. C when the fuel cell operates with high frequency load current due to the increased internal losses.

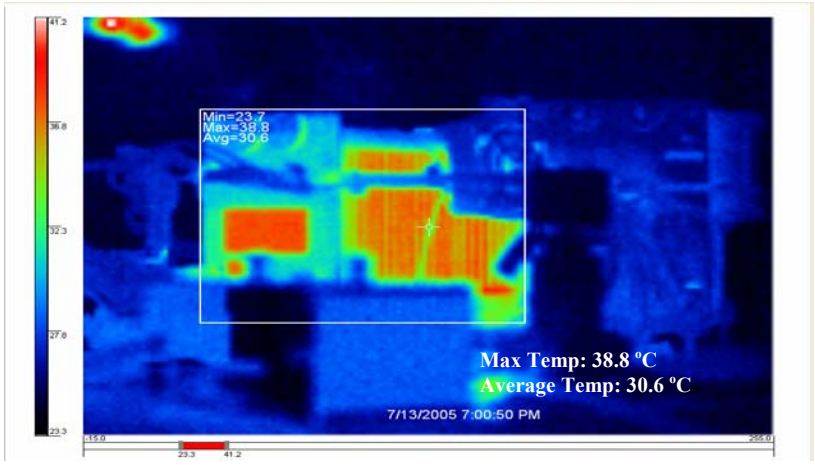

a)

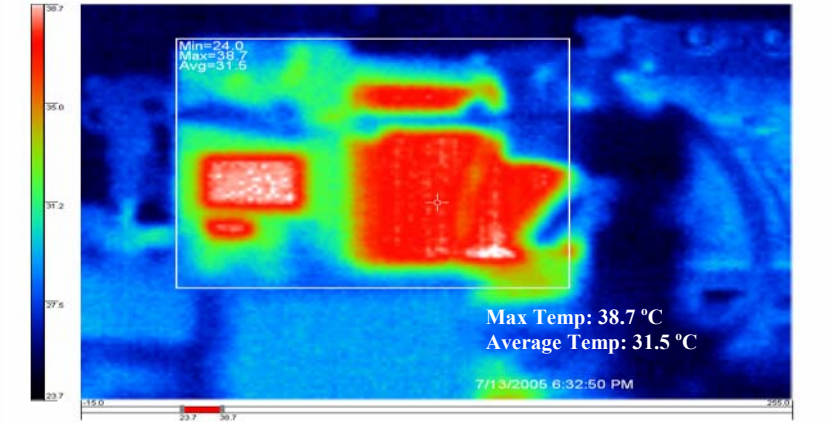

b)

Figure 20 Thermal analysis of the 20W fuel cell stack

From these experimental results it can be concluded that the presence of high frequency ripple currents (10 kHz – 200 kHz) does not impact negatively the performance of the fuel cell stack. This is especially convenient in the case of connecting a DC-DC converter at the terminals of the fuel cell. In this case the current being drawn from the fuel cell has a ripple current at the converter switching frequency. Since this frequency is normally high (above 30 kHz) the additional hydrogen consumed by the fuel cell and heat produced by it is not significant.

2.3.3. Experimental measurements for 30W FC

In order to contrast the results obtained in sections 2.3.1 and 2.3.2 the experiment was repeated in a 30W PEM fuel cell. Figure 21a shows the per unit increment in hydrogen consumption of the fuel cell stack as function of the ripple current frequency when the average output current of the stack is kept constant. From the figure it can be seen that the fuel cell consumes up to a 7% more hydrogen when the current being supplied has a current ripple below 1 kHz. For frequencies in the range of 10 to 200 kHz the hydrogen consumption varies as function of the frequency but as an average the fuel cell consumes 1% more hydrogen than when the load current is purely DC. Figure 21b shows the per unit output power of the fuel cell when the average value of the load current is kept constant and the frequency of the ripple is varied. From the result shown in figure 21b it can be seen that the power delivered to the load is lower at low frequencies. The fuel cell delivers up to 30% less power when the current ripple has a frequency in the range of 10-1000 Hz. As the frequency of the current ripple increases the output power of the fuel cell approaches its DC characteristic, and for frequencies above 10 kHz due the internal power loss the fuel cell can deliver 5% less power.

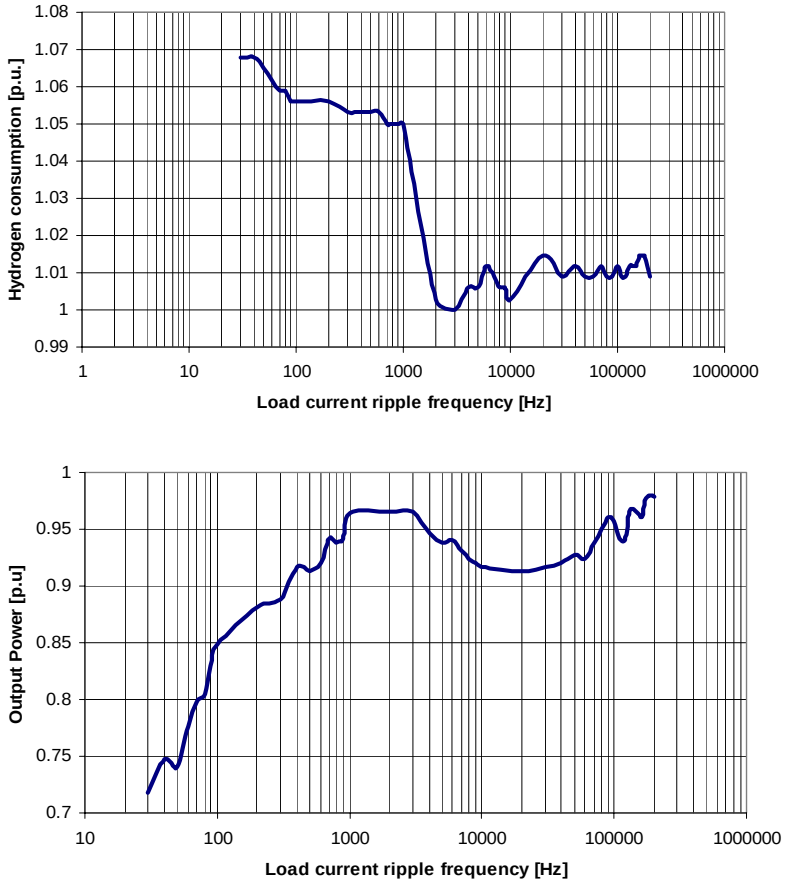

Figure 21 Hydrogen and output power of the 30 W fuel cell as function

Thermal analysis of the fuel cell stack working under DC load and high frequency current ripple (20 kHz) is shown in figure 22. The output power in both cases is the nominal power of the stack that is 30W. As can be observed from this figure the effect of operating under 20 kHz translates into a rise of 0.4 deg C. in the average stack temperature.

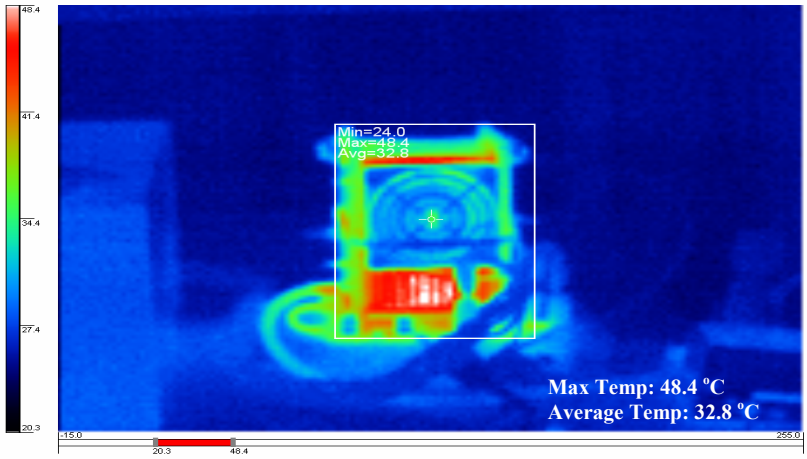

a) DC current 5. A,(Vo = 6.18, Po = 30.93, φ = 0.378 l/min)

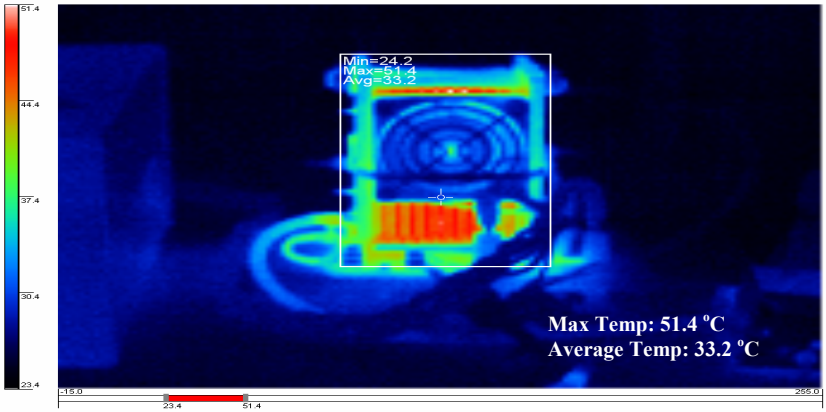

b)20 kHz pulsating current load of 6.36 Arms,(Vo = 6.12, Po = 30.70, φ = 0.391 l/min)

Figure 22 Thermal analysis of the 30W fuel cell stack

2.3.4 Effect of current duty cycle

In the case of discontinuous conduction mode it is also interesting to evaluate the effect of the duty cycle of the current on the stack performance. For this the duty cycle of a fixed frequency (1 kHz) current vas varied along with its peak value in order to maintain the output power of the fuel cell constant. Figure 23 shows the resulting hydrogen consumption.

It can be observed from this figure that for currents with duty cycles between 40 to 80% the amount of hydrogen being consumed by the stack is above its nominal value by less than 5%. For duty cycles below 40 % the amount of hydrogen being consumed increases as the duty cycle is reduced. This is due to the magnitude of the current for these duty cycles. In the case of a 10% duty cycle the peak current is 10 times the nominal fuel cell current.

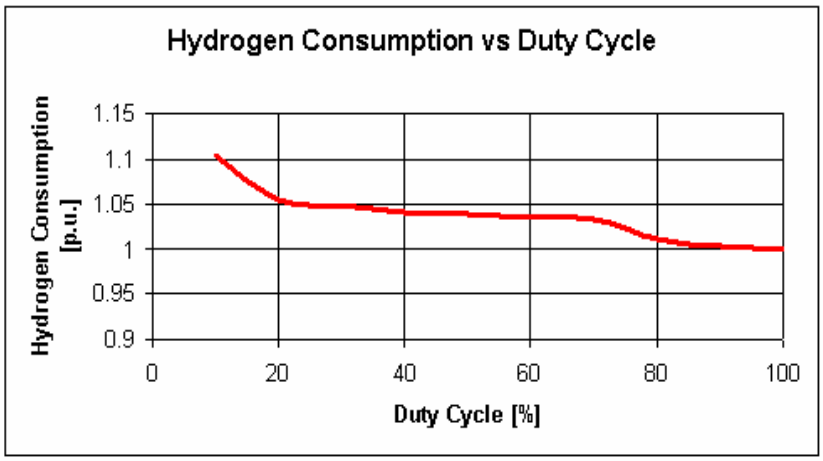

Figure 23 Hydrogen consumption as function of duty cycle

2.4. Conclusions

In this chapter the electrical equivalent circuit for PEM fuel cells has been discussed. And in addition a method for experimentally obtaining the parameters in the equivalent circuit was presented. The effect of discontinuous conduction on the performance of the fuel cell stack has been studied. It has been shown that when the load current of the fuel cell is not purely DC the hydrogen consumption increases and the output power of the fuel cell decreases. The magnitude of this effect is a function of the frequency of the

ripple current. Also it has been shown both analytically and experimentally that for load currents with a low frequency ripple (below 1 kHz) the hydrogen consumption increases up to 7% while the output power of the fuel cell decreases up to 30%. On the other hand if the frequency of the ripple current is high, above 20 kHz, the hydrogen being consumed by the fuel cell increases in the range from 1% to 3%, while its output power decreases by 5%. Also it was shown that the thermal performance of the fuel cell is not severely affected by the presence of high frequency ripple currents (i.e. due to discontinuous mode of operation).

CHAPTER III

DC-DC CONVERTER STABILITY ANALYSIS IN FUEL CELL POWERED PORTABLE ELECTRONIC SYSTEMS

3.1. Introduction

Fuel cells can be considered as a soft voltage source [19-21], this due to the load dependent nature of its output voltage. A typical fuel cell stack output voltage experiences a 2 to 1 variation from no load to full load. Also, since each cell in a fuel cell stack has a low output voltage (0.6V to 0.7V at full load), it is necessary to stack many in series to obtain a reasonable output voltage. Due to their low output voltage, coupled with no-load to full-load variation of the fuel cell terminal voltage, a DC-DC boost converter becomes necessary (figure. 24). On the other hand fuel cells have a complex internal impedance which can influence the dynamic characteristics of the power converter controller [22- 25].

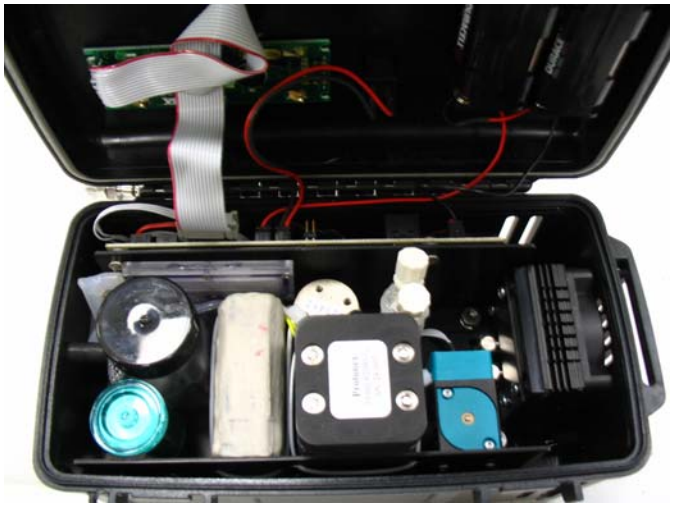

a) An example 30W portable fuel cell system

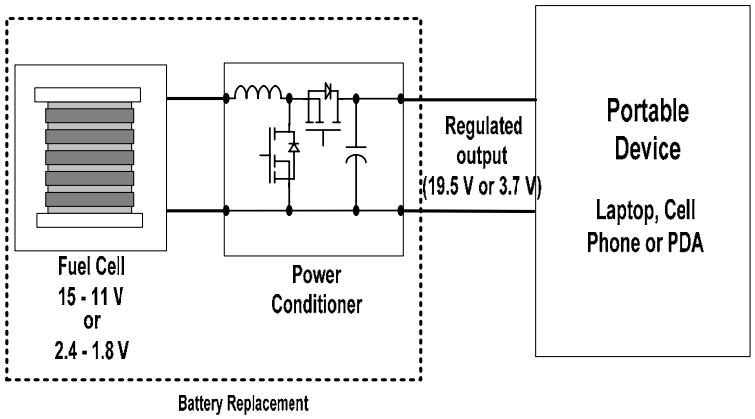

b) Fuel cell powered portable electronic system

Figure 24 Portable fuel cell system

Interaction between the internal impedance of the fuel cell may also lead to instabilities and oscillations in the controller operation. Moreover for low power applications dead ended fuel cells are used. In this type of fuel cells a valve is opened at regular intervals to purge the products of the chemical reaction. This transient disturbance may also affect the operation of the system.

The purpose of this chapter is to explore these problems by means of analytical tools and to obtain design guidelines to minimize the effect of the fuel cell internal characteristics in the performance of the power conversion unit.

3.2. Stability analysis

In most practical applications, due to the low voltage of the fuel cell, the use of a boost type DC-DC converter is required. The interaction of the two systems has to be analyzed in order to ensure proper dynamic response as well as stability of the overall system. Normally the design of power supplies is carried out assuming that the impedance of the source is small enough to not interfere with the operation and dynamic performance of the converter. But the use of a fuel cell as the power source, which has complex internal impedance, alters the control characteristic of the DC-DC converter. Another point to be analyzed is the behavior of the system during the purging of the fuel cell. During the purge interval the voltage produced by the stack is reduced, which in turn reduces the power that the fuel cell can deliver.

3.2.1 Steady state stability

From the fuel cell terminals point of view any DC-DC converter operating in closed loop can be considered as a constant power load. This is because regardless of the voltage being produced by the fuel cell stack the output voltage of the DC-DC converter is maintained at a constant voltage. In particular for the case of a boost converter, if there are variations in the voltage produced by the fuel cell stack the converter increases or

reduces its input current in order to maintain its output voltage constant. In general for a fuel cell powered DC-DC converter system to be stable in steady state the V-I characteristic of the fuel cell and the constant power locus of the DC-DC converter have to intersect at one point, this sets the operating condition of the system. If the two curves do not intersect the source is not able to meet the power demanded by the load. Figure 25 shows the V-I characteristic (Normal V-I) of the 30 W fuel cell whose parameters where obtained in Chapter II. This figure also shows the constant power locus of a 30W boost converter for full and half load. As can be observed from Figure 25 the constant power locus intersects the V-I of the fuel cell, and therefore the power requirements of the load are met.

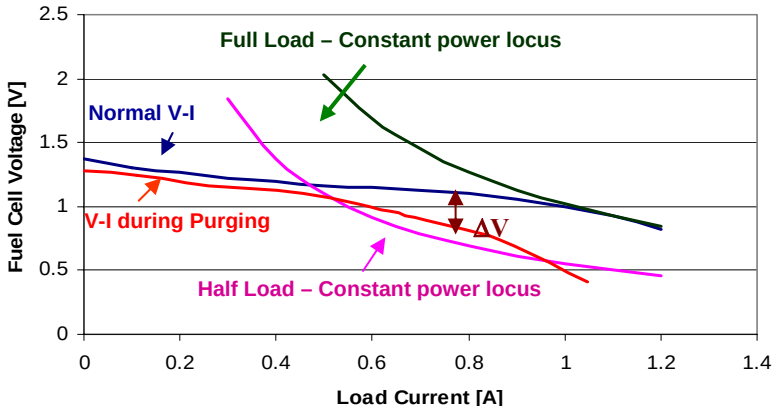

Figure 25 Fuel cell V-I characteristic and load constant power locus

For low power applications, 150W and below, dead ended PEM fuel cells are normally used. In this particular kind of fuel cell hydrogen enters the stack at the anode,

and there is a solenoid valve located at the cathode which opens at regular intervals to release the products of the chemical reaction. The opening of the valve is referred to as purging. During the purging interval the voltage produced by the fuel cell drops due to the reduction in internal pressure. The magnitude of this voltage drop is a characteristic of the fuel cell, and it is a function of the load current, fuel cell parameters, and the duration of the purging period. Figure 26 shows the voltage profile of the 30W stack during a purge.

It can be seen that for this particular fuel cell the duration of the purging interval is 2.5 seconds and the voltage drops by 2.24V for a load current of 1.73 A. Figure 25 shows the V-I characteristic measured for the 30W fuel cell during the purge interval. As can be observed from Figure 25 during the purge the fuel cell voltage drops by a quantity ΔV. In order to maintain the output power constant the DC-DC converter will require a higher current, which will produce an additional voltage drop at the fuel cell terminals. This in turn will produce and additional increase in the converter current. In other words a positive feedback takes place, which finally results in instability.

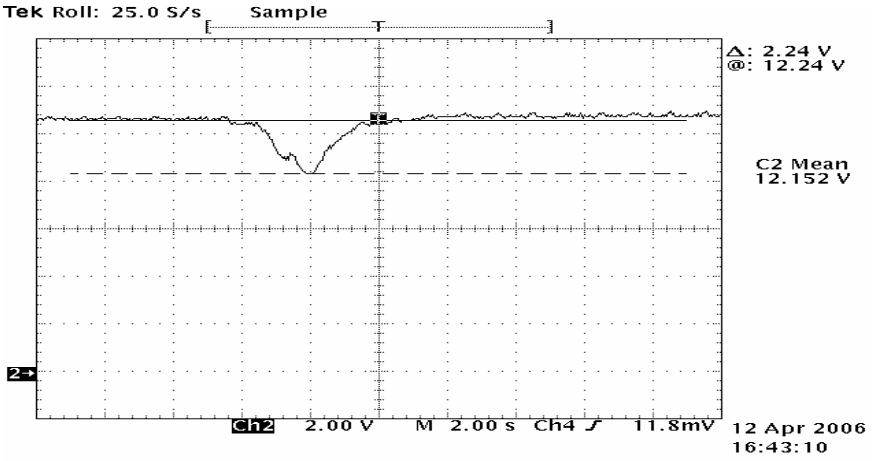

Figure 26 Fuel cell voltage during the purging interval for a 30W stack supplying 1.73A

To avoid this problem two approaches can be taken. One of them is to control the boost converter in order to limit its output load during the purging interval. But this approach has the disadvantage of derating the total output power of the system. An alternative approach it to supply the power difference produced during the purge by using a supercapacitor. The size of the capacitor is calculated in terms of the energy that the capacitor has to supply during the duration of the purge, and can be calculated by:

$$C = \frac{2\Delta P_o t_p}{\Delta V^2} \qquad (8)$$

where ΔP_o is the difference between the power that the fuel cell can supply during the purge and the power required by the load, t_p is the duration of the purge and ΔV is the voltage drop in the capacitor. In the case of the 30W fuel cell under study the duration of the purge is 2.5 seconds, and the voltage drops to 0.75 p.u at full load. In this case the

supercapacitor needs to supply 25% of the output load during 2.5 seconds. If a maximum voltage drop of 2 V is allowed during the purge from (8) the required capacitance is 10F.

3.2.2 Transient stability

Due to the characteristics of the internal impedance of the fuel cell the dynamics of the DC-DC converter are affected. The controller of power converter normally is designed to provide appropriate amount of phase and magnitude margins in order to meet the stability criteria. But once the fuel cell is connected to the input terminals of the power converter as shown in figure 27 the output impedance of the fuel cell comes into play.

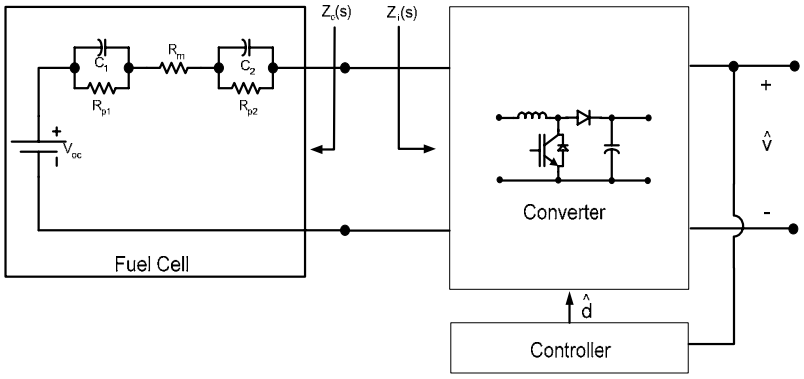

Figure 27 Fuel cell DC-DC converter system

If the internal impedance of the fuel cell is considered, Middlebrook's extra element theorem [9] can be used to analyze the effect of the fuel cell into the dynamics of the

converter. Applying the theorem the system shown in figure 28 results, where the fuel cell output impedance is modeled as an extra element in the system.

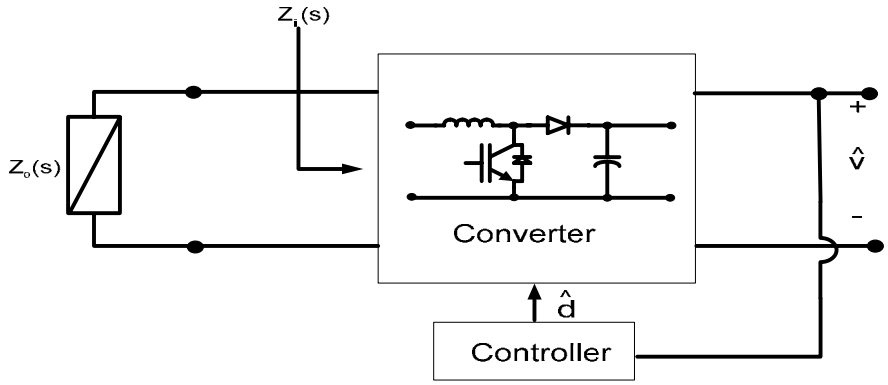

Figure 28 Modeling of the fuel cell impedance effect

It can be found that the control to output transfer function of the converter when the fuel cell is considered is given by (9)

$$G_{vd}(s) = \left(G_{vd}(s)\big|_{Z_o=0}\right)\frac{1+\dfrac{Z_o(s)}{Z_N(s)}}{1+\dfrac{Z_o(s)}{Z_D(s)}} \qquad (9)$$

Where $G_{vd}(s)\big|_{Z_o=0}$ is the converter transfer function when the supply is an ideal voltage source, $Z_N(s)$ is the input impedance of the converter under the condition that the feedback controller operates ideally, $Z_D(s)$ is the input impedance of the converter under the assumption that $\hat{d}(s)=0$, and $Z_o(s)$ is the output impedance of the fuel cell. From analyzing equation (9) it becomes apparent that the transfer function of the converter is

modified by the output impedance of the fuel cell. Moreover it can be shown that by connecting the fuel cell to the DC-DC converter all the transfer functions are modified including the control to output, the line to output and the converter output impedance. In order to minimize the effect in the dynamics of the converter it has been shown [9] that the following impedance inequalities have to be met.

$$\|Z_o\| << \|Z_N\| \qquad (10)$$

$$\|Z_o\| << \|Z_D\| \qquad (11)$$

Similarly the converter output impedance of the converter is not affected if

$$\|Z_o\| << \|Z_e\| \qquad (12)$$

$$\|Z_o\| << \|Z_D\| \qquad (13)$$

where Z_e is the converter input impedance when its output is shorted. A typical fuel cell power converter system is shown in figure 24. Due to the low output voltage of the fuel cell the converter of choice for this kind of applications is a boost converter. The small signal model for a boost converter is shown in figure 29a. If the fuel cell equivalent circuit model is added to the circuit the small signal equivalent shown in figure 29b is obtained. From figure 29a the input impedances of the system $Z_N(s)$ and $Z_D(s)$ are given by:

$$Z_N(s) = -D'^2 R\left(1 - \frac{sL_b}{D'^2 R}\right) \qquad (14)$$

$$Z_D(s) = D'^2 R \frac{\left(1 + s\frac{L_b}{D'^2 R} + s^2 \frac{L_b C_b}{D'^2}\right)}{(1 + sRC)} \qquad (15)$$

where D is the converter duty cycle L_b and C_b are the inductor and capacitor of the converter and R its load resistance.

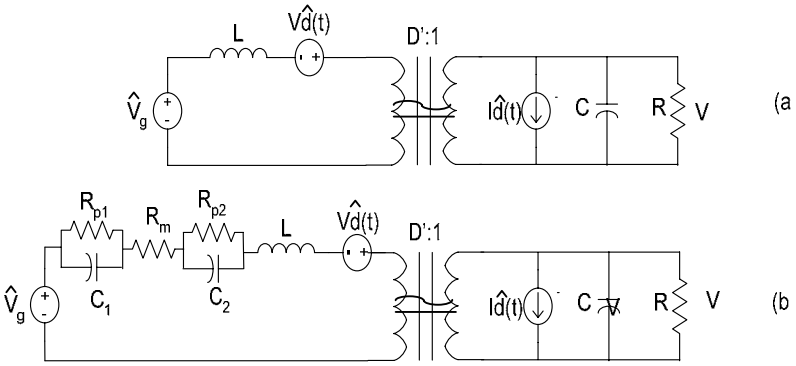

Figure 29 Small-signal models for boost converter. b) When connected to a fuel cell

From the fuel cell equivalent circuit discussed in Chapter II its output impedance is given by (16).

$$Z_o = \frac{s^2(R_m R_{p1} R_{p2} C_1 C_2) + s(R_m(R_{p1}C_1 + R_{p2}C_2) + R_{p1}R_{p2}(C_1 + C_2)) + R_m + R_{p1} + R_{p2}}{s^2(R_{p1}R_{p2}C_1C_2) + s(R_{p1}C_1 + R_{p2}C_2) + 1} \quad (16)$$

By plotting the magnitudes of the converter input impedances and fuel cell output impedance (14-16) for the fuel cell parameters shown in Table II and for a 30W boost converter designed to operate in continuous conduction with a 250μH inductance and 250μF output capacitance the graph of figure 30 is obtained.

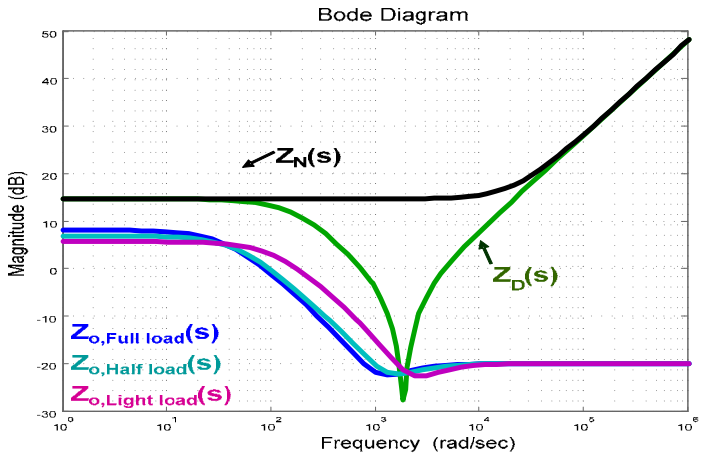

Figure 30 Impedances for fuel cell boost converter system

It can be observed from figure 30 that the magnitudes of the converter input impedance and the fuel cell output impedance are of comparable magnitudes. From (9) in order to minimize the effect of the fuel cell in the dynamics of the system the impedance inequalities (10)-(11) have to be met. Normally the "much greater than" condition (<<) can be considered to be true if there exist at least 6dB of difference between the magnitude of the converter and fuel cell impedances. As can be seen from figure 30 the inequalities may not be satisfied for low frequencies and at the resonant frequency of the boost inductor and output capacitor. Therefore it is important to verify the stability of the system as part of the system design. At low frequencies the inequalities (10)-(11) are met as long as the DC-DC converter input power is less or equal to the rated power of the fuel cell. On the other hand to meet the design criteria at the resonant frequency of the input impedance of the boost converter either the converter or the fuel cell impedances have to be modified. A method of modifying the output impedance of the fuel cell is by connecting a supercapacitor in parallel. The effect of the

parallel capacitor is displacing the output impedance of the fuel cell to the left as shown in figure 31, thus increasing the distance between the output impedance of the fuel cell and the input impedance of the boost converter. This in turn helps satisfying the impedance inequalities. The modified output impedance of the fuel cell-supercapacitor system can be calculated by:

$$Z_o = \frac{s^3(R_m R_{y1} C_1 R_{y2} C_2) + s^2(R_m(R_{y1}C_1 + R_{y2}C_2)}{s^3(R_m C_{sc} R_{y1} C_1 R_{y2} C_2) + s^2(C_{sc}(R_m(R_{y1}C_1 + R_{y2}C_2) + R_{y1}R_{y2}(C1+C2)) + R_{y1}C_1 R_{y2}C_2)} \ldots\ldots$$
$$\ldots\ldots \frac{+ R_{y1}R_{y2}(C1+C2)) + R_{y1} + R_{y2} + R_m}{+ s(C_{sc}(R_{y1} + R_{y2} + R_m) + R_{y1}C_1 + R_{y2}C_2) + 1} \quad (17)$$

where C_{sc} is the capacitance of the supercapacitor.

Figure 31 shows the fuel cell output impedance (17) and DC-DC input impedance frequency responses for different super capacitor values (100mF and 1F). As can be observed from this figure the capacitance needed to modify the output impedance of the fuel cell in order to satisfy (10)-(13) is relatively small. And in general the amount of capacitance calculated to compensate for the voltage drop during the purging period is sufficient to ensure that the impedance inequalities are met.

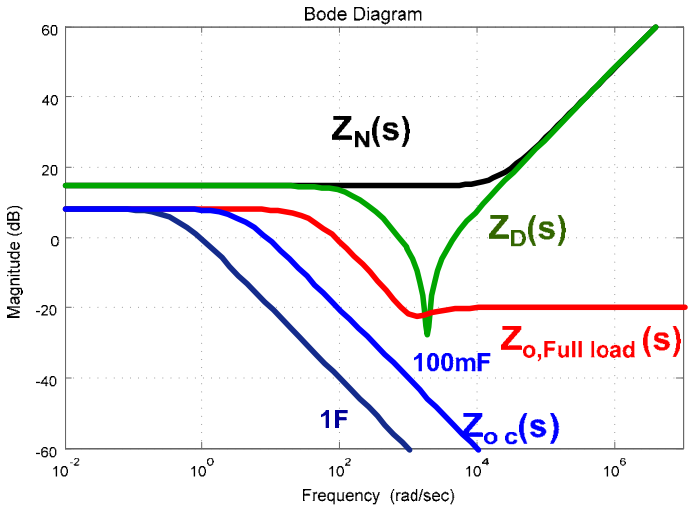

Figure 31 Effect of adding a supercapacitor in parallel with the fuel cell

3.3. Experimental results

In order to verify the theoretical analysis experimental measurements were made. For this a 30W fuel cell and boost converter were used. The output voltage of the fuel cell varies from 16V for no load to 10V for full load as shown in figure 25. The internal parameters of the fuel cell are shown in Table II. The boost converter is designed to maintain a 19.5 V output voltage and it is rated for 30W, which is suitable to supply a laptop computer. Figure 32 shows the transient response of the boost converter for a load change from zero to full load when supplied by a source which follows the steady state V-I characteristic of the fuel cell (figure 25). It can be seen from this figure that the output voltage presents no oscillations due to the change in the input supply (16-12V) and load (no load to full load).

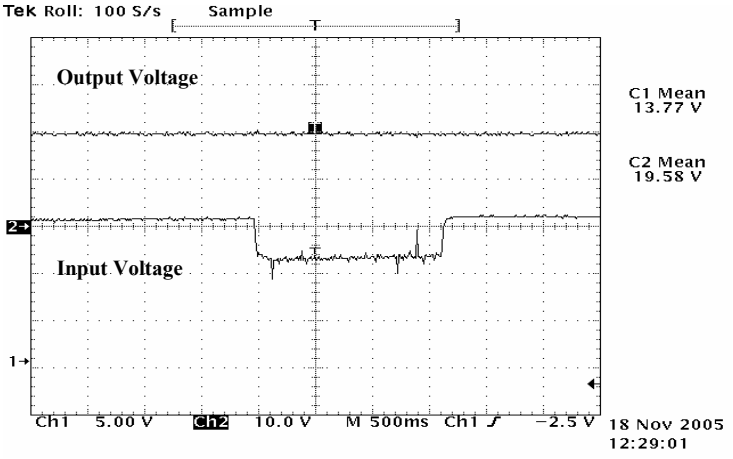

Figure 32 Converter supplied from power supply

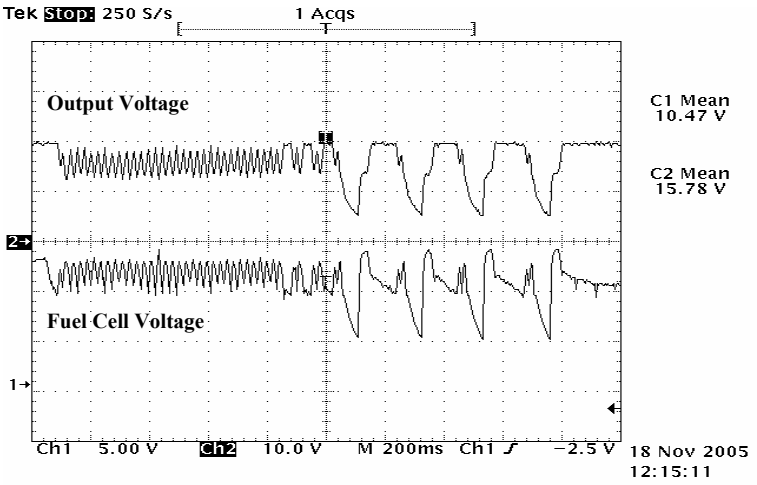

Figure 33 Converter supplied from fuel cell

Figure 33 shows the response of the system for the same load step when the fuel cell is used as input supply; as can be seen in this case both input and output voltage oscillate widely until the load is removed.

Figure 34 shows the response of the system once a 10F supercapacitor is connected across the terminals of the fuel cell.

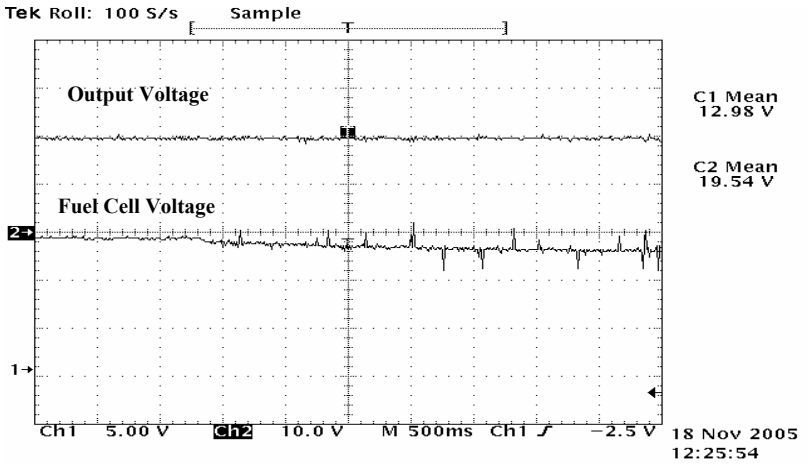

Figure 34 Converter supplied from fuel cell and super capacitor

It can be observed that in this case there is no oscillation in either input or output voltage. Also the input voltage decreases slowly until the new steady state is reached.

3.4. Conclusions

In this chapter stability analysis of fuel cell powered DC-DC converters for portable applications has been discussed. It has been shown that fuel cell internal impedance can significantly affect the dynamics of the DC-DC converter. Also the behavior of the fuel

cell during purging has been discussed. The reduced power available during purging has been shown to be another possible cause for instability. To overcome these problems the use of supercapacitors connected in parallel with the fuel cell has been proposed. An approach to calculate the value of the supercapacitor to achieve stability has been derived. Experimental results from a 30W fuel cell-boost converter system demonstrate the validity of the proposed analysis. Finally, stability and good dynamic behavior has been shown to be possible with the use of supercapacitors connected to the output of the fuel cell.

CHAPTER IV

NEW TRANSFORMER-LESS DC-DC CONVERTERS FOR FUEL CELL APPLICATIONS

4.1. Introduction

As more countries ratify the Kyoto protocol aiming to reduce the emission of greenhouse gases produced by combustion of fossil fuels, along with rampaging high oil prices and concerns regarding the safety and disposal of by-products of nuclear generation has created the need of clean power generation systems. This presents a unique opportunity for the development and implementation of distributed generation.

Distributed generation normally uses environmentally friendly energy sources such as fuel cells, solar panels and micro hydroelectric plants to produce electric power. Among these fuel cells have been considered as the primary energy source for the next generation distributed power generation, since they are highly efficient, modular and clean; however, as a drawback the DC voltage generated by a fuel cell stack varies widely, normally from 2 in per unit to 1 in per unit. Further the voltage produced by fuel cells is low in magnitude and therefore for applications where the output power is in the kilowatt range input voltages and currents can easily have the same order of magnitude. Thus they present challenging characteristics for the design of the power conditioning system required to interface the fuel cell to the utility grid or ac loads common in

residential applications. By the fore mentioned reason a step-up DC-DC conversion stage is essential to generate an adequate input voltage for the DC-AC inverter stage (200V typically for a 120 V AC output). Normally the DC-DC converters used to accomplish this task take advantage of a high frequency transformer to provide the voltage gain required. But the use of transformer based DC-DC converter has some disadvantages such as increased size and cost.

Recently transformer-less converters have been proposed to reduce the size and cost of the power conversion units in applications where no electrical isolation is required [4, 5, 26]. But they lack of an adequate voltage gain, and sometimes require a dual input voltage.

In this chapter a new DC-DC converter topology is proposed to step up the fuel cell voltage and provide a stable dc-link for the DC-AC inverter. The proposed DC-DC power conversion unit consists of a hybrid connection of two two-level DC-DC converters. This produces an independently controllable dual voltage output. As it will be shown the use of the proposed topology along with a DC-AC inverter eliminates the need for a transformer to provide the required voltage gain. As a result, proposed topology has the following advantages:

- Operates from a single input voltage
- No transformer is required to achieve a voltage gain of 5 in per unit
- If a single phase inverter is connected at its output the system can generate $120V_{AC}$ output from a $40V_{DC}$ input source without the use of a transformer.

4.2. Proposed converter

The proposed high gain converter is constructed by connecting DC-DC converter modules in a series-parallel connection. This is the inputs of the modules are connected in parallel to the input supply and their output are connected in series as shown in figure 35.

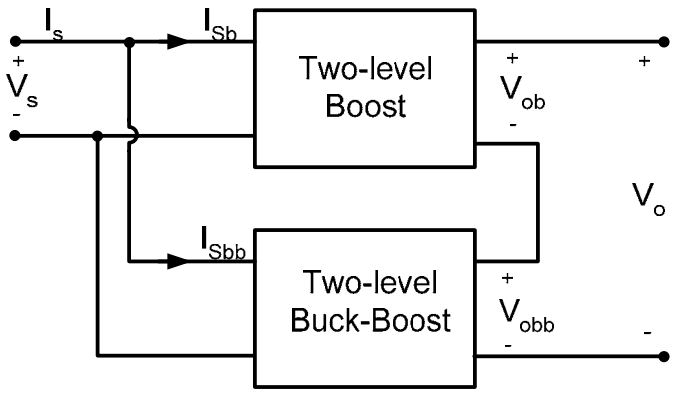

Figure 35 Block diagram if the proposed converter

Since the modules used to construct the converter do not have isolation between input and output, it becomes necessary for one of the modules to produce a negative output voltage. In the case of conventional DC-DC converters this converter can be constructed by using a boost converter for module 1 and a buck-boost converter for module 2. This approach is shown in figure 36.

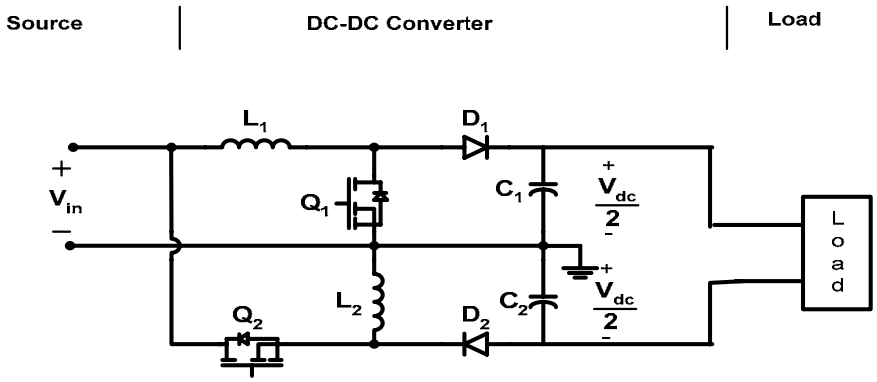

Figure 36 Circuit schematic of proposed converter

The operation of the DC-DC converter can be broken down into two stages as shown in figure 37. The two elemental converters that compose the proposed DC-DC converter are a boost converter which charges the capacitor C_1 and a buck-boost converter charging capacitor C_2. These two converters are operated in an interleaved fashion in order to reduce the input current ripple.

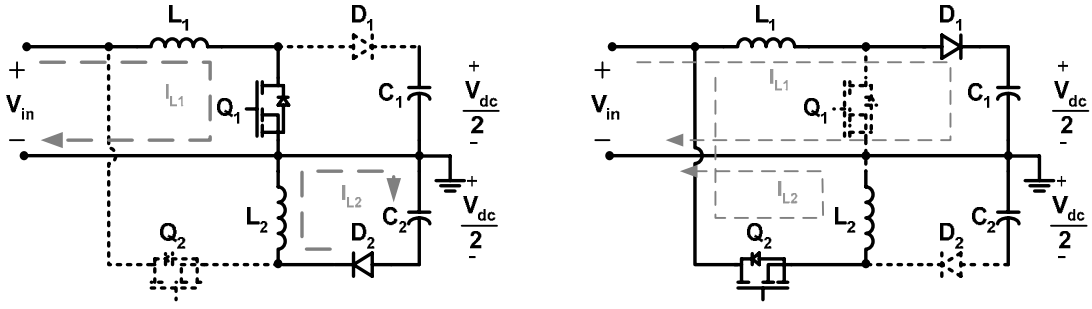

Figure 37 DC-DC converter operation stages

During the first period of operation (figure 37a) the switch Q_2 is open and Q_1 is closed thus charging inductor L1. This state has duration T_1 given by:

$$T_1 = D_1 T_S \tag{18}$$

where Ts is the switching period of the converter and D_1 is the duty cycle produced by the converter controller in order to follow the voltage reference. Also during this time period the energy stored in inductor L_2 during the previous state is delivered to the capacitor C_2 charging it.

In a similar fashion during the state shown in figure 37b the switch Q_1 is opened allowing the energy stored in the inductor L_1 to charge capacitor C_1. While switch Q_2 is closed charging inductor L_2. This state is maintained for a time T2 given by:

$$T_2 = D_2 T_S \tag{19}$$

where Ts is the switching period of the converter and D_2 is the duty cycle produced by the converter controller. Since the voltage gain characteristics of the boost and buck-boost converters are different the duty cycles D_1 and D_2 will be different, i.e. $T_1<T_2$. In fact in order to get a voltage gain of 2 the buck-boost converter is required to operate with a duty cycle D_2 around 0.65, thus there will be certain overlapping between the states shown in figures 38a and 38b. This is not a problem since the two converters can operate in a decoupled fashion. However since the maximum voltage gain of each of the modules is limited to 2 p.u.; the maximum voltage gain that the converter can achieve is 4 p.u. To achieve a higher voltage gain a different type of converter needs to be used for each of the modules. A better approach is to use two level DC-DC converters as shown in figure 38a. It uses as building blocks a two-level boost converter [27] and a two-level buck-boost converter. As can be seen from figure 38b, the inputs of the converters are

connected in parallel and their outputs are in series, thus combining the voltage gains of each converter. The overall voltage gain of 5 per unit can be realized. The operation of the DC/DC converter can be explained by analyzing the two converters separately and then combining their input/output relationships.

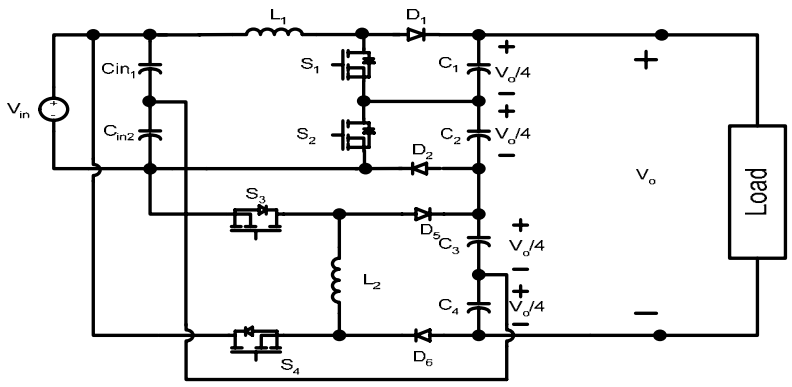

a) Proposed high-gain dc-dc converter for fuel cell power systems

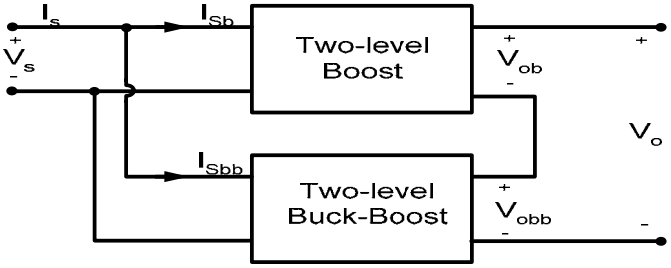

b) Connection block diagram
Figure 38 Proposed high gain converter

4.2.1 Two-level boost DC-DC converter

The operation of the two-level boost converter (figure 39) is detailed in [27] for single phase power factor correction applications. And its operation states are repeated here for completion. These states are distributed along the switching period and the

duration of each state is determined by the duty cycle D. During one switching period the following switching state sequence is applied. If the voltage drop across diodes D_1 and D_2 is neglected to simplify the analysis, the equations describing the different states are:

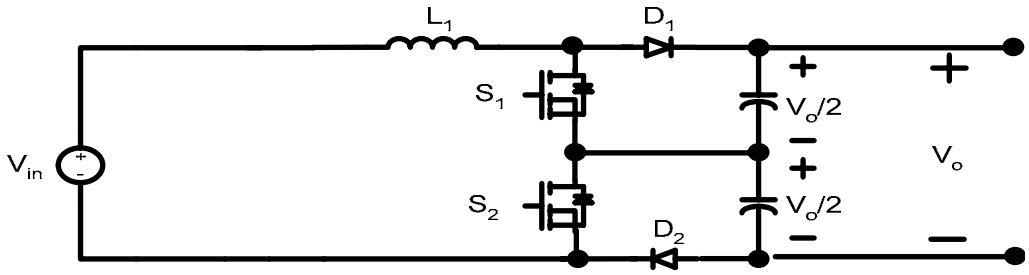

Figure 39 Two-level boost converter

1. Inductor charging state 1

Switches S_1 and S_2 are closed to charge inductor L_1. During this switching state diodes D_1-D_2 are reverse biased, as shown in figure 3a. During this stage the inductor voltage is $V_L = V_s - 2R_{DS}I_L - R_L I_L$. The capacitor currents for this converter state are $i_{C1} = i_{C2} = -I_o$.

2. Energy transfer to capacitor C_1 state

Switch S_1 is opened and switch S_2 remains closed. Diode D_1 conducts and diode D_2 remains reverse biased as shown in figure 40b. During this stage the energy stored in the inductor is delivered to the capacitor C_1 charging it. The inductor voltage in this case

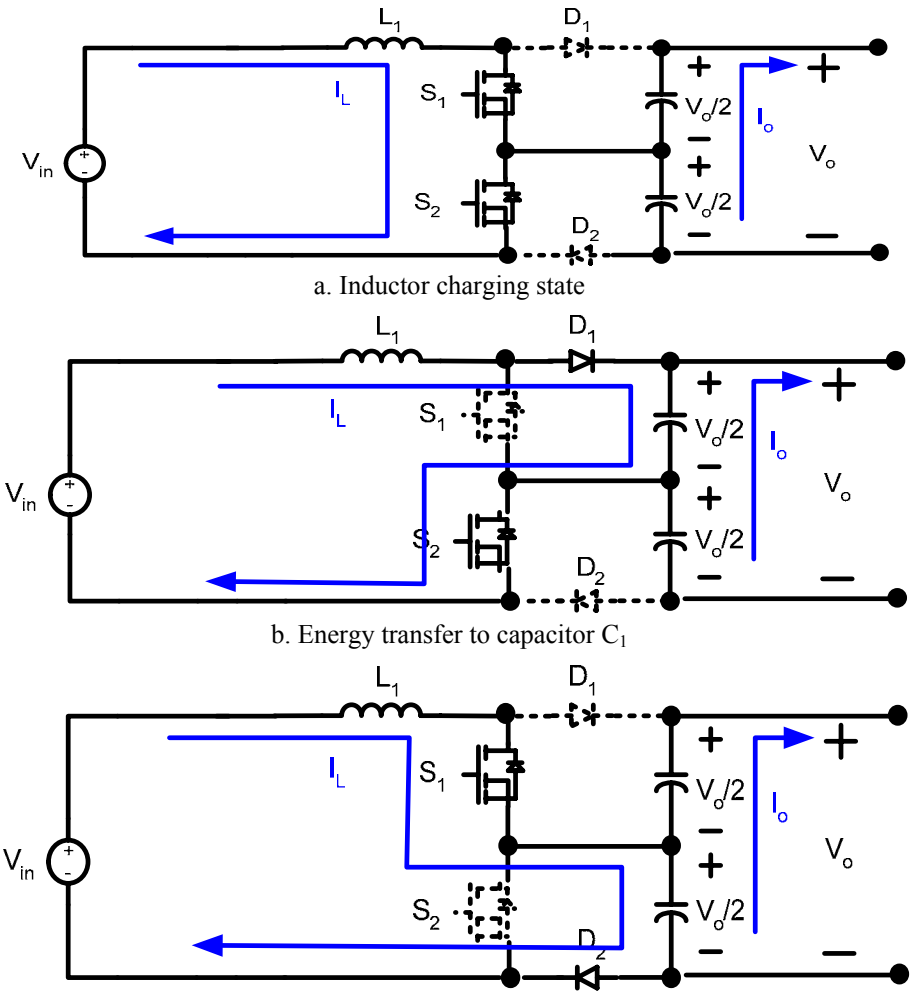

a. Inductor charging state

b. Energy transfer to capacitor C_1

c. Energy transfer to capacitor C_2

Figure 40 Two level boost operation modes

is $V_L = V_S - \frac{Vo}{2} - R_L I_L - R_{DS} I_L$. For this converter state the capacitor currents are given by $i_{C1} = I_L - I_o$, and $i_{C2} = -I_o$

3. Inductor charge state 2

Again switches S_1 and S_2 are closed to charge the inductor L_1, and diode D_1-D_2 are reverse biased, as shown in figure 40a. During this stage the inductor voltage is $V_L = V_s - 2R_{DS} I_L - R_L I_L$. The capacitor currents for this converter state are $i_{C1} = i_{C2} = -I_o$.

4. Energy transfer to capacitor C_2 state

Switch S_2 is opened and switch S_1 remains closed. Diode D_2 conducts and diode D_1 remains reversed biased as shown in figure 40c. During this stage the energy stored in the inductor is delivered to the capacitor C_2, and the voltage across the inductor is given by $V_L = V_s - \frac{Vo}{2} - R_L I_L - R_{DS} I_L$. For this converter state the capacitor currents are given by $i_{C1} = -I_o$, and $i_{C2} = I_L - I_o$.

The duration of each converter state can be obtained from figure 41. In steady state the switching pattern used for the converter operation is shown in the figure 41. From this figure and assuming that the inductor was charged during the previous switching cycle, state 2 is applied for a time given by $t_{S1} = \frac{(1 - D)Ts}{4}$. Then the inductor is

charged during a time t_c given by $t_c = \frac{DTs}{2}$. Once the inductor is charged state 4 is applied to the converter for a time $t_{S2} = \frac{(1-D)Ts}{2}$. After this the inductor is charged again for a time period $t_c = \frac{DTs}{2}$. Once we finished charging the inductor, circuit will again enter the state 2 for a time $t_{S1} = \frac{(1-D)Ts}{4}$, to complete the one period cycle.

To obtain the voltage gain characteristic of the converter the inductor volt-second balance over one switching period is calculated. From that calculation the voltage gain characteristic of the converter is obtained to be:

$$V_o = V_s \frac{2}{(1-D)} \frac{1}{1+\frac{4(Rds\,(1+D)+RL)}{(1-D)^2 R}} \qquad (20)$$

From this analysis the inductor and input currents are calculated and are given by:

$$I_L = I_o \frac{2}{(1-D)} \qquad (21)$$

$$I_S = I_L \qquad (22)$$

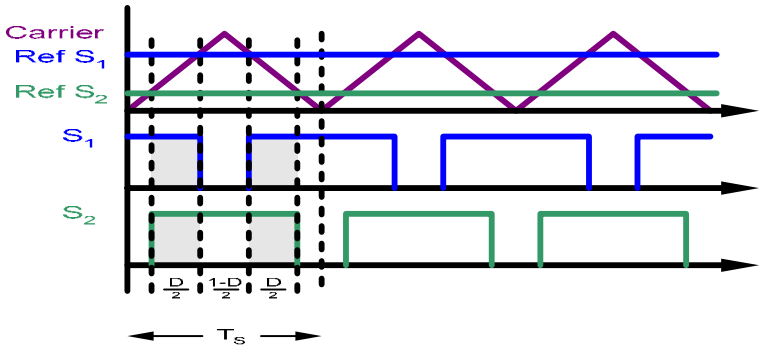

Figure 41. Switching pattern

Also from the analysis of the different switching states of the converter we can obtain the average equivalent circuit of the two level boost converter. Figure 42 shows the complete equivalent circuit including the losses in the inductor, MOSFET and diodes.

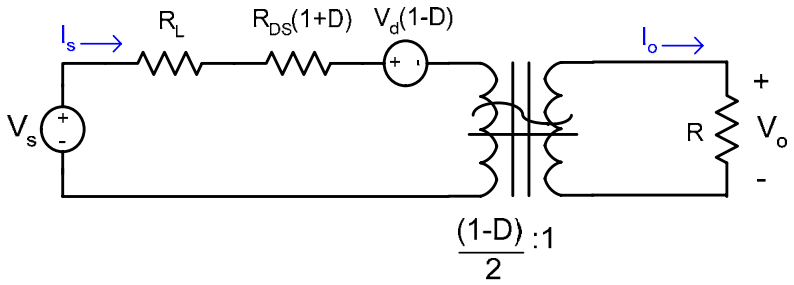

Figure 42. Average equivalent circuit

4.2.2. Two-level buck-boost DC-DC converter

The operation of the two-level buck-boost converter (figure 43) can be explained in the same manner as was done with the two-level boost converter. If we neglect the voltage drop in the diodes the equations for the switching states of the converter for one switching period are obtained as follows:

1. Inductor charge state1

Switches S_1 and S_2 are closed to charge inductor L. Diodes D_1-D_2 are reverse biased, as shown in figure 43a. During this stage the inductor voltage is $V_L = V_s - 2R_{DS}I_L - R_L I_L$. The capacitor currents for this converter state are $i_{C1} = i_{C2} = -I_o$.

2. Energy transfer to capacitor C_1 state

Switch S_1 is opened and switch S_2 remains closed. Diode D_1 conducts and diode D_2 remains reverse biased as shown in figure 43b. During this stage the energy stored in the inductor is delivered to the capacitor C_1 by charging it to a voltage $V_{C1} = V_L + \frac{Vs}{2} - R_L I_L - R_{DS} I_L$. For this converter state the capacitor currents are given by $i_{C1} = I_L - I_o$ and $i_{C2} = -I_o$.

3. Inductor charge state 2

Again switches S_1 and S_2 are closed to charge the inductor L and diode D_1-D_2 are reverse biased, as shown in figure 43a. During this stage the inductor voltage is $V_L = V_s - 2R_{DS}I_L - R_L I_L$. The capacitor currents for this converter state are $i_{C1} = i_{C2} = -I_o$.

4. Energy transfer to capacitor C_2 state

Switch S_2 is opened and switch S_1 remains closed. Diode D_2 conducts and diode D_1 remains reversed biased as shown in figure 43c. During this stage the energy stored in the inductor is delivered to the capacitor C_2 charging it to a voltage $V_{C1} = V_L + \frac{Vs}{2} - R_L I_L - R_{DS} I_L$. For this converter state the capacitor currents are given by $i_{C1} = -I_o$, and $i_{C2} = I_L - I_o$.

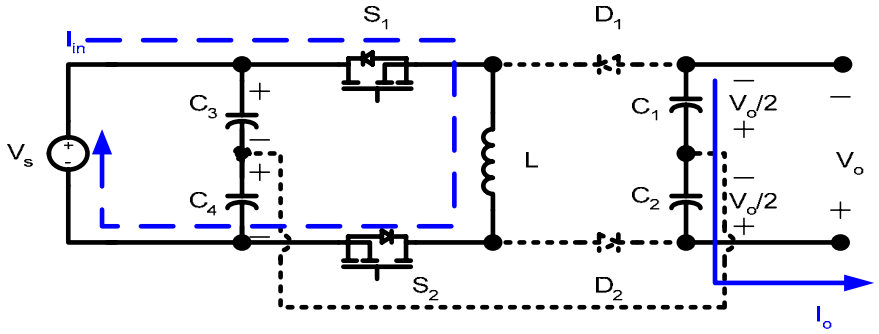

a. Inductor charging state

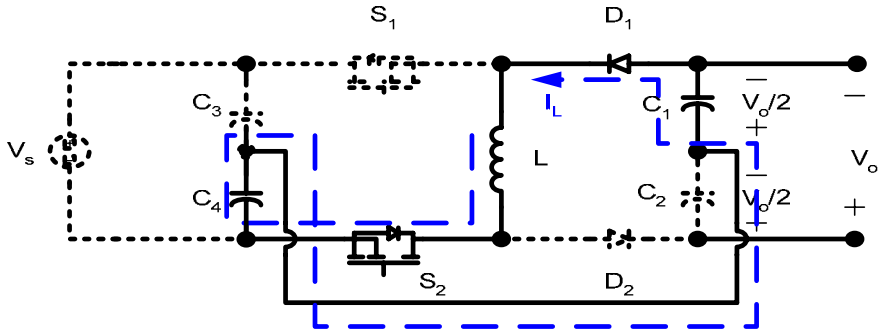

b. Energy transfer to capacitor C_1

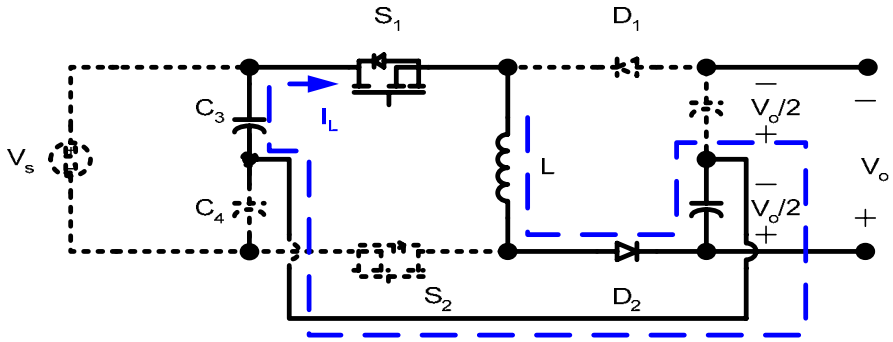

c. Energy transfer to capacitor C_2

Figure 43 Two level buck boost

The duration of each converter state can also be obtained using the method shown in figure 41. From this figure and assuming that the inductor is charged from the previous switching cycle state 2 is applied for a time given by $t_{S1} = \frac{(1-D)Ts}{4}$. Then the inductor is charged during the time t_c given by $t_c = \frac{DTs}{2}$. Once the inductor is charged, state 4 is applied to the converter for a time $t_{S2} = \frac{(1-D)Ts}{2}$. After this the inductor is charged again for a time period $t_c = \frac{DTs}{2}$. Once we finished charging the inductor, circuit will again enter the state 2 for a time $t_{S1} = \frac{(1-D)Ts}{4}$, to complete the one period cycle.

To obtain the voltage gain characteristic of the converter the inductor volt-second balance over one switching period is calculated. From that calculation the voltage gain characteristic of the converter is:

$$V_o = V_s \frac{(1+D)}{(1-D)} \frac{1}{1+\frac{4(Rds\ (1+D)+RL)}{(1-D)^2 R}} \quad (23)$$

Using the same analysis the inductor and input currents are calculated and are given by:

$$I_L = I_o \frac{2}{(1-D)} \quad (24)$$

$$I_S = I_o \frac{(1+D)}{(1-D)} \quad (25)$$

In a similar fashion as in the case of the two level boost converter, we obtain the average equivalent circuit of the two level buck-boost converter from the switching state

analysis. Figure 44 shows the resulting equivalent circuit which incorporates the losses due to the inductor, switches and diodes.

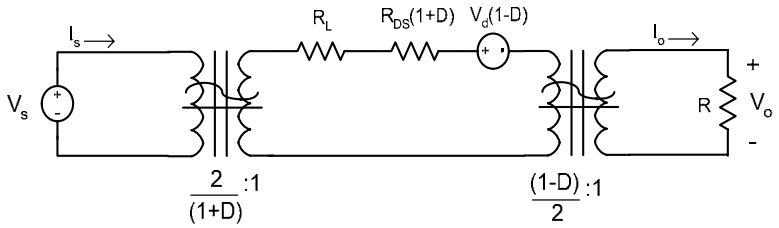

Figure 44 Average equivalent circuit

4.2.3. Proposed four level DC-DC converter

As discussed in the previous sections, the proposed converter shown in figure 38 is realized by combining the two-level boost and buck-boost converters to obtain a higher voltage gain. The boost and buck-boost converters have their input terminals connected in parallel and their output terminals connected in series as shown in figure 38b. To obtain the total voltage gain and efficiency of the four level converter the output voltage and input currents of the individual converters are properly combined. From Figure 38b the output voltage of the four-level converter can be calculated by adding the output voltages of the two-level boost (20) and the two-level buck-boost converters (23).

$$V_o = V_{o,boost} + V_{o,buck-boost}$$

$$= V_s \left[\frac{2}{(1-D_1)} \frac{1}{1+\frac{4(Rds(1+D_1)+RL)}{(1-D_1)^2 R}} + \frac{(1+D_2)}{(1-D_2)} \frac{1}{1+\frac{4(Rds(1+D_2)+RL)}{(1-D_2)^2 R}} \right] \quad (26)$$

In the same manner the input current of the four-level converter is obtained by adding the input currents of the individual converters (22) and (25). The resulting expression is then given by:

$$I_{S,4-level} = I_o\left[\frac{2}{(1-D_1)} + \frac{(1+D_2)}{(1-D_2)}\right] \qquad (27)$$

The efficiency of the four-level converter when inductors and semiconductor losses are included can be obtained by using the average equivalent circuits of figures 42 and 44. Using this method the efficiency of the converter is the given by:

$$\eta = \frac{P_o}{P_{in}} = \frac{V_o\,(Vs, D_1, D_2)\,I_o}{V_S\,I_S\,(I_o, D_1, D_2)} = \frac{1}{\dfrac{2}{(1-D_1)} + \dfrac{(1+D_2)}{(1-D_1)}}\left(\begin{array}{l}\dfrac{2}{(1-D_1)}\dfrac{1}{1+\dfrac{4(R_{DS}\,(D_1+1)+R_L)}{(1-D_1)^2 R}} + \\ \dfrac{D_2+1}{1-D_2}\dfrac{1}{1+\dfrac{4(R_{DS}\,(D_2+1)+R_L+Vd\,(1-D_2))}{(1-D_2)^2 R}}\end{array}\right) \qquad (28)$$

where D_1 and D_2 are the two-level boost and two-level buck-boost duty cycles respectively. Plotting (7) and (9) for different inductor resistance versus load resistance ratios (R_L/R) the graphs shown in figure 45 are obtained. It can be observed from figure 45 that although in theory this converter allows to get a voltage gain of 8 p.u; a practical implementation of the converter considering losses in the inductor and semiconductors can produce a maximum voltage gain of 6 p.u if the converter efficiency is to be kept above 80%.

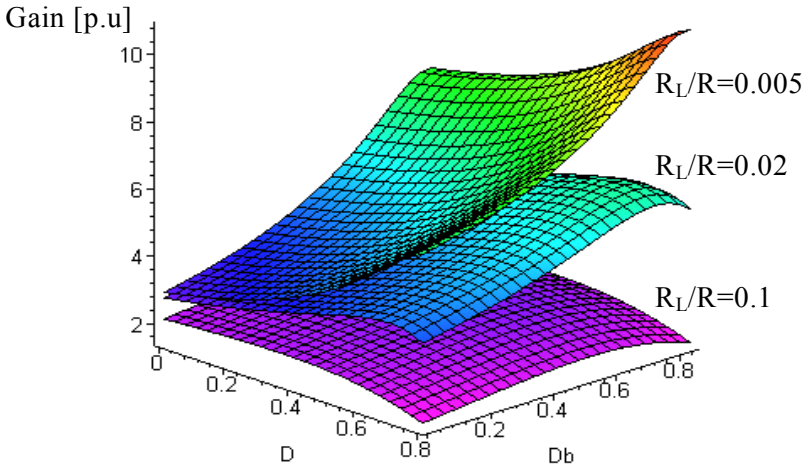

a. voltage gain

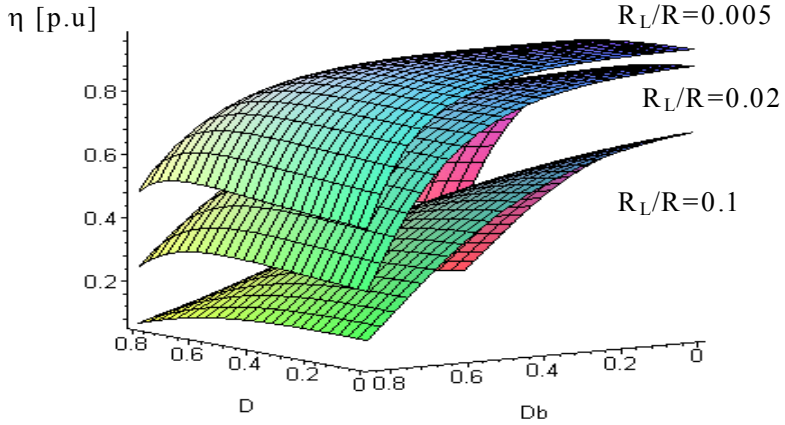

b. estimated efficiency

Figure 45 Converter voltage gain and efficiency

4.3. Design example

A design example of a 45Vdc to 200 Vdc, 1 kW DC-DC converter is outlined in this section. To generate 200 V_{dc} at the converter output the total voltage gain required is 5, so it is needed that each stage supplies a voltage gain of 2.25p.u. By using equation (1), and considering that the switch on resistance as 80 mΩ and inductor resistance as 0.5 Ω, we obtain that the boost converter has to be operated with a duty cycle D_1 = 0.32.

Similarly by using equation (4) we obtain that the duty cycle of the buck-boost converter to be $D_2 = 0.54$. To calculate the value of the inductor for the two level boost converter equation (29) is derived from figures 39 and 41.

$$L = \frac{R(1-D)D}{8 f_s} \tag{29}$$

Designing the converter to operate in continuous conduction in a load range from 10% to 100% at a switching frequency of 50 kHz we obtain that a 218 μH inductor is needed. In the case of the inductor for the two level buck-boost converter from figures 4 and 6 we can obtain an equation (30).

$$L = \frac{R(1-D)D}{4(1+D) f_s} \tag{30}$$

From (30) and designing for the same switching frequency and load range as the boost converter we obtain that the inductor required has a value of 248 μH. For the design of the values of capacitors C1 – C4 equation (31) can be used.

$$C = \frac{V_o D}{4R\Delta V f_s} \tag{31}$$

For an output voltage ripple of less than 1% we obtain that the capacitor values are 100 μF. The current and voltage for the switches in the two level boost converter can be obtained from (19) and the output voltage of the boost stage. Thus switch current is 7.35 A, and the switch voltage stress of the boost stage is 250 V. In the case of the switches for the two level buck-boost converter the switch current can be calculated from (24) and

it results to be 10.6 A. The switch voltage stress is two times the output voltage of the buck-boost stage, i.e. 250 V.

4.4. Experimental results

A laboratory prototype of the proposed converter was built to verify the analysis and simulations. The converter was implemented using four IRFPS40N60K MOSFETs and four DSEI 12-20 diodes. The inductors were designed and wound on toroidal iron powder cores and their value was measured to be 250 µH with a series resistance of 0.5 Ohms.

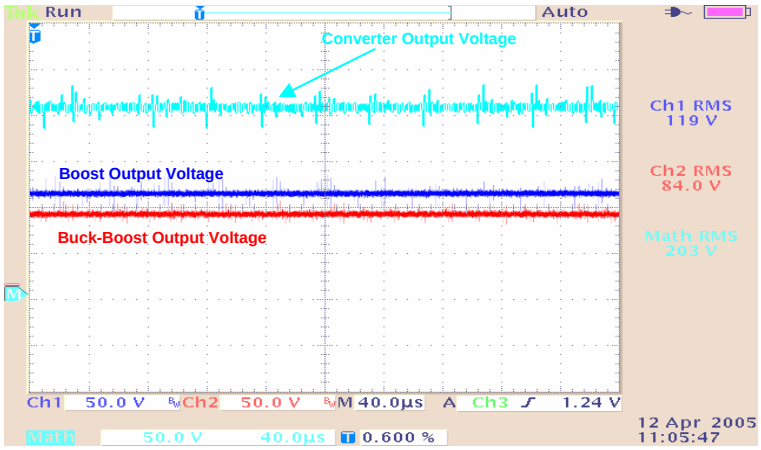

Figure 46 Converter output voltage

Figure 46 shows experimental waveforms for the converter operating from a 45 V_{dc} input source. The output voltage of the converter is measured to be 204 V and the output power is 0.5 kW. In figure 46 the top traces correspond to the voltage across the output capacitors of each converter block, i.e. C_1/C_2 and C_3/C_4. As can be observed from the figure the output voltage of the boost stage is 110 V and the voltage of the buck-boost stage is 94 V. This confirms that each converter block is providing a voltage gain of 2.44 p.u. and 2.09 p.u. respectively. The voltage gains of the converters are set at different values in order to maintain the inductor rms current in each converter at a similar level. This in turn has the effect of splitting the losses evenly between the two stages. The traces in figure 47 show the inductor current waveforms measured at the output of the current sensors. The scaling factor of the sensors is 2.84 A/V. As can be seen from the figure the currents in the two inductors are kept at the same value, 7.24 A in this case. The total input current of the converter is measured to be 14.6 A.

Figure 48 shows the voltage across switches S1 and S3. As can be observed from this figure the voltage stress of the switches is 2.5 times the output voltage of the converter.

Figure 49 shows the converter efficiency measured from the prototype for different output loads. As can be seen from the figure the efficiency of the converter is above 75 % for light loads and as the load increases it improves to values above 80%.

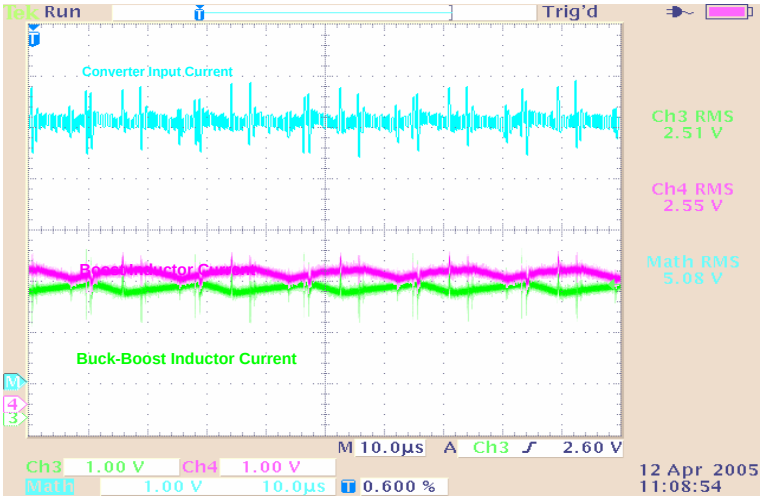

Figure 47 Converter inductor currents and input current

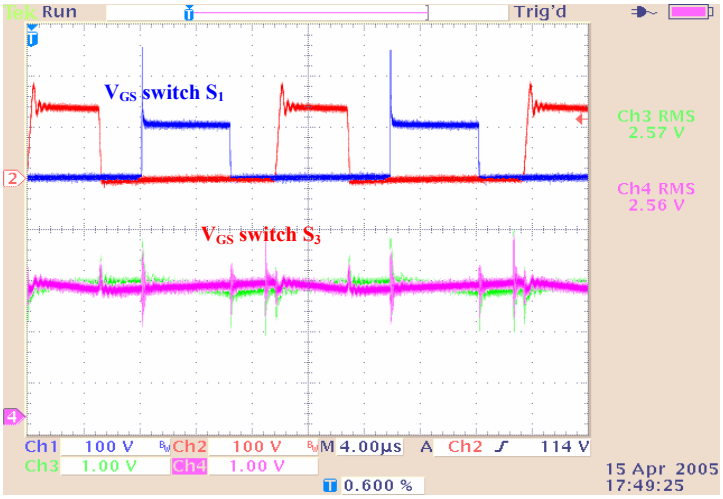

Figure 48 Switch voltage stress

4.5. Converter efficiency improvement

As shown in figure 49 the efficiency measured from the prototype converter is in the range of 80%. For higher efficiency the inductor losses need to be reduced by optimizing the design of the magnetic core and by limiting the resistive losses of the magnetic wire. Further improvement in efficiency can be obtained by replacing diodes $D_1 – D_4$ by using MOSFET synchronous rectifiers. Figure 50 shows the converter topology a for higher efficiency design.

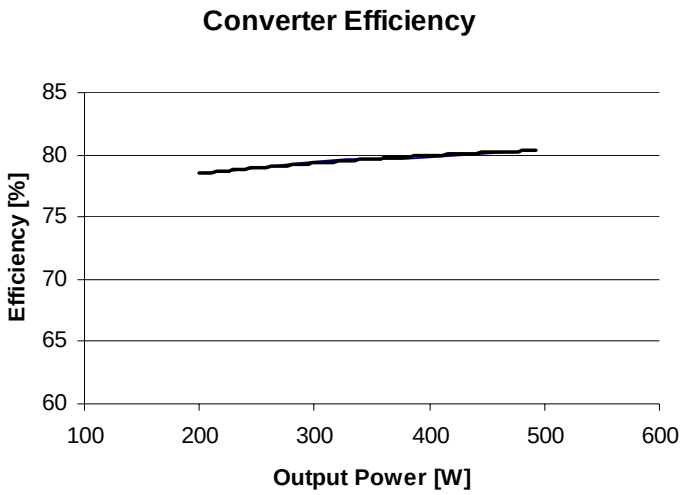

Figure 49 Measured converter efficiency

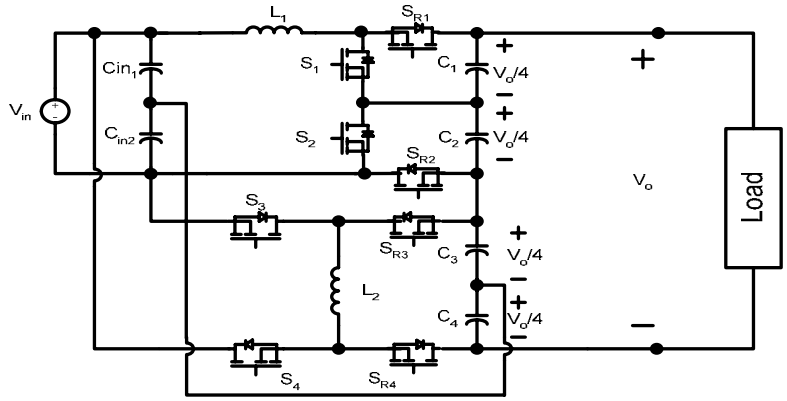

Figure 50 Synchronous rectifier approach

The efficiency of the modified converter can now be calculated using the same analytical method used to obtain the efficiency of the original converter using diodes. From the analysis the efficiency of the converter when synchronous rectifiers are used is derived to be as shown in equation (32).

$$\eta = \frac{P_o}{P_{in}} = \frac{V_o\,(Vs, D_1, D_2) I_o}{V_S I_S (I_o, D_1, D_2)} = \tag{32}$$

$$\frac{1}{\dfrac{2}{(1-D_1)} + \dfrac{(1+D_2)}{(1-D_1)}} \left(\begin{array}{l} \dfrac{2}{(1-D_1)} \dfrac{1}{1+\dfrac{4(2R_{DS}+R_L)}{(1-D_1)^2 R}} \\ + \dfrac{D_2+1}{1-D_2} \dfrac{1}{1+\dfrac{4(2R_{DS}+R_L+Vd\,(1-D_2))}{(1-D_2)^2 R}} \end{array} \right)$$

The efficiency of the converter when using diodes and synchronous rectifiers can be compared from the plots shown in figure 51. This figure shows the calculated efficiency of the converter for different duty cycles calculated from equations (28) and (32). For

example if the duty cycles of the boost and buck-boost converters are set at the values calculated in the design example, D_1= 0.32 and D_2=0.54. The efficiency when using diodes is 80%, whereas if synchronous rectifiers are used the efficiency of the converter is calculated to be 85.3 %. That is the efficiency of the DC/DC converter improves by 5% if synchronous rectifiers are used. Further if the losses in the inductor can be reduced and the inductor resistance to load resistance ratio can be improved from 0.01 in the experimental prototype to 0.007 the efficiency of the converter can be improved up to 91%.

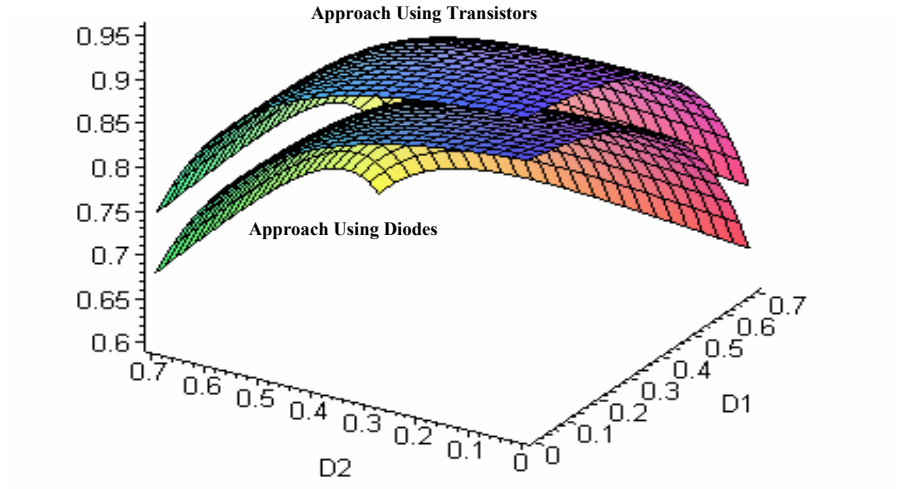

Figure 51 Efficiency improvement with synchronous rectifiers

4.6. Conclusions

In this chapter a high-gain transformer-less DC-DC converter suitable for fuel-cell applications has been presented. The proposed converter employs a two level boost and a two level buck-boost converter in cascade to obtain a high voltage gain. The fact that this converter does not require a transformer to obtain the voltage gain needed to supply a single phase inverter can significantly reduce the cost and size of the system. The proposed converter operation has been shown to result in low input current ripple, which can contribute to low EMI. Experimental results demonstrate the feasibility of the proposed DC-DC converter, and show that a voltage gain of 5 p.u is obtainable.

CHAPTER V

A MODULAR FUEL CELL, MODULAR DC-DC CONVERTER CONCEPT FOR HIGH PERFORMANCE AND ENHANCED RELIABILITY

5.1. Introduction

Fuel cells are electrochemical devices that process hydrogen and oxygen to generate electric power, having water vapor as their only by-product. The voltage resulting from the reaction of the fuel and oxygen varies with the load, and ranges from 0.8 V at no load to about 0.4 V for full load. Due to their low output voltage it becomes necessary to stack many cells in series to realize a practical system. For low power applications the number of cells that needs to be connected in series is small, but as power increases the number of cells that are required in the stack increases rapidly [28-30]. A conventional fuel cell system (figure 52a) consists of a stack of cells connected in series and a DC-DC converter to step-up its terminal voltage. In such a system the output power is limited by the state of the weakest cell. The state of a cell can be inferred from the voltage across its terminals, which is affected by parameters such as fuel and air pressure, and membrane humidity. Furthermore if a stack contains mal-functioning or defective cells the whole stack has to be taken out of service until major repairs are done. In order to circumvent

these problems the modular fuel cell and DC-DC converter shown in figure 52b are presented in this chapter. The proposed approach has the following advantages:

i) The power generated by the different sections in the modular fuel cell stack can be independently controlled by the DC-DC converter.

ii) Sections containing better performing cells can produce more power and the current drawn from sections containing under-performing cells can be limited in order to minimize internal losses.

iii) If a section of the stack is faulty, the DC-DC converter controlling the faulty stack can be disenabled and bypassed, while the rest of the system can continue operation at reduced power

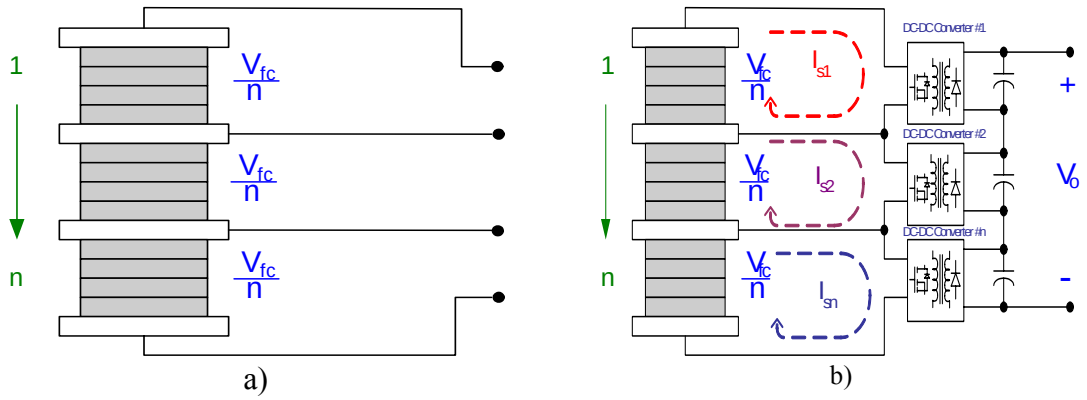

Figure 52 Taped fuel cell stack concept

5.2. Modular fuel cell stack

Fuel cell stacks are constructed by stacking several individual cells, which is equivalent to connect many voltage sources in series. The fuel and oxygen input lines to each of the cells in the stack are connected in parallel in order to ensure that the pressure on the anode and cathode of each cell in the stack the stack is kept at a similar level. This is done by means of manifolds which connect the fuel and oxygen lines to the actual cells in the stack as shown in figure 53.

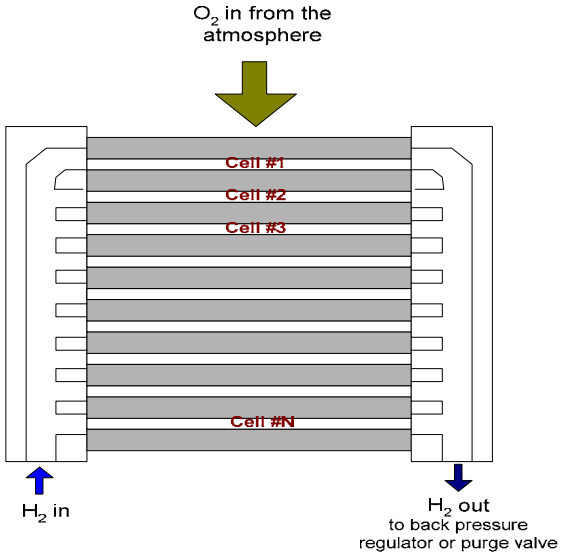

Figure 53 Fuel cell construction

The voltage produced by each of the cells in the stack is a function of fuel pressure, membrane humidity and state of the catalyst. The fuel pressure on each cell is in theory constant due to the input manifold, but in reality it may drop due to water condensation or other obstructions. Cells receiving a lower pressure will produce a reduced voltage. The membrane humidity may vary from cell to cell depending on the heat distribution in

the fuel cell. Cells with a drier membrane will produce less voltage and cell with a moisturized membrane will produce a voltage closer to its nominal. On the other hand the hydrogen supply may be contaminated with a small amount of carbon monoxide (CO), which is normally a by-product of fuel reformers used to extract hydrogen from other fuels such as natural gas. The platinum catalyst used in PEM fuel cell stacks has a good affinity with CO, thus if the fuel is contaminated the platinum traps the CO reducing the active area in the membrane. This in turn has the effect of reducing the voltage produced by the cell.

All these reasons contribute to an un-even voltage distribution through the fuel cell stack. Most of these problems are minimal if the stack is kept short, 5-10 cells. But in longer stacks they pose a problem. As an example figure 54 shows the V-I characteristic measured from the different cells from a 24 cell 12 V/ 150 W stack.

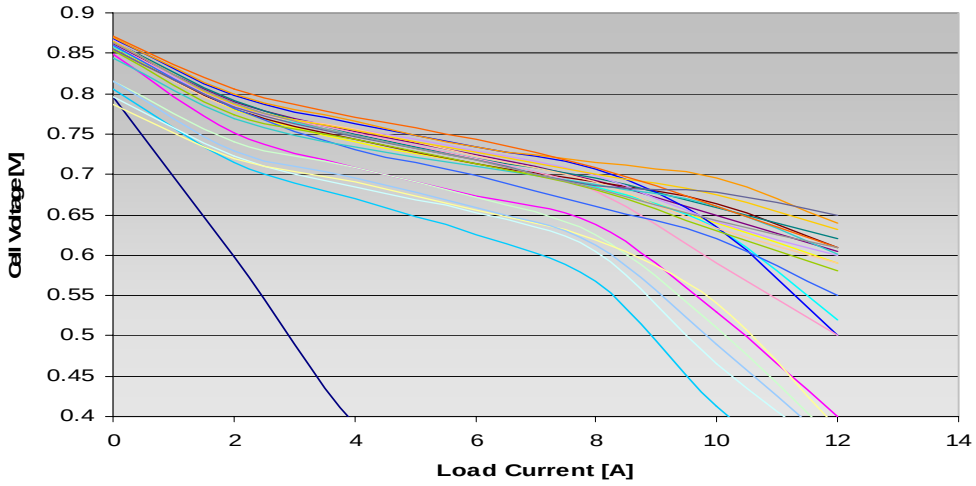

Figure 54 Individual cell V-I

As can be observed from figure 54 the voltage produced by each cell in this particular stack can be classified in three categories. First there is a group of cells that clearly have a healthy V-I characteristic. It can be observed that most of the cells in the stack can be included into this group. Then there is a reduced group of cells in the stack that have lesser performance, this since their voltage drops quickly with the load current. Finally as can be seen from figure 54 this stack contains one cell whose voltage collapses rapidly with the load current. This cell is a bad cell. Ultimately the effect of having under performing cells in the stack is the reduction of the maximum output power that the stack can deliver. Figure 55 shows the power (watts) generated by each individual cell.

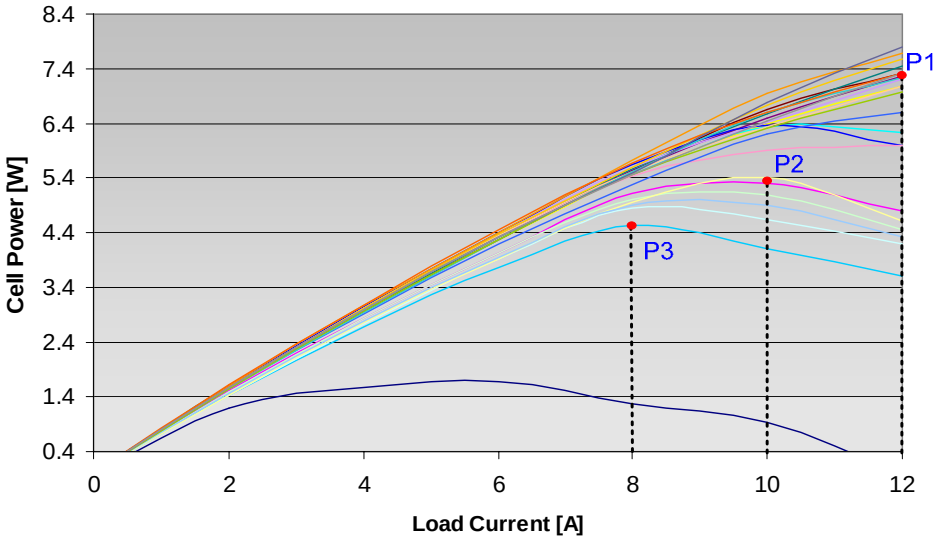

Figure 55 Individual cell P-I

Comparing points P1, P2, and P3 in figure 55, it becomes evident that under performing cells in the stack can produce less power than the cells that are in good operating condition. In addition if the current flowing through an underperforming cell goes above the point of maximum power generation no additional power is gained. Moreover the internal loses in the cell increase, thus the efficiency of the system drops and its temperature raises. From these results in order to optimize the operation of the stack one should be able to control the current flowing through each cell in the tack. However such an approach proves to be impractical as well as un-economical. A better approach is to control a group of cells in order to maximize their performance. To do this it becomes necessary to divide the fuel cell stack into sections which can be controlled individually. A convenient approach is to divide the stack in sections of 5-10 cells as shown in figure 52. By having access to these additional terminals allows to load each section in a different manner which in turn allows maximizing the power generation of the stack. The construction of such a stack does not differ much from the conventional construction approach, and can be done by inserting metal plates between the last and first cell in two consecutive sections. However care needs to be taken in order not to obstruct the fuel distribution manifolds. Figure 56 shows a schematic diagram of the proposed approach as well as a picture of a 12V 150W prototype, which is divided into three sections. An additional advantage of having a taped fuel cell stack as shown in figure 56 is that if a faulty section is detected. Power extraction from the said section can be stopped while the rest of the stack can remain in operation. This has the obvious advantage of increasing the reliability of the overall system.

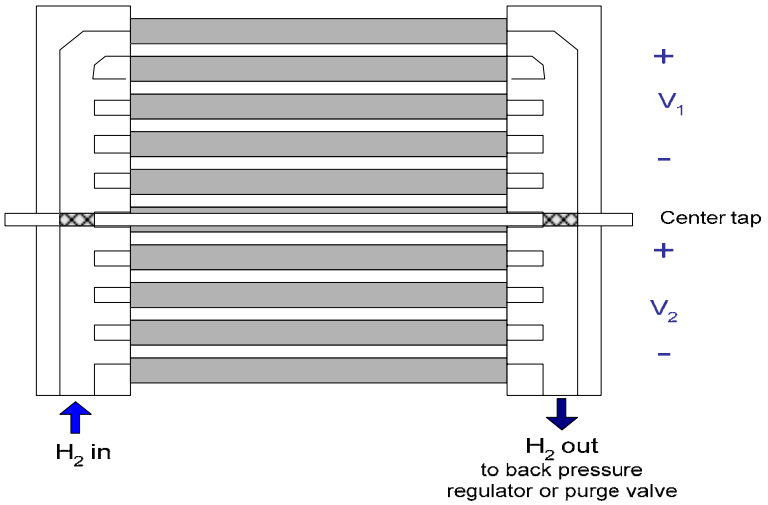

a) Schematic drawing

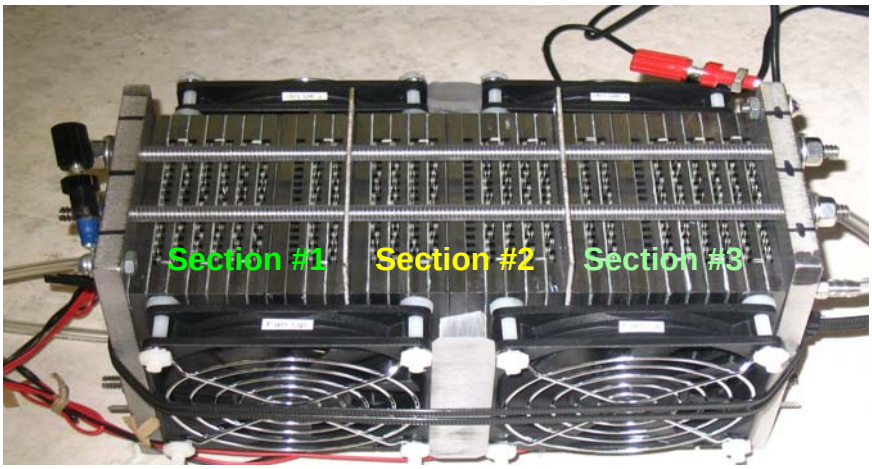

b) Prototype

Figure 56 Proposed taped fuel cell stack

Figure 57 shows the V-I characteristic for each of the sections in the prototype fuel cell stack. It can be observed that the performance of the three sections is different. From the figure nominal current (12A) can be drawn from sections 1 and 3 before their voltage drops below their minimum voltage (4V). On the other hand section 2 can only supply a maximum current of 8A before its voltage collapses.

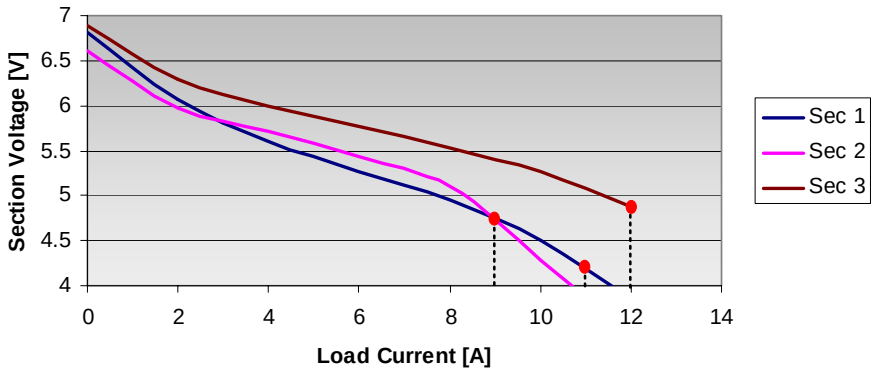

Figure 57 V-I characteristic of sectioned fuel cell

Figure 58 shows the power produced by each section in the fuel cell stack as function of the load current. As can be seen from this figure the section of the stack with lower performance, section 2, reaches its maximum output power at a current of 10A. After this the power that it produces decreases if the load current is increased, which clearly indicates an increase in its internal losses.

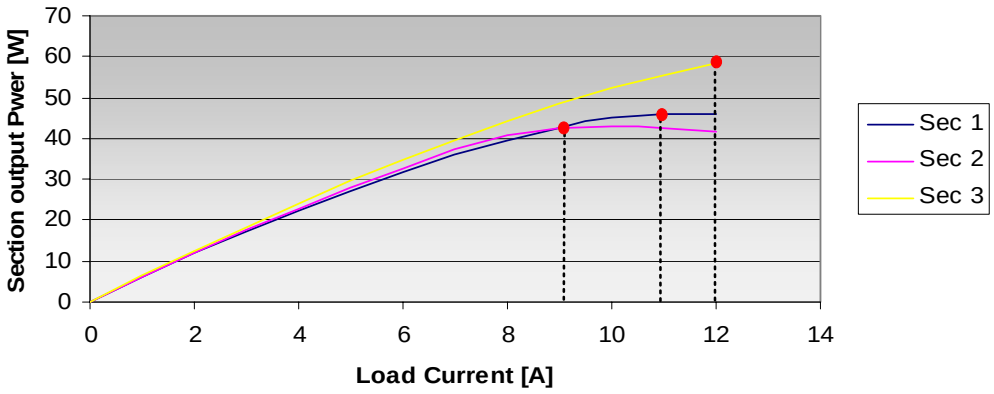

Figure 58 P-I characteristic of sectioned fuel cell

If a traditional approach is used the current in the stack should be limited by the weakest section, 9A in this case, but due to the modular construction of the system the other sections can be operated at different load currents to optimize their operation. A comparison of the maximum output power that the stack can generate with the two approaches is shown in Table III.

Table III
Conventional and modular approach comparison

	Conventional	Modular
Section 1	**42W**	**42 W**
Section 2	**43W**	**47 W**
Section 3	**49 W**	**58 W**
Total Power	**134 W**	**147 W**

From figures 57, 58, and Table III it becomes apparent that to optimize the power generation in the fuel cell it is necessary to independently control the current drawn from each of the sections in the stack. In order to control each section of the fuel cell stack independently the power converter needs to provide three independently controllable inputs. In addition to this the DC-DC converter has to be controlled accordingly.

5.3. Proposed modular DC-DC converter

The modular fuel cell design shown in figure 56 is divided into three sections of 8 cells each, and the terminals of each section are accessible to connect a load. To take advantage of such a fuel cell stack a multi input DC-DC converter is required. The converter should have three individually controllable inputs and one output. In addition, since the positive terminal of one section in the stack also serves as the negative terminal for the next section. The converter should provide isolation between input and output in order to avoid circulating currents. A converter meeting these specifications can be constructed by using an arrangement of isolated DC-DC converter modules. Where the inputs of each module are connected across one of the sections of the fuel cell and their outputs are connected in series in order to add the output voltages of the different modules and thus obtaining a higher output voltage. Such a modular DC-DC converter is shown in figure 59.

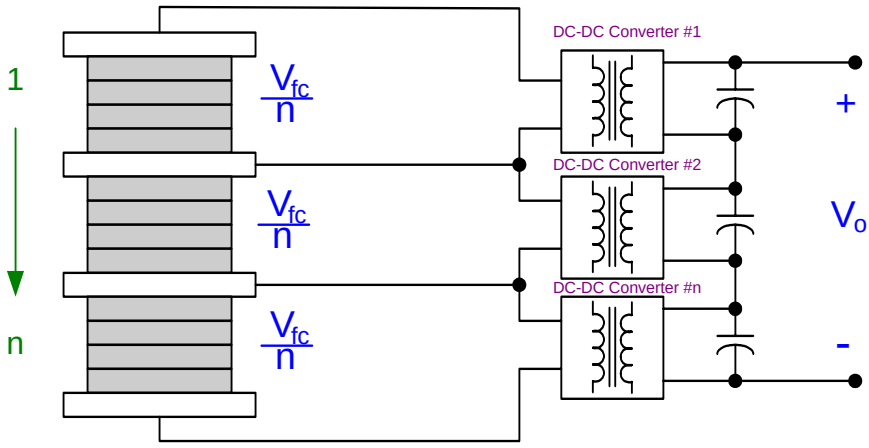

Figure 59 Proposed modular DC-DC converter

Each of the modules used to construct the DC-DC converter in figure 59 is implemented by using an isolated step-up topology such as fly-back, push-pull, forward or full Bridge. Among these the push-pull converter is a good option for step-up applications with output powers above 50W due to their low semiconductor stress, and component count. Figure 60 shows the schematic diagram of the proposed modular DC-DC converter implemented using three push-pull modules.

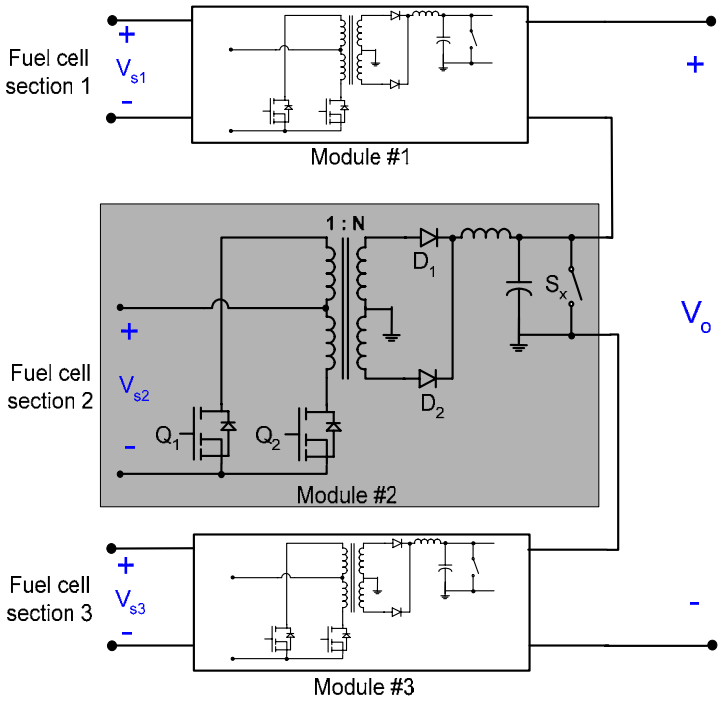

Figure 60 Module schematic

As discussed earlier in this chapter another of the advantages of constructing a fuel cell stack with several taps is that faulty sections of the stack can be by-passed, while the rest of the stack can continue operation. To implement this function each of the modules used to construct the DC-DC converter should be able to stop extracting power from the section they are connected to and set their output impedance to zero. This can be accomplished by removing the gating signals to the transistors. In addition it is necessary to add a switch (S_x) at the output of each module to short circuit the output capacitor of the converter and thus bypassing the module.

In order to optimize the power extraction from each of the sections in the fuel cell an appropriate control scheme needs to be devised. Since the voltage across the terminals of

each section in the stack is a good indication of how much power it can generate, this information can be used to better distribute the power extracted from each section. A section producing a higher voltage can generate more power than a section that produces a lower voltage. Thus by controlling the load current of each section proportionally to their terminal voltages has the effect of having a higher load in the healthier sections and a lower load in the sections that can not produce as much power. This in turn, reduces internal losses and improves the overall efficiency of the system. The proposed scheme can be implemented by having each of the modules in the DC-DC converter produce a different voltage at their output terminals. This in turn produces a different load current at their input terminals and therefore a different loading to the fuel cell section to which they are connected. Figure 61 shows the control scheme for the proposed modular converter.

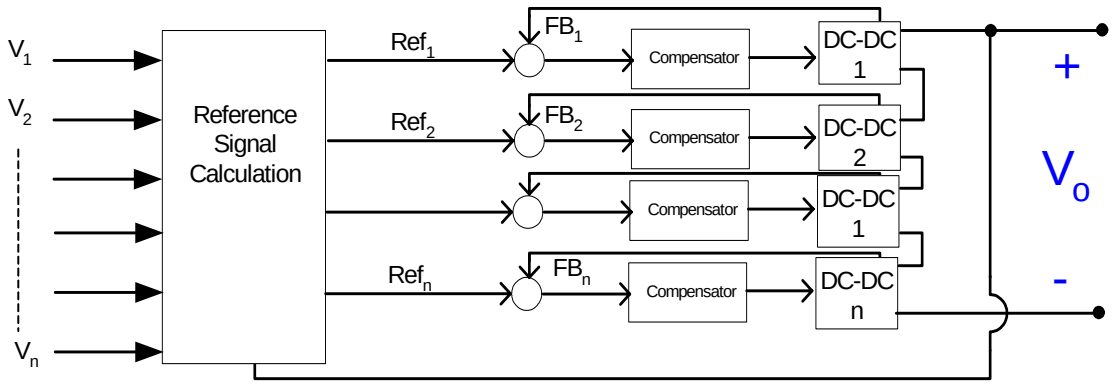

Figure 61 Proposed control scheme

Each of the modules that compose the DC-DC converter has an internal control loop to regulate their output voltage. The reference signals to each of the modules are set in order to control the loading of the sections of the stack and to maintain the output voltage of the DC-DC converter. The calculation of the different reference signals (Ref_1-Ref_n) is calculated by taking into account the voltage produced by each of the sections in the stack and the number of modules that compose the DC-DC converter. Each of the reference signals is calculated by a weighting function according to equation (36):

$$\text{Ref}_n = \frac{V_n}{\sum_{1}^{NAC} V_i} \tag{36}$$

In (36) V_n is the voltage produced by the "n^{th}" section in the fuel cell stack, V_i is the voltage produced by the "i^{th}" section in the stack, and NAC is the total number of active sections in the stack. Thus the reference signal for the "n^{th}" module is given by the ratio between the voltage produced by the "n^{th}" section in the fuel cell stack and the total voltage produced by the stack. The number of active sections in the stack is defined by all the sections that produce a voltage above a minimum value. Now if one of the sections produces a lower voltage, that section can be considered as faulty. Thus it cannot produce power and needs to be discarded. In this case the controller reduces NAC by one and sets the reference signal to the respective module to zero. Additionally this has the effect of increasing the reference signals of the remaining modules to compensate for the loss of one of the modules.

5.4. Experimental results

To verify the operation of the proposed converter a laboratory prototype was built. The test system is composed of a 150W 12V fuel cell stack divided into three 8 cell sections, and a DC-DC converter composed of three modules. The DC-DC converter is designed to supply a 22V load, thus if all the sections in the fuel cell produce an even output voltage each module needs to provide one third of the output voltage and output power. However, since the modules have to be designed for the condition of faulty sections, each is designed in order to provide half of the output voltage of the DC-DC converter and one third of its output power. This is 11V and 50W. The DC-DC converter and modules are as shown in the schematic in figure 60.

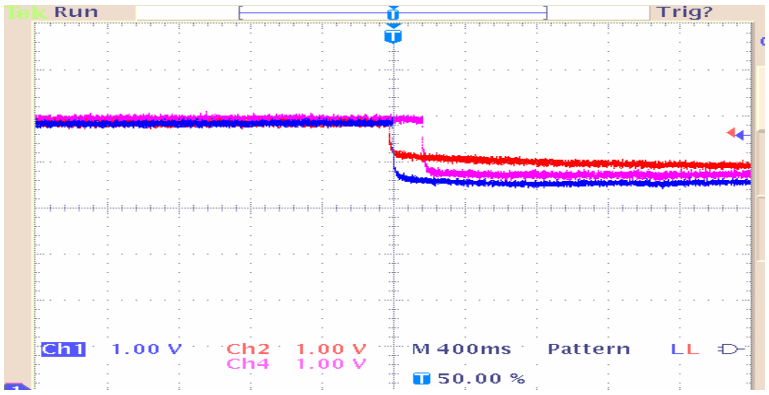

Figure 62 Section voltages during load transient

Figure 62 shows the voltage across each of the sections in the stack when the output load goes from 40% load to 90%. In this figure trace 1 shows the voltage in section 3, trace 2 the voltage in section 1 and trace 4 the voltage in section 2. As can be seen from the figure initially the voltages of the three sections are different levels (5.7, 5.9, and 8V)

and after the load is increased the controller of the DC-DC converter adjust the reference of each of the modules in order to find a new equilibrium. The time it takes to the voltages produced by the different sections in the stack to settle down into the new operating point may differ due to the difference in the internal time constant of the sections, which is a function of the health of each section. A healthy section has smaller internal impedance and its voltage reacts faster. Figure 63 shows the currents drawn from each of the sections in the stack. It can be observed from figure 63 that before the transient the currents drawn by each module is different. During the first load condition the current drawn by sections 1 (trace 2), 2 (trace4), and 3 (trace 1) are 4.5A, 3A and 4 A respectively.

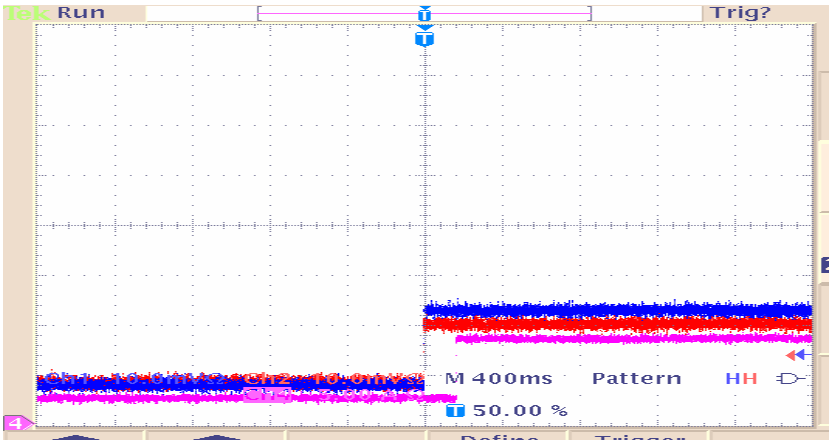

Figure 63 Section load currents

After the load transient the references for the modules are adjusted in order to accommodate to the new load condition. In this case the currents of sections 1, 2 and 3

are 10A, 7 and 11.5A. This result could be anticipated from figure 58 which shows the load current- output power characteristic of the different sections in the stack.

The other functionality offered by the proposed converter is the ability to discard a section of the fuel cell if the controller detects that the voltage across its terminals drops below a certain threshold. The test system is rated for 12V at full load, thus the voltage of the sections at full load is 4V. Therefore if a section is faulty its terminal voltage will fall below this value. For this reason the threshold level in the controller was set to 3.8V. Figure 5.13 shows the behavior of the system when a faulty section is detected, in this case section 2.

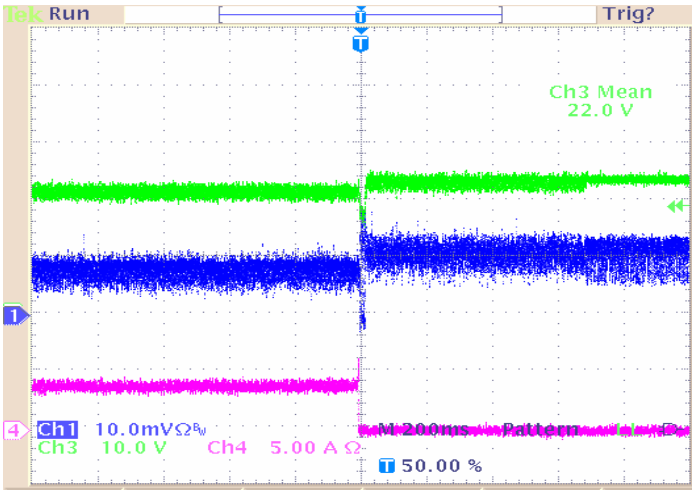

Figure 64 Detection of a faulty section

In figure 64 trace 1 corresponds to the current drawn from section 3, trace 3 the output voltage of the DC-DC converter and trace 4 the current drawn from section 2. It can be observed that once the fault condition is detected the current drawn from the

faulty section (section 2) falls to zero. At the same time the current drawn from the other sections in the stack increase in order to maintain the output voltage of the system (trace 3). Figure 65 shows thermal images of the fuel cell stack operating in both single stack and modular stack modes. The current being drawn by the load for the single stack case was 7.25 A, and the voltage of the stack was measured to be 12, that is the nominal voltage of the fuel cell for full load. The power generated by the stack was measured to be 87W. Figure 65a shows the case of the fuel cell operating in single stack mode while the load draws a current of 8A. It can be observed that the temperature distribution is quite un-even due to the presence of bad cells in section 2, while sections 1 and 3 show a lower temperature indicating that they are under used.

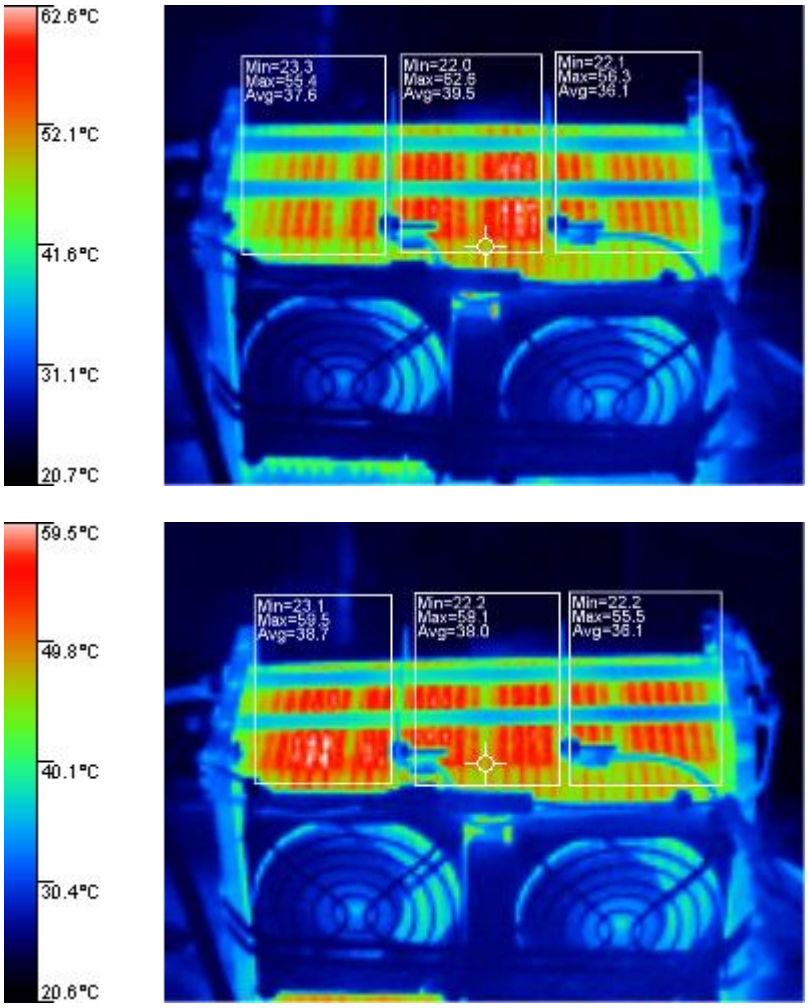

Figure 65 Thermal comparison of conventional and modular fuel cell

The case of the modular stack and DC-DC converter was tested next. During this test the voltage across each of the sections was regulated to 4V, the nominal voltage for each section. The currents drawn from sections 1, 2 and 3 in the stack were measured to be 10A, 6A, and 9A respectively. Thus the power generated by the fuel cell in this case is 102W. Figure 65b shows the fuel cell stack operating in modular mode and connected to the proposed modular converter. It can be seen that in this case the temperature

distribution is even. And that in the case of the modular system the fuel cell generates 15% more power than if the conventional approach is used.

5.5. Conclusions

In this chapter a modular fuel cell stack and DC-DC converter and their advantages were presented. The voltage produced by each cell in a fuel cell stack is a function of several parameters. Due to variations in these parameters the voltage distribution through the stack is un-even. Moreover the maximum power that can be generated by the stack is limited by the weakest cells in the stack. In addition if a stack contains faulty cells operation of the system needs to be discontinued until repairs are made.

To avoid these problems and optimize the power generation in long fuel cell stacks a modular fuel cell design is introduced. The proposed fuel cell system is divided into sections whose voltage and load current can be controlled independently in order to optimize its operation. To take advantage of the proposed tapped fuel cell a modular DC-DC converter and control scheme are introduced.

The proposed modular DC-DC converter controls the current drawn from the each of the sections in the fuel cell in terms of their terminal voltages. This in turn has the effect of better distributing the load across the section in the stack, which reduces extra heating and internal losses.

Experimental results show the effectively of the proposed modular DC-DC converter and control scheme.

CHAPTER VI

COMMON MODE VOLTAGE ANALYSIS IN UTILITY CONNECTED FUEL CELL SYSTEMS

6.1. Introduction

Since fuel cells produce a low output voltage with a large variation from no load to full load it becomes necessary to use a switching power converter in order to interface with the loads. Because of rapid changes in voltages and currents within a switching converter, power electronic equipment is a source of electromagnetic interference (EMI) [31]. This interference can affect the operation of other equipment as well as the one producing the interference. The EMI produced by the converter can be transmitted in two forms: radiated and conducted. Switching converters supplying power to the utility generate conducted noise that is normally several orders of magnitude higher than the radiated noise, this due to the fact that power converters are normally encased in metal cabinets that serve as a shield that blocks the radiated component of the EMI [32-33].

The operation of any power converter produces two types of outputs, a differential output and a common mode output. The differential output is the intended output voltage and current of the system. On the other hand the common-mode output is a voltage or current measured between the output lines of the converter and ground. The transmission of the common-mode noise is entirely trough “parasitic” or stray capacitors and stray

electric and magnetic fields. These stray capacitances exist between various system components and between components to ground.

Analysis of common mode voltage and current in fuel cell systems is done in this chapter in order to find design guidelines to minimize its effects on the system components and nearby equipment.

6.2. Generation and effects of common mode voltage

Common mode noise is a type of electrical noise induced on signals with respect to a reference ground. Common mode noise problems imply a source of noise and a means of coupling noise by conduction or radiation and circuit susceptible to magnitude, frequency and repetition rate of the noise impressed. Normally equipment susceptible to common mode noise includes low power circuitry used for control and supervision, such as digital signal processors (DSP) and pulse with modulation integrated circuits (PWM IC's). Thus the common mode noise can impact both nearby equipment as well as the converter that is producing the noise.

In general switch mode power converters can use three types of modulation schemes pulse width modulation (PWM), pulse frequency modulation (PFM), and resonant switching. Among these modulation types PWM is by far the most widely used in the industry due to its simple implementation and single frequency operation. A PWM output voltage has abrupt transitions to and from the dc bus voltage [31]. These transitions have the effect of inducing large current spikes, due to the dV/dt, on stray capacitances to ground distributed throughout the circuit as shown in figure 66.

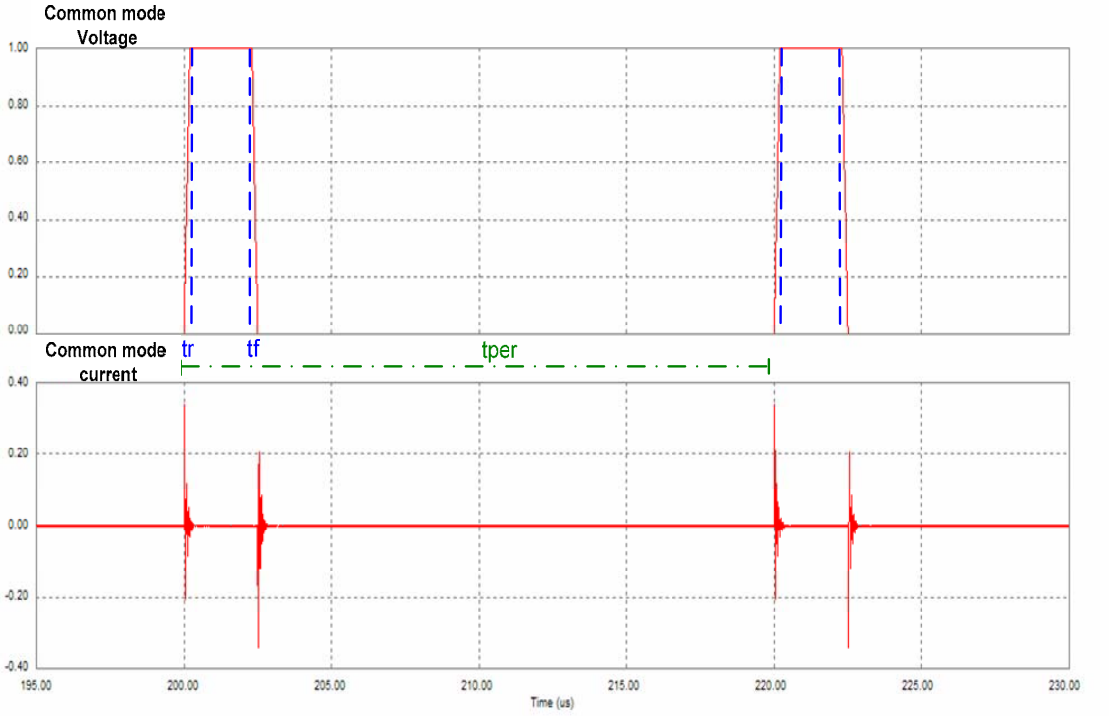

Figure 66 Effect of common mode dv/dt in stray capacitances

The time it takes the voltage to change from one voltage level to the other is essentially controlled by the semiconductor switching time (rise and fall time). The transition time of a semiconductor is inherent to the technology used for the particular device. For example the transition times for insulated gate bipolar transistors (IGBT) is in the range from 0.05 to 0.2 μs, and for metal oxide field effect transistors (MOSFET) it ranges from 50 – 80 ns. That is the dv/dt produced by the operation of MOSFET's can be 2.5 to 4 times larger than in the case of IGBT's. The time it takes to transition from a voltage level to another (rise time, t_r, and fall time, t_f) determine an equivalent noise coupling frequency which can be calculated by (37) as follows [32]:

$$f_n = \frac{0.38}{t_{rise}} \tag{37}$$

Thus MOSFET's generate noise in a frequency ranging from 4.75 MHz to 7.6 MHz. On the other hand IGBT's have a noise coupling frequency in the range from 1.6 MHz to 6.4 MHz. That is the coupling frequency of MOSFET devices is up to 5 times higher than IGBT. Typically a combination of MOSFET and IGBT devices is used for fuel cell applications. This since the power conditioning units are normally constructed in a two stage approach composed of a step-up DC-DC converter and a cascaded inverter which are implemented by MOSFET's and IGBT's respectively. And thus both types of noise coupling frequencies exist in these systems.

Since power converters are enclosed in metal cabinets most of the electro magnetic interference (EMI) is due to conducted noise current circulating through ground. Figure 67 shows a typical fuel cell power conditioning system, parasitic capacitances to ground and some of the paths through which the common mode currents can flow [34].

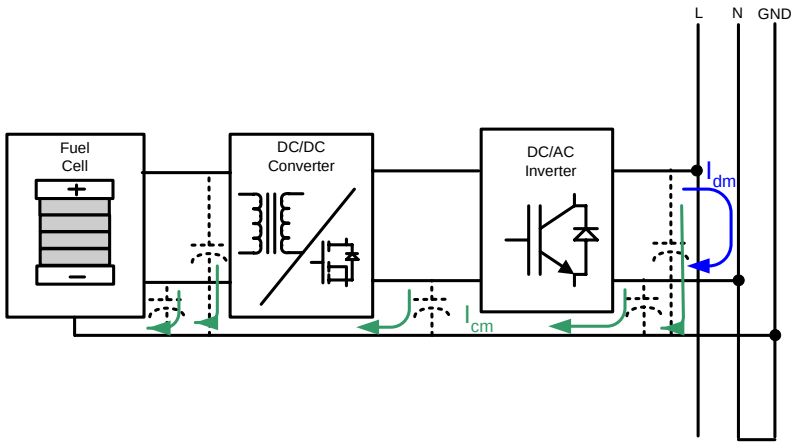

Figure 67 System parasitic capacitances and common mode coupling paths

The effect of the common mode noise induced by these currents on other equipment is a function of the distance separating the noise generation and reception. Therefore it is important to keep the circulation paths of common mode currents as short as possible.

6.3. Analysis of common mode voltage in single phase fuel cell systems

Single phase systems are normally used for lower power applications. In these applications the fuel cell output terminals are connected to a step-up DC-DC converter. The output of the DC-DC converter is connected to a single phase inverter whose output is then connected to the e utility, resulting in the system as shown in figure 68 [34].

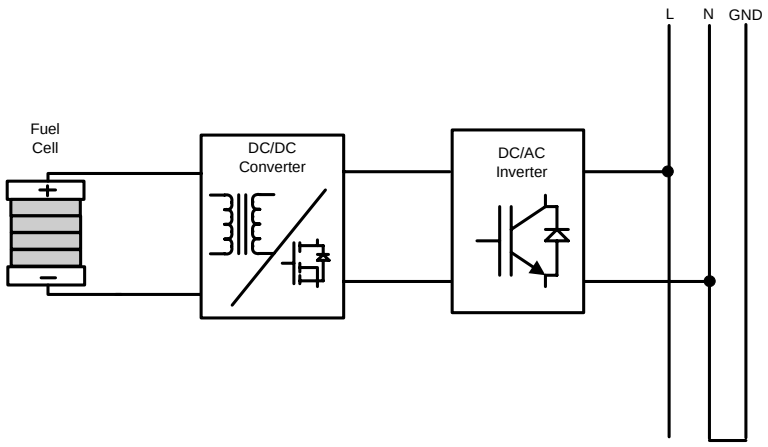

Figure 68 Single stack single phase system

From the point of view of common mode noise two different conditions can be identified for this system. These two cases depend on whether or not the fuel cell is connected to ground or not.

6.3.1. Floating fuel cell stack

If neither of the terminals of the fuel cell stack is connected to ground the stack is said to be floating with respect to ground. In this case the system can be modeled as shown in figure 69 which includes the parasitic capacitances that appear from different points in the circuit to ground [34-36].

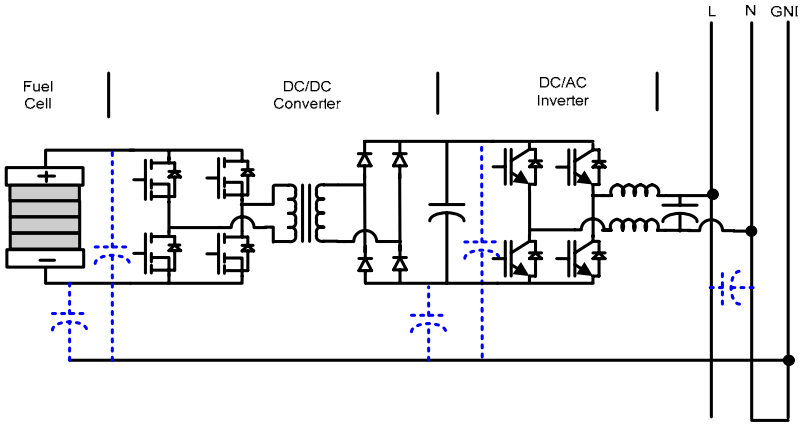

Figure 69 Single stack ungrounded system

As can be seen from this figure even though the fuel cell stack is not grounded parasitic capacitances appear from its terminals to ground. To perform the common mode analysis the equivalent common mode circuit (figure 70) can be obtained from figure 69 [37-38]. In this circuit each of the switching legs in the DC-DC converter, rectifier and inverter can be modeled as a common mode voltage source. The transformer in the DC-DC converter is modeled by lumped capacitances from primary and secondary to ground, which represent the distributed parasitic capacitances of each

turn to ground in both primary and secondary [39]. An additional capacitance from secondary to primary models the parasitic capacitance between primary and secondary.

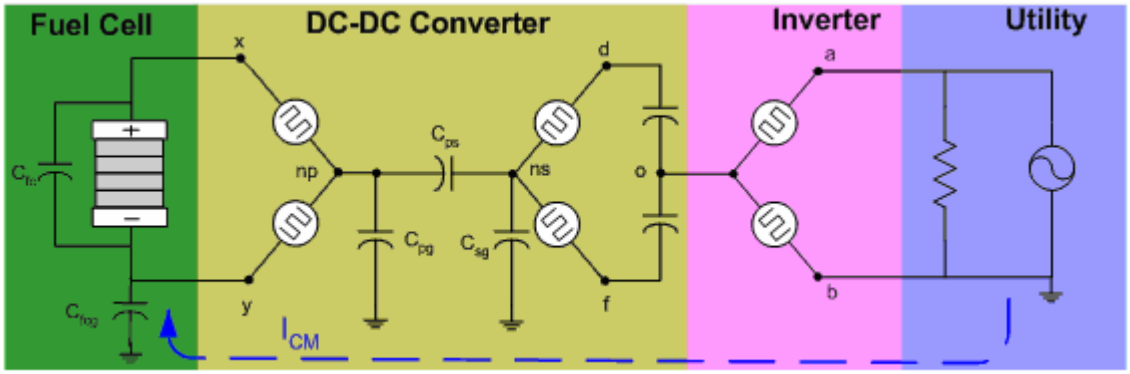

Figure 70 Common mode equivalent circuit

From figure 70 the output voltage of the system is given by:

$$V_{ab} = V_{ao} - V_{bo} \tag{38}$$

And since in this case the inverter corresponds to a single phase type we have that

$$V_{bo} = -V_{ao} \tag{39}$$

Thus the voltage between the point "o" and ground can be calculated by

$$V_{og} = -V_{bo} = V_{ao} \tag{40}$$

Also from figure 70 it can be found that the voltage from the center point of the secondary transformer winding to ground is given by:

$$V_{nsg} = V_{og} = V_{ao} \tag{41}$$

The voltage at the center point of the transformer primary winding can be found from the capacitor divider formed by the primary to secondary parasitic capacitance (C_{ps}) and the primary to ground parasitic capacitance (C_{ng}). This voltage can be calculated from (42)

$$V_{pg} = \frac{C_{ps}}{C_{ps} + C_{ng}} V_{nsg} \tag{42}$$

The voltage to ground that appears from each of the terminals of the fuel cell stack can then be obtained from the equivalent circuit of figure 70 in terms of V_{pg} and is given by (43) and (44).

$$V_{fc+} = V_{pg} + \frac{V_{fc}}{2} \tag{43}$$

$$V_{fc-} = V_{pg} - \frac{V_{fc}}{2} \tag{44}$$

Therefore it can be concluded that an AC voltage is superimposed to the voltage produced by the fuel cell stack. The magnitude of this voltage is a function of the ratio of the parasitic capacitances present in the high frequency transformer used to construct the DC-DC converter.

The magnitude of the common mode current flowing through ground, I_{cm} in figure 70 can then be calculated by:

$$I_{CM} = C_{fcg} \frac{dV_{ft-}}{dt} \tag{45}$$

This analysis is verified by means of computer simulations using PSim. The circuit schematic used for simulating this case is shown in figure 71, which corresponds to a

typical single phase system. The input voltage of the system is 48V and its output is 240V, 60Hz.

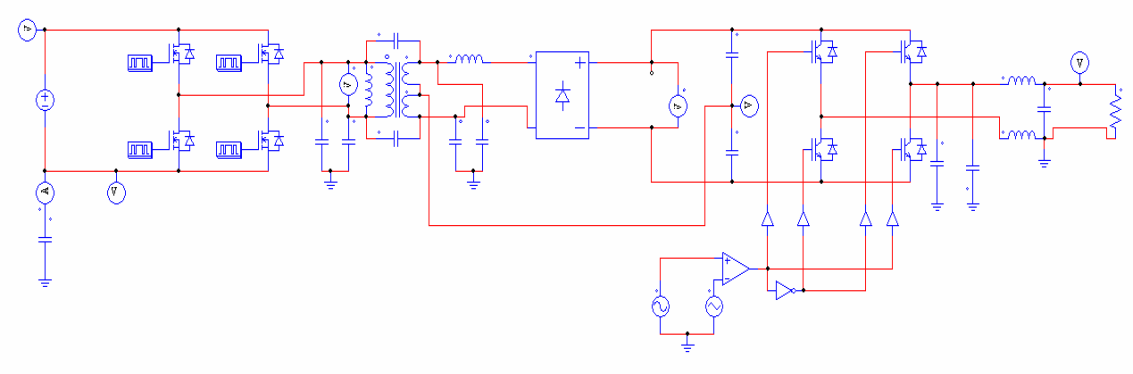

Figure 71 Circuit schematic

The values used for the parasitic capacitance between the fuel cell and ground C_{fcg} is 100pF and the parasitic capacitances for the transformer are C_{pg} = 100 pf, C_{sg} = 100 pF, and C_{ps} = 50 pF. Figure 72 shows the resulting common mode current I_{cm}, voltage V_{ao} and the output voltage of the system. From this figure it can be observed that the common mode current is as high as 7A. Also the number of current spikes in the common mode current is higher around the zero crossing of the output voltage of the system. This is due to the PWM modulation which produces more and narrower pulses as the reference voltage approaches zero.

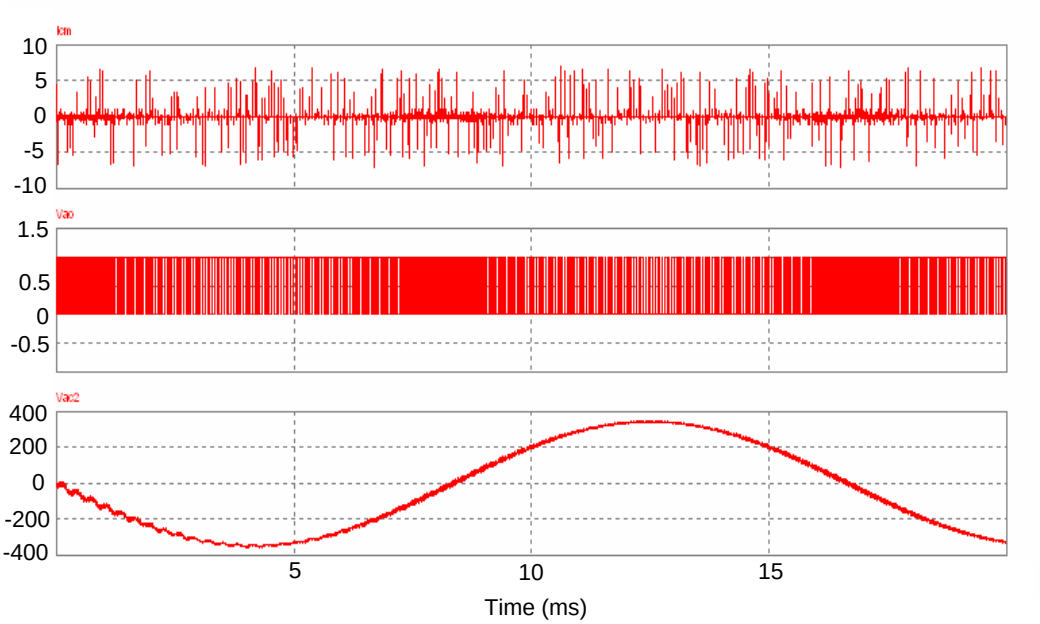

Figure 72 Simulation result for floating single phase system

To better observe the effect of the rise and fall times of the switching the waveforms for the common mode current and voltage V_{ao} are magnified in figure 73. As can be seen from the figure the current spikes are due to the fast transitions of V_{ao}. The magnitude of these transitions is a function of the parasitic capacitances, the magnitude of the DC-link voltage and the raise and fall time of the semiconductors as was shown in equations (37) and (45).

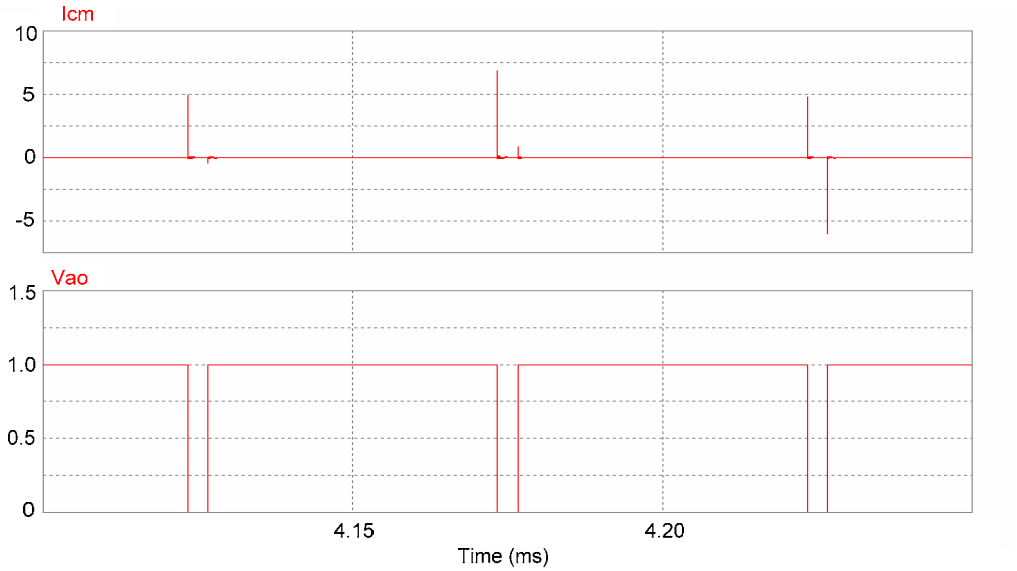

Figure 73 Voltage V_{ao} and common mode current I_{cm}

As can be observed from figure 73 the common mode current has peak values up to 7A, which is of considerable amplitude when it comes to producing EMI interference.

6.3.2. Grounded fuel cell stack

As was shown in equations (43) and (44) if the fuel cell is floating an AC voltage is superimposed to the voltage produced by the fuel cell stack. For safety reasons in most practical systems one of the terminals of the stack needs to be tied to ground, which is normally the negative one. The circuit schematic and common mode equivalent circuits for this case are shown in figures 74 and 75 respectively. The analysis of the common mode voltage done previously for the floating stack is valid up to equation (41).

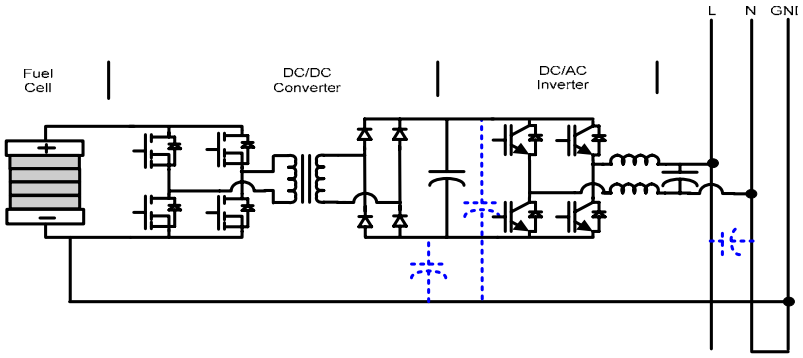

Figure 74 Circuit schematic for grounded fuel cell system

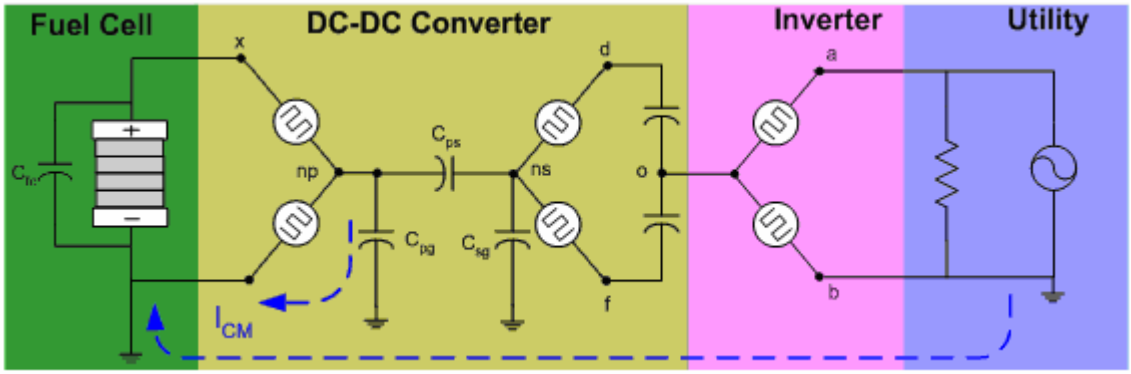

Figure 75 Common mode equivalent for grounded fuel cell system

From figure 75 the common mode current not only has a component due to the voltage that appears between point "o" and ground but also due to the common mode voltage source V_{npg}. It can be calculated by equation 46.

$$I_{CM} = C_{ps}\frac{d(V_{nsg} - V_{npg})}{dt} + C_{pg}\frac{dV_{npg}}{dt} \qquad (46)$$

A simulation is run in order to verify the result obtained in equation (46), and the resulting common mode current is shown in figure 76. As can be seen from figure 76 the common mode current is considerably larger in this case. The peak common mode

current for this case reaches 22A; this is about three times higher than the case when the stack is not grounded. The increment in the common mode current is due to the smaller parasitic impedance that appears between the circuit and ground, since one of the ends of the fuel cell is connected to ground facilitating the circulation of common mode currents. In addition for this configuration a second common mode voltage source comes in to play further increasing the magnitude of the current.

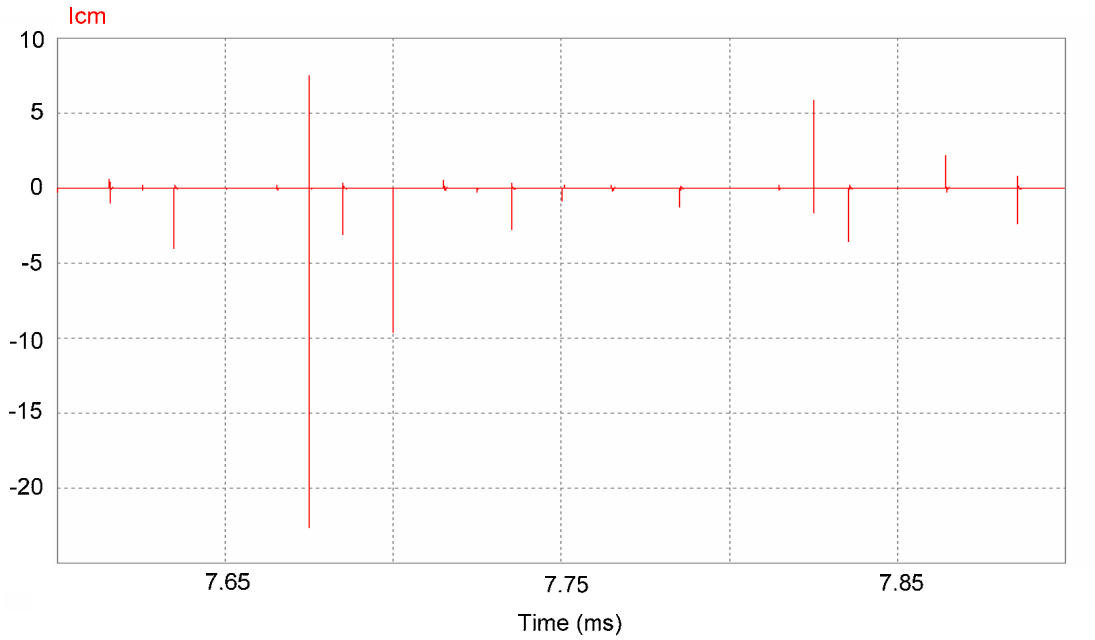

Figure 76 Common mode current for system with grounded fuel cell stack

6.4. Analysis of common mode voltage in three phase fuel cell systems

Single phase systems are used for low power applications (10-15kW), but as the power levels increase three phase systems are better suited. Figure 77 shows the block

diagram of a typical three phase fuel cell system. As can be observed from figure 77 in this case the last stage of the system is replaced with a three phase inverter.

For safety reasons normally the neutral of the three phase system is tied to ground and it may or may not be available depending on whether the distribution is done using three, four or five wires.

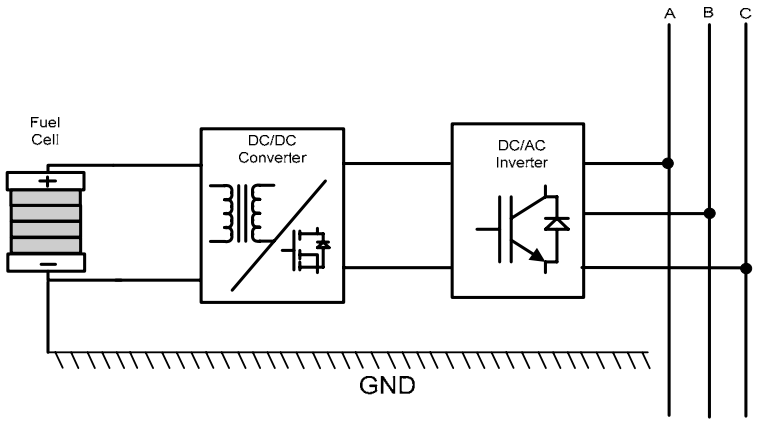

Figure 77 Three phase system block diagram

To analyze this system first the common mode equivalent circuit has to be obtained. As done in the previous sections each of the inverter legs is modeled as a common mode voltage source. Also the same common mode transformer model used in the single phase case is included in the common mode equivalent circuit for the three phase system. Figure 78 shows the resulting equivalent circuit for the three phase fuel cell inverter system.

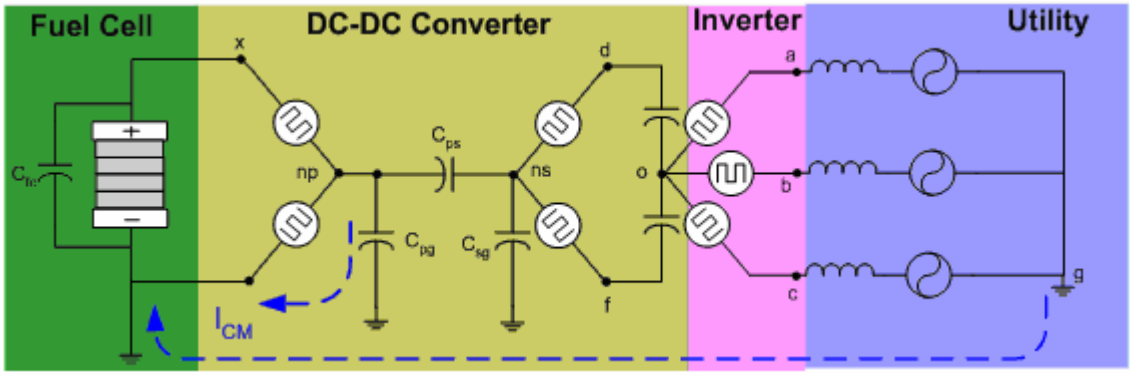

Figure 78 Grounded fuel cell system

From figure 78 the voltage from the pint "o" to ground can be calculated by:

$$V_{og} = \frac{V_{ao} - V_{ag} + V_{bo} - V_{bg} + V_{co} - V_{cg}}{3} = \frac{V_{ao} + V_{bo} + V_{co} - (V_{ag} + V_{bg} + V_{cg})}{3} \qquad (47)$$

Assuming that the utility voltage is balanced we have that $V_{ag} + V_{bg} + V_{cg} = 0$, thus

$$V_{og} = \frac{V_{ao} + V_{bo} + V_{co}}{3} \qquad (48)$$

Now since,

$$V_{dns} - \frac{V_C}{2} = \frac{V_C}{2} - V_{fns} \qquad (49)$$

We have that $V_{nsg} = V_{og}$. Also from figure 78 we have that the voltage V_{npg} is given by the common mode voltage source connected between ground and the point "np". From these equations and from the equivalent circuit (figure 78) the common mode current for the three phase case can be calculated by:

$$I_{CM} = C_{ps}\frac{d(V_{nsg} - V_{og})}{dt} + C_{pg}\frac{dV_{npg}}{dt} \qquad (50)$$

A three phase fuel cell inverter system connected to a 640 V utility bus was simulated in order to verify the circulation of common mode current through ground and validate the preceding analysis. The voltage supplied by the fuel cell stack in this case is 330V and the output of the system is 640 Vrms, 60Hz. Figure 79 shows the schematic diagram of the circuit used for the simulation in PSim.

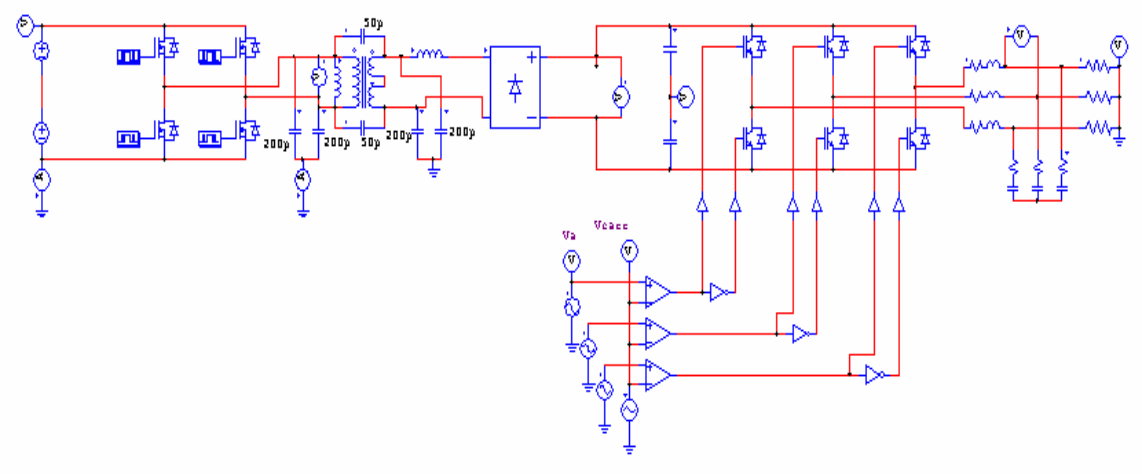

Figure 79 Circuit schematic for simulation

The common mode current obtained from the simulation is shown in figure 80. As can be observed from the figure the peak amplitude of the common mode current is about 2.5 times larger than in the single phase case. This is due mainly by two reasons, first since the converter supplies power to a 640 V utility, the DC link voltage is higher than in the single phase case, and therefore dV/dt is also higher. Secondly from equation (47) the common mode voltage in a three phase system is given by three common mode voltage sources instead of only one for the single phase case (40).

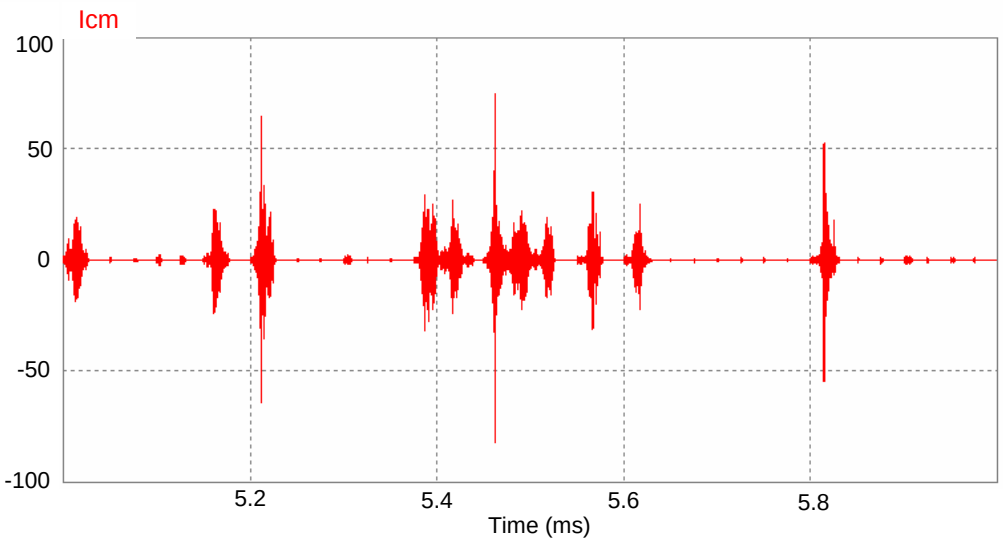

Figure 80 Common mode current for the three phase case

6.5. Reduction of common mode current

As shown in the previous sections the power converters used to interface the fuel cell stack to single phase and three phase systems produce a common mode current that circulates trough ground. The short duration and high amplitude of the current spikes in the common mode current contribute to generate conducted EMI, which can affect the operation of low power electronic circuitry. The amount of EMI generated is proportional to the magnitude of the current pulses in the common mode current. For this reason it becomes necessary to reduce their magnitude. From equations (46) and (50) it can be seen that the common mode current is generated by the common mode voltage sources of the DC-DC converter and DC-AC inverter. Also since the voltage in the DC link between the DC-DC converter and inverter is several times higher than the voltage produced by the fuel cell; the component of the common mode current generated by the inverter is dominant in the overall common mode current. Further analyzing equations

(46) and (50) it becomes clear that to limit the main component of the common mode current the capacitance C_{ps} in the equivalent circuit has to be reduced. In the common mode equivalent circuit this capacitance stands for the parasitic capacitance between the primary and secondary of the high frequency transformer used in the DC-DC converter, as can be seen in figure 81a.

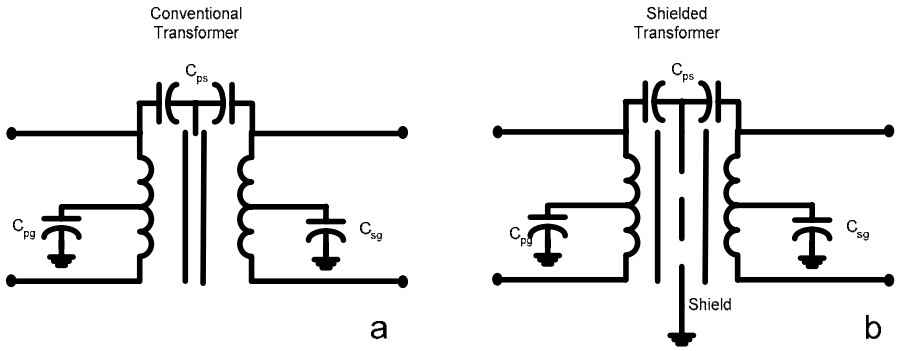

Figure 81 Conventional and shielded transformers

A practical way of reducing the value of this capacitance is by using a shield in the transformer. The shield is then connected to ground (figure 81b), reducing the capacitive coupling between primary and secondary. Figure 82 shows the circuit schematic and common mode equivalent circuit for the single phase power converter. It can be observed form figure 82b that when a shielded transformer is used to implement the DC-DC converter stage, the circulation path for the common mode current no longer exits.

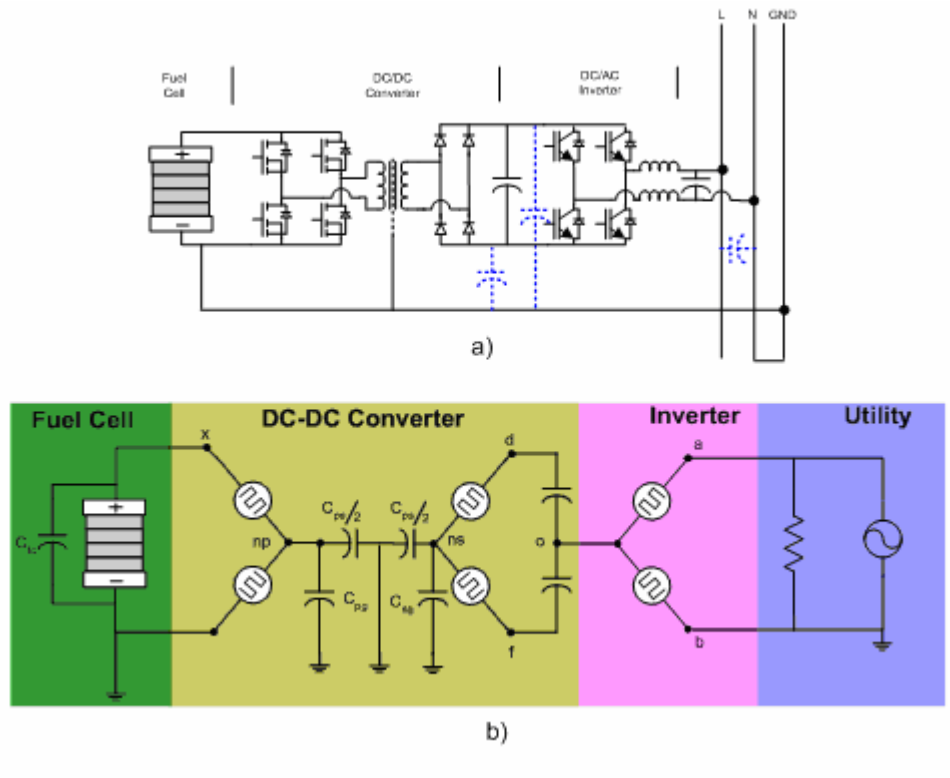

Figure 82 Single phase system with shielded transformer

The other case under consideration is the power converter for a three phase system. If the equivalent common mode circuit for the three phase power converter shown in figure 78 is modified to include the shielded transformer as was done in the single phase case the equivalent circuit shown in figure 83 is obtained. As can be observed from figure 83 the effect of introducing a shield in the high frequency transformer of the DC-DC converter is splitting the primary to secondary coupling capacitance; which is then connected to ground. The end effect of this, as in the single phase case, is breaking the circulation path for the common mode current.

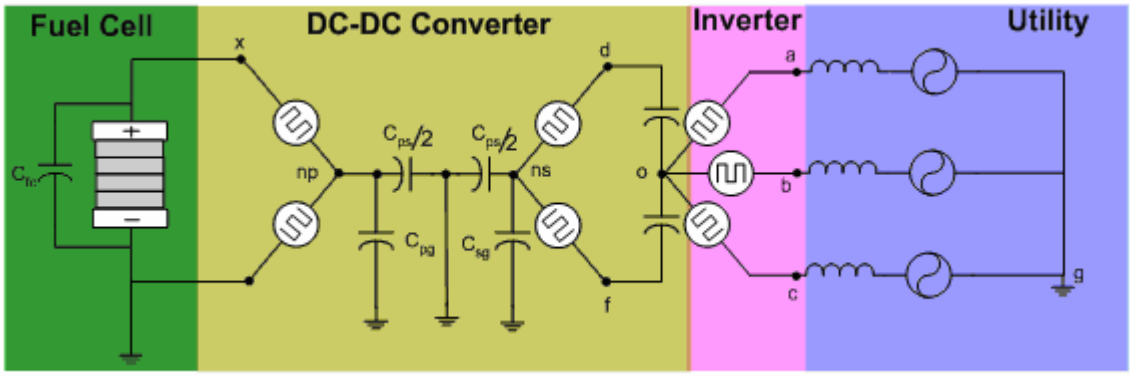

Figure 83 Common mode equivalent circuit for three phase system with shielded transformer

To verify the effectiveness of the shielded transformer the single phase and three phase systems were simulated on PSim and the common mode current was measured. Figure 84 shows the common mode current obtained for the single phase system when a shielded transformer is used.

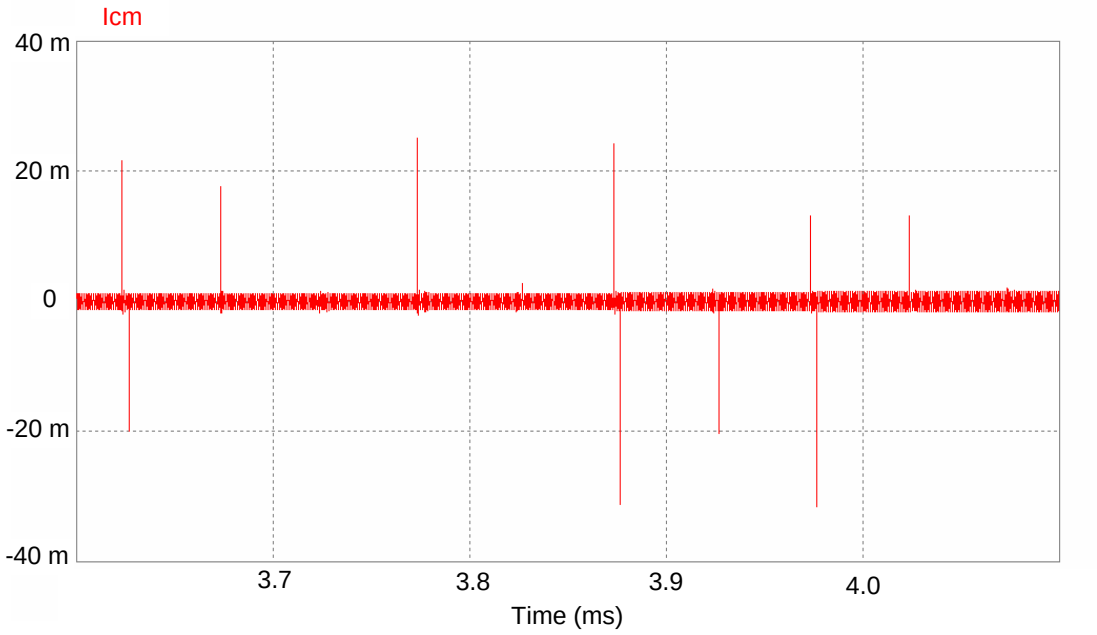

Figure 84 Common mode current for single phase system with shielded transformer

As can be seen from figure 84 the common mode current is significantly reduced. In this case the peak amplitude of the current 25 mA. This is the common mode current is three orders of magnitude smaller than the current present when a normal transformer is used to implement the DC-DC converter.

The case of the three phase system is studied next. The same three phase fuel cell power converter shown in figure 78 is simulated. But in this case the parasitic capacitance from transformer primary to secondary is reduced to 0.05 pF to account for the shielding in the transformer. Figure 85 shows the common mode current obtained from the simulation, as can be observed from the figure the peak common mode current in this case reaches 52 mA.

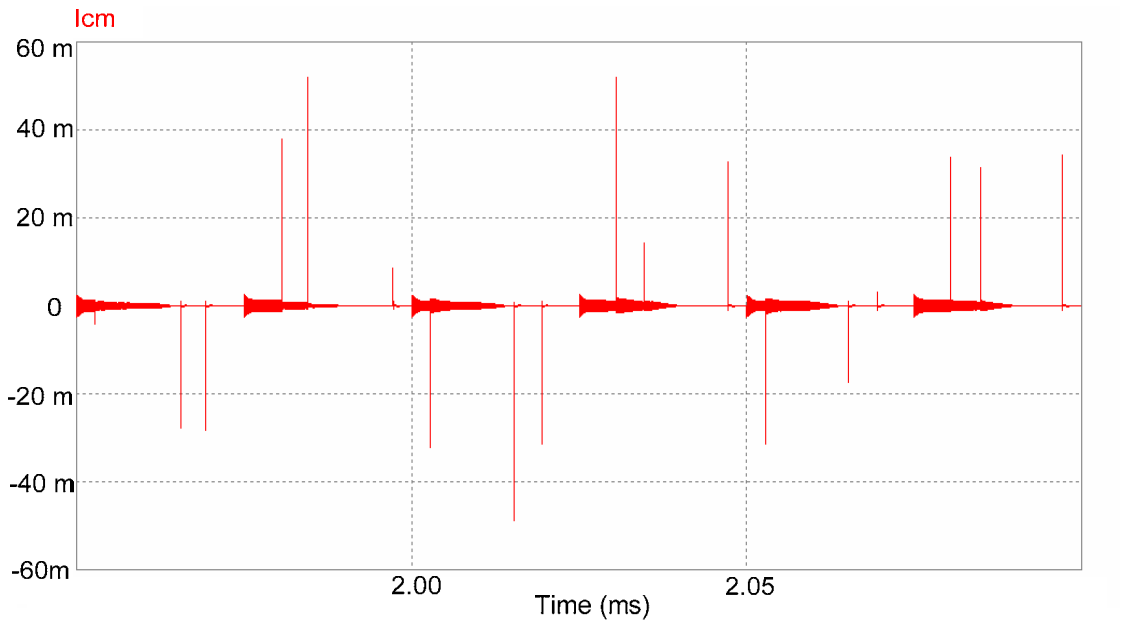

Figure 85 Common mode current for three phase system with shielded transformer

A comparison of the results obtained from simulating the single phase and three phase systems with and without the shielded transformer is shown in table IV.

Table IV

Comparison of common mode currents with and without shielded transformer

System Type	Conventional Transformer	Shielded Transformer
Single phase	22 A	55 A
Three phase	25 mA	52 mA

From the comparison of the results shown in table IV one can see that the common mode current is greatly reduced by the introduction of a shield in the high frequency transformer in the DC-DC converter. The magnitude of the reduction in the peak value of the common mode current is about three orders of magnitude smaller.

From these results it is possible to conclude that by using a shielded transformer the common mode current can be minimized, which contributes to a reduce the conducted EMI.

6.6. Conclusions

In this chapter the origin and effects of common mode voltage and currents in fuel cell power converters were discussed. It was shown that common mode currents are produced by rapid voltage transitions normal to the operation of power electronics

converters and the presence of parasitic capacitances to ground. The magnitude of these currents is a function of the rise and fall time of the semiconductor devices, the magnitude of the voltage and the value of the parasitic capacitances in the system. They can have magnitudes as high as 50 A and a very short duration. These short current pulses can cause interference in nearby circuits and may lead them to miss operate and fail.

The problem of common mode currents was analyzed for typical single phase and three phase fuel cell power conditioners and it was shown that both systems can produce currents of considerable amplitude.

To tackle this problem the use of shielded transformers in the DC-DC converter stage was proposed. And it was shown by means of computer simulations that the magnitude of the common mode current can be significantly reduced. This helps minimizing the generation of conducted EMI.

CHAPTER VII

CONCLUSIONS

Alternative energy sources have gained wide acceptance in the last two decades. Fuel cells, solar panels, wind mills and micro hydroelectric plants appear as good alternatives to produce electric power. Among these, fuel cells have been considered as the primary energy source for next generation power for residential, transportation and portable applications.

Fuel cells generate electrical energy by combining oxygen with a hydrogen-based fuel, such as methanol. Their main advantages are clean operation, simple maintenance, and modularity. However they generate a low voltage across their terminals, and therefore it is necessary to stack many cells to obtain a practical system. In addition they exhibit a large voltage variation from full load to no load. For this reason the use of a power converter becomes necessary to interface the fuel cell with the loads.

Using power electronic converters to interface the fuel cell with the loads introduces ripple currents in the current drawn from the fuel cell. To analyze the effect of these currents in the performance of the fuel cell stack an equivalent circuit model was shown. The parameters of this equivalent circuit are obtained from experimental measurements taken from the fuel cell.

DC-DC converters can be operated either in continues or discontinued conduction mode. From these two modes of operation discontinues conduction mode can be considered the worst case scenario, since the magnitude of the ripple current is comparable in magnitude to the DC component of the current. Thus the effect of discontinues conduction mode on the operation of the stack would be more significative. It was shown that when the load current of the fuel cell is not purely DC the hydrogen consumption of the stack increases and the output power of the fuel cell decreases. The magnitude of this effect is a function of the frequency of the ripple current. Also it was shown both analytically and experimentally that for load currents with low frequency ripple (below 1 kHz) the hydrogen consumption increases up to 7% while the output power of the fuel cell decreases up to 30%. On the other hand if the frequency of the ripple current is high, above 20 kHz, the hydrogen consumed by the fuel cell increases in the range from 1% to 3%, while its output power decreases by 5%. Also it was shown that the thermal performance of the fuel cell is not severely affected by the presence of high frequency ripple currents (i.e. due to discontinuous mode of operation).

Since fuel cells have a complex internal impedance its effect on the operation of the power converter was studied. It was shown that the internal impedance of the fuel cell can significantly affect the dynamics of the DC-DC converter. Also the behavior of the fuel cell during purging was discussed. The reduced power available during purging of the stack has been shown to be another possible cause for instability. To overcome these problems the use of supercapacitors connected in parallel with the fuel cell has been proposed. An approach to calculate the value of the supercapacitor to achieve stability

has been derived. Experimental results from a 30W fuel cell-boost converter system demonstrate the validity of the proposed solution. Finally, stability and good dynamic behavior has been shown to be possible with the use of supercapacitors connected to the output of the fuel cell.

Because of the low voltage produced by fuel cell stacks, most applications require that the power converter provides a large voltage gain. Traditionally this is accomplished by including a high frequency transformer in the DC-DC converter. This increases its size and cost. To reduce the cost and volume of the system a high gain transformer-less DC-DC converter was presented. The proposed converter employs a two level boost and a two level buck-boost converter in cascade to obtain a high voltage gain. It was shown that the proposed converter operation results in low input current ripple, which can contribute to lower EMI. Experimental results demonstrate the feasibility of the proposed DC-DC converter, and show that a voltage gain of 5 p.u. is obtainable.

Conventional fuel cells are constructed by stacking many cells. The main disadvantage of this approach is that the power that the system can generate is limited by the weakest cell in the stack. In addition if one or more cells fail the whole system has to be decommissioned. To tackle this problem a new modular fuel cell stack and DC-DC converter were introduced. The proposed approach divides the fuel cell stack into different sections that can be operated and controlled independently. This has the advantage of increasing the reliability of the system, since if one of the sections in the stack fails the rest of the fuel cell can remain in operation at reduced output power. In addition the power generation of the system can be optimized by controlling the current

drawn from each section in terms of the voltage they produce. It was shown that this technique results in a 10-14% additional power generation.

Rapid changes in voltage and currents normal to the operation of DC-DC converters generate common mode voltages and currents that circulate through ground. The effect of these common mode currents contributes to the generation of electromagnetic interference, which can produce miss operation in nearby equipment. It was shown that common mode currents appear in single phase and three phase utility interactive systems. To minimize the magnitude of common mode currents the use of shielded transformers was discussed and analyzed. It was shown that by introducing a shield between the primary and secondary windings of the high frequency transformer in the DC-DC converter the circulation of common mode currents can be drastically reduced.

REFERENCES

[1] Campbell, C. J.; *The Golden Century of Oil 1950-2050: The Depletion of a Resource*; 1st edition, New York, Springer.

[2] Hubbert, M; " Oil, the Dwindling Treasure"; *National Geographic*, June, 1974; pp. 792-825

[3] Lynch, M; " CRYING WOLF: Warnings about oil supply", available at http://sepwww.stanford.edu/sep/jon/world-oil.dir/lynch/worldoil.html

[4] Luo, F. L.," Luo-Converters, a series of new DC-DC step-up (boost) conversion circuits"; in Proc. *International Conference on Power Electronics and Drive Systems, 1997*; vol.2, pp. 882 – 888, May 1997

[5] Bayer, E.;" Optimized control of the "flying"-capacitor operating voltage in "gear-box"-charge-pumps-the key factor for a smooth operation"; in Proc*. IEEE PESC '03*, vol. 2, pp 610 – 615, June 2003

[6] Correa, J.; Farret, F.; Canha, L.; Simones, M.;" An Electrochemical –Based Fuel Cell Model Suitable for Electrical Engineering Automation Approach"; *IEEE Trans. on Ind. Electronics*, Vol. 51, No. 5, pp 1103-1112, October 2004

[7] Amphlett R.; Mann, R.; Peppley B.; Roberge, P.; Rodigues, A.;"A Practical PEM Fuel Cell Model For Simulation Vehicle Power Sources"; in *Proc. of the Tenth Annual Battery Conference on Applications and Advances*, pp 221 – 226, Jan. 1995

[8] Ceraolo, M.; Miulli, C. Pozio, A.; "Modeling static and dynamic behavior of proton Exchange membrane fuel cells on the basis of electro-chemical description"; *Journal of Power Sources*, No. 113, pp 131-144, , January 2003

[9] Erickson, R.; Maksimović, D.; *Fundamentals of Power Electronics*; Second Edition; Boston, Kluwer Academic Publishers, 2001

[10] Cengelci, E; Enjeti, P.; Singh, C.; Blaabjerg, F.; Pederson, J.K.; "New medium voltage PWM inverter topologies for adjustable speed AC motor drive systems**";** in *Proc. IEEE APEC'98*, vol. 2, pp 565 – 571, February 1998

[11] Rendusara, D.; Enjeti, P**.;"** An improved inverter output filter configuration reduces common and differential modes dv/dt at the motor terminals in PWM drive systems"; *IEEE Trans. on Power Electronics*, vol. 13, issue 6, pp 1135 – 1143, November 1998

[12] Palma, L.; Enjeti, P.;" An inverter output filter to mitigate dV/dt effects in PWM drive system"; in *Proc. IEEE APEC'02*, vol. 1,pp 550 – 556, March 2002

[13] Ogasawara, S.; Akagi, H**.;"** Modeling and damping of high-frequency leakage currents in PWM inverter-fed AC motor drive systems"; *IEEE Trans. on Ind. Applications*, vol. 32, issue 5, pp 1105 – 1114, September 1996

[14] Poh Chiang Loh; Holmes, D.G.; Fukuta, Y.; Lipo, T.A.;" A reduced common mode hysteresis current regulation strategy for multilevel inverters"; *IEEE Trans. on Power Electronics*, vol. 19, issue 1, pp 192 – 200, January 2004

[15] Loh, P.C.; Vilathgamuwa, D.M.; Gao, F.; Gajanayake, C.J.; Gay, L.W.; Leong, P.F.;" Random Pulse-Width Modulated Neutral-Point-Clamped Inverter With Reduced Common-Mode Switching"; in *Proc. IEEE PEDS'05,* vol. 2, pp 1435 – 1440, November 2005

[16] Haoran Zhang; Von Jouanne, A.; Shaoan Dai; Wallace, A.K.; Fei Wang**;"** Multilevel inverter modulation schemes to eliminate common-mode voltages"**;** *IEEE Trans. on Ind. Applications*, vol. 36, issue 6, pp 1645 – 1653, November 2000

[17] Xie, C.; Pavio, J.; Hallmark, J.; Bostaph, J.; Fisher, A.;" Key requirements of micro fuel cell system for portable electronics"; in *Proc. IEEE IECEC '02*, page(s): 603 – 606, July 2004;

[18] Ellis, M; Spakovsky, M.; Nelson, D.;" Fuel Cell Systems: Efficient, Flexible Energy Conversion for the 21st Century"; in *Proc. of the IEEE*, vol. 89, no 12, pp 1808-1818, December 2001

[19] Jiang, R.;Chu, D.;" Voltage-time behavior of a polymer electrolyte membrane fuel cell stack at constant current discharge", *Journal of Power Sources*, No. 92, pp 193-198, January 2001

[20] Smith, M.; Cooper, K.; Johnson D.; Scriber, L.; "Comparison of Fuel Cell Electrolyte Resistance Measurement Techniques"; *Fuel Cell Magazine*, pp 26-31, April/May 2005

[21] Niemann, J.; "Unraveling Fuel Cell Electrical Measurements", *Fuel Cell Magazine*, pp 32-37, April/May 2005

[22] Alfayyoumi, M.; Nayfeh, A.H.; Borojevic, D.; "Input filter interactions in DC-DC switching regulators"; in *Proc. IEEE PESC 99*, vol. 2, pp 926 – 932July 1999

[23] Mitchell, D.M.; "Power line filter design considerations for DC-DC converters"**;** *IEEE Ind. Applications Magazine*, vol. 5, issue 6, pp 16 – 26, Nov.-Dec. 1999

[24] Siri, K.; "Study of system instability in solar-array-based power systems**"**; *IEEE Trans. on Aerospace and Electronic Systems*, vol. 36, issue 3, pp 957 – 964, July 2000

[25] Erich, S.Y.; Polivka, W.A.; "Input filter design criteria for current-programmed regulators"; *IEEE Trans. on Power Electronics*, vol. 7, issue 1, pp 143 – 151, Jan. 1992

[26] N.Kasa, T. Iida, H. Iwamoto, "An Inverter using buck-boost Type Chopper Circuits For Popular Small-scale Photovoltaic Power System,", in *Proc. IEEE IECON '99* , vol. 1 , pp 185 – 190, Dec. 1999

[27] M.T. Zhang, Y. Jiang, F.C. Lee, M.M. Jovanovic, "Single-phase three level boost power factor correction converter", in *Proc. IEEE APEC '95*, vol. 1, pp 434 – 439, March 1995

[28] M. Pagano, L. Piegari, "Electrical networks fed by fuel-cells for uninterruptible electrical supply," in *Proc. IEEE ISIE'02*, vol. 3, pp. 953-958, May 2002

[29] R. Gopinath; S. Kim; J-H. Hahn; Webster, M.; J. Burghardt; S. Campbell; D. Becker; P. Enjeti; M. Yeary; J. Howze;*"* Development of a low cost fuel cell inverter system with DSP control**";** in *Proc. IEEE PESC'02*, vol. 1, pp 309-314 vol.1, June 2002

[30] W. Choi; P. Enjeti; J.W. Howze;" Fuel cell powered UPS systems: design considerations"; in *Proc. IEEE PESC '03*, vol. 1, pp 385 – 390, June 2003

[31] Akagi, H**.;"** Influence of high dv/dt switching on a motor drive system: a practical solution to EMI issues"**;** in *Proc. IEEE ISPSD '04*, pp 139 – 142, May 2004

[32] Skibinski, G.; Pankau, J.; Sladky, R.; Campbell, J.;"Generation, control and regulation of EMI from AC drives"; in *Proc. IEEE IAS '97*, vol. 2, pp1571 – 1583, Oct. 1997

[33] Gulez, K.; Mutoh, N.; Ogata, M.; Harashima, F.; Ohnishi, K.;" A new approximation method of estimating common mode (CM) model impedance parameters for EMI emissions in motor drive system"**;** in *Proc. IEEE International Symposium on Intelligent Control*, pp 648 – 653, Oct. 2002

[34] Y. Xue, L. Chang, S.B. Kjæer, J. Bordonau, T. Shimizu, "Topologies of Single-Phase Inverters for Small Distributed Power Generators: An Overview "; *IEEE Trans. on Power Electronics*, vol. 19, issue 5 , pp 1305 – 1314, Sept. 2004

[35] Junping He; Jianguo Jiang; Jiangjiang Huang; Wei Chen**;"** Model of EMI coupling paths for an off-line power converter"**;** *in Proc. IEEE APEC '04*; vol. 2, Page(s): 708 – 713, February 2004

[36] Gitau, M.N**.;"** Modeling conducted EMI noise generation and propagation in boost converters"; in *Proc. IEEE ISIE'00*, vol. 2, pp: 353 – 358, December 2000

[37] Rendusara, D.A.; Cengelci, E.; Enjeti, P.N.; Stefanovic, V.R.; Gray, J.W**.;"** Analysis of common mode voltage-"neutral shift" in medium voltage PWM adjustable speed drive (MV-ASD) systems"; *IEEE Trans. on Power Electronics,* vol. 15, issue 6, pp 1124 – 1133, November 2000

[38] Rendusara, D.; Enjeti, P.;" New inverter output filter configuration reduces common mode and differential mode dv/dt at the motor terminals in PWM drive systems"; in *Proc. IEEE PESC '97*, vol. 2, pp1269 – 1275, June 1997

[39] A. Greenwood; *Electrical Transients in Power Systems*; Second Edition, New York, John Wiley & Sons

VITA

Leonardo Manuel Palma Fanjul graduated with a Bachelor of Engineering from Universidad de Concepción, Concepción, Chile in 1999. During the year 2000 he worked as a part-time engineer doing consulting. He joined the master's program in electrical engineering at Texas A&M University in January 2001, and received his Master of Science degree in August 2003. Since then he has been pursuing his PhD degree at Texas A&M University which he received in December 2006.

His interests include power electronics, motor drives, energy storage devices, control systems and alternative energy applications.

He can be reached at palma@ieee.org or through the Department of Electrical Engineering, Texas A&M University, College Station, TX 77843, mail stop 77843-3128.